A LASER-DRIVEN PELLET ACCELERATOR FOR CTR FUEL INJECTION

Jeffrey Craig Hoy

A LASER-DRIVEN PELLET ACCELERATOR FOR CTR FUEL INJECTION

by

JEFFREY CRAIG HOY

B.S., United States Naval Academy

(1976)

SUBMITTED IN PARTIAL FULFILLMENT

OF THE REQUIREMENTS FOR THE

DEGREE OF MASTER OF

SCIENCE

at the

MASSACHUSETTS INSTITUTE OF TECHNOLOGY

August, 1977

A LASER-DRIVEN PELLET ACCELERATOR FOR CTR FUEL INJECTION

by

JEFFREY CRAIG HOY

Submitted to the Department of Nuclear Engineering on 12 August, 1977 in partial fulfillment of the requirements for the degree of Master of Science in Nuclear Engineering

ABSTRACT

The high-speed ballistic injection of a solid spherical pellet of deuterium-tritium ice into a magnetically confined thermonuclear reactor plasma has been suggested as a technique for controlled thermonuclear reactor fueling. This experiment is intended to be a preliminary test of the feasability of accelerating macroscopic fuel pellets using a pulsed ruby laser operating in the conventional mode. Pellet velocities in the range of 10^3-10^4 m/sec are required to enable the pellets to penetrate and effectively refuel the reactor plasma. In this study, cellulose acetate pellets were used to simulate deuterium-tritium fuel. When placed in a vacuum enclosed tube, they were accelerated by the reaction to the laser induced ablation cloud from the exposed half of the pellet. Pellet velocities of over 200 m/sec were achieved. The velocities were measured by stroboscopic photography, and the pellets were weighed to determine the fraction ablated.

Thesis Advisor: Peter A. Politzer
Title: Assistant Professor of Nuclear Engineering

ACKNOWLEDGMENTS

The author would like to express his gratitude to the United States Navy, for permitting him to pursue his graduate studies at the Massachusetts Institute of Technology this past year, while on active duty.

The author sincerely appreciates the helpful suggestions and advice given by his thesis advisor, Assistant Professor Peter A. Politzer, as well as by Professor Lawrence M. Lidsky, Assistant Professor Louis S. Scaturro, and the other members of the Applied Plasma Physics Group of the Nuclear Engineering Department. Special thanks are due to Mark L. McKinstry, who gave most generously of his time and contract money. He was a constant source of encouragement and information throughout this project. The author is also indebted to his MIT undergraduate assistant, Douglas H. Baird, lab technicians Melvin Alpert and Kenneth Rettman, and Professor Emeritus Harold E. Edgerton of MIT for the use of his stroboscopic photography equipment.

Last but not least, the author wishes to express his deep appreciation and affection to his family and friends, who in many intangible ways, helped to make his work more enjoyable.

The funds for this project were made available through the United States Energy Research and Development Administration (Contract No. FY-76-S-02-2431).

TABLE OF CONTENTS

ITEM	PAGE
ABSTRACT	2
ACKNOWLEDGMENTS	3
TABLE OF CONTENTS	4
LIST OF FIGURES	6
LIST OF TABLES	9
CHAPTER I: INTRODUCTION AND BACKROUND	10
1.1 FOREWORD	10
1.2 BACKROUND	12
1.2.1 FUELING A CONTROLLED THERMONUCLEAR REACTOR	12
1.2.2 REACTOR FUELING BY PELLET INJECTION	15
1.2.3 MACROSCOPIC PELLET ACCELERATORS	20
1.2.4 LASER-DRIVEN PELLET ACCELERATORS	23
1.2.5 PELLET COMPOSITION, PROPERTIES, AND BEHAVIOR	25
1.3 ORGANIZATION AND OBJECTIVES OF THE THESIS	31
CHAPTER II: LASER PELLET ACCELERATOR DESIGN	33
2.1 INTRODUCTION	33
2.2 LASER SYSTEM	34
2.3 VACUUM SYSTEM	37
2.4 BARREL ASSEMBLY	39
2.5 VELOCITY DIAGNOSTIC SYSTEM	43
2.6 PELLETS	47
2.7 ACCESSORY EQUIPMENT	52
2.8 SUMMARY	53

TABLE OF CONTENTS (Cont.)

ITEM	PAGE
CHAPTER III: EXPERIMENTAL PROCEDURE AND RESULTS	56
3.1 LASER CAVITY ALIGNMENT	56
3.2 LASER-BARREL ALIGNMENT	57
3.3 LASER OUTPUT ENERGY MEASUREMENT AND CALIBRATION	57
3.4 LASER PULSE SHAPE MEASUREMENT	60
3.5 STROBE INTERVAL MEASUREMENT	60
3.6 PELLET FIRING AND VELOCITY MEASUREMENT	63
3.6.1 PROCEDURE	63
3.6.2 DATA COLLECTION	66
3.6.3 DATA REDUCTION AND ANALYSIS	83
CHAPTER IV: DISCUSSION AND CONCLUSIONS	93
4.1 DISCUSSION	93
4.2 CONCLUSIONS	96
APPENDIX	99
BIOGRAPHICAL NOTE	105
REFERENCES	106

LIST OF FIGURES

NUMBER	TITLE	PAGE
1.1	DEPTH OF FUEL PELLET PENETRATION AS A FUNCTION OF INJECTION SPEED	17
1.2	FUELING RATE AND PERCENTAGE OF REACTOR CHARGE PER PELLET FOR A 5000 Mw(t) CTR	19
1.3	REQUIRED ACCELERATING VOLTAGE FOR FUEL PELLETS OF DIFFERENT RADII	24
1.4	CONVERSION EFFICIENCY OF INCIDENT LASER ENERGY TO PELLET KINETIC ENERGY	30
2.1	K-1 LASER HEAD - INTERNAL VIEW	35
2.2	LASER CAVITY, FOCUSING LENS, AND SUPPORT PLATFORM	36
2.3	VACUUM SYSTEM LAYOUT	38
2.4	VACUUM CHAMBER WITH BARREL ASSEMBLY INSTALLED	40
2.5	LASER POWER SUPPLY AND VACUUM GAUGE CONTROL PANEL	41
2.6	E.G.G. DOUBLE FLASHLIGHT SOURCE, REAR PANEL	44
2.7	PHOTODIODE CURRENT AMPLIFIER	46
2.8	CELLULOSE TRIACETATE PELLET DIAMETER DISTRIBUTION	48
2.9	CELLULOSE TRIACETATE PELLET MASS DISTRIBUTION	49
2.10	MER STRUCTURE OF CELLULOSE TRIACETATE	51
3.1	LASER OUTPUT AS A FUNCTION OF CAPACITOR BANK VOLTAGE	59
3.2	LASER PULSE SHAPE	61
3.3	STROBE FLASH INTERVAL VARIATION AND PULSE SHAPE	62
3.4	PELLET PHOTOGRAPH SCALE REFERENCE	64
3.5	PELLET VELOCITY AS A FUNCTION OF BARREL DEPTH FOR SHOT NUMBERS 1-36	68

LIST OF FIGURES (Cont.)

NUMBER	TITLE	PAGE
3.6	PELLET VELOCITY AS A FUNCTION OF BARREL DEPTH FOR SHOT NUMBERS 37-48	69
3.7	TYPICAL DOUBLE-EXPOSURE PELLET PHOTOGRAPH	70
3.8	PELLET VELOCITY AS A FUNCTION OF BARREL DEPTH FOR SHOT NUMBERS 49-54	71
3.9	TYPICAL DOUBLE-EXPOSURE DOUBLE-PELLET PHOTOGRAPH	72
3.10	PELLET VELOCITY AS A FUNCTION OF BARREL DEPTH FOR SHOT NUMBERS 55-59	73
3.11	PELLET VELOCITY AS A FUNCTION OF BARREL DEPTH FOR SHOT NUMBERS 60-70	74
3.12	PELLET VELOCITY AS A FUNCTION OF BARREL DEPTH FOR SHOT NUMBERS 71-80	75
3.13	PELLET VELOCITY AS A FUNCTION OF LASER OUTPUT	76
3.14	TYPICAL DOUBLE-PELLET AND QUADRUPLE-PELLET DOUBLE-EXPOSURE PHOTOGRAPHS	77
3.15	PELLET VELOCITY AS A FUNCTION OF BARREL DEPTH FOR SHOT NUMBERS 86-92	78
3.16	FRACTION OF PELLET ABLATED AS A FUNCTION OF BARREL DEPTH FOR SHOT NUMBERS 49-54	79
3.17	FRACTION OF PELLET ABLATED AS A FUNCTION OF BARREL DEPTH FOR SHOT NUMBERS 60-70	80
3.18	FRACTION OF PELLET ABLATED AS A FUNCTION OF BARREL DEPTH FOR SHOT NUMBERS 71-80	81
3.19	FRACTION OF PELLET ABLATED AS A FUNCTION OF LASER OUTPUT	82
3.20	TIME SPENT IN BARREL AS A FUNCTION OF BARREL DEPTH FOR SHOT NUMBERS 1-36	86
3.21	TIME SPENT IN BARREL AS A FUNCTION OF BARREL DEPTH FOR SHOT NUMBERS 37-44	87

LIST OF FIGURES (Cont.)

NUMBER	TITLE	PAGE
3.22	TIME SPENT IN BARREL AS A FUNCTION OF BARREL DEPTH FOR SHOT NUMBERS 55-59	88
3.23	TIME SPENT IN BARREL AS A FUNCTION OF BARREL DEPTH FOR SHOT NUMBERS 60-70	89
3.24	TIME SPENT IN BARREL AS A FUNCTION OF BARREL DEPTH FOR SHOT NUMBERS 71-80	90
3.25	TIME SPENT IN BARREL AS A FUNCTION OF LASER OUTPUT	91
A.1	STROBE DIAL TIME INTERVAL AS A FUNCTION OF ACTUAL STROBE TIME INTERVAL	99

LIST OF TABLES

NUMBER	TITLE	PAGE
1.1	U.S. ENERGY RESERVES	11
1.2	FUELING CHARACTERISTICS OF REFERENCE DESIGN FUSION REACTORS	14
1.3	ESTIMATES OF MAJOR EXPERIMENTAL PELLET FUELING REQUIREMENTS	21
1.4	CATALOGUE OF ACCELERATING DEVICES FOR 2 mm DIAMETER DT PELLETS	22
1.5	MECHANICAL PROPERTIES OF SOLID n-DEUTERIUM	27
2.1	SELECTED PHYSICAL PROPERTIES OF CELLULOSE TRIACETATE	50
A.1	RUBY LASER CALIBRATION DATA	100
A.2	PELLET ACCELERATION DATA	101

CHAPTER I

INTRODUCTION AND BACKROUND

1.1 FOREWORD

Since the beginning of the 1970's, and especially after the Arab Oil Embargo in the Fall of 1973, increasing national attention has been focused on the availability and economics of energy. In the past 35 years, man has used as much energy as during the whole of his previously recorded history. He will probably use the same amount again in the next fifteen years, and the same again in the following seven years. At present,our primary resources for energy production are the fossil fuels, namely oil, coal, and natural gas. The present reserves of fossil fuels are dwindling rapidly in the face of exponentially increasing demands and they are plagued with air-pollution problems. The resources of fissile fuels are more abundant, as shown in Table 1.1, but also limited, especially in the light of President Carter's recent efforts to kill the breeder reactor program in the United States. Clearly, the institutions of our civilization that make possible such a high standard of living, including medicine, agriculture, transportation, and industry, are all extremely dependent upon our energy resources.

Consequently, tremendous amounts of time and money have been invested studying new sources of power and optimal

TABLE 1.1

U.S. ENERGY RESERVES

[1]

Fuel		Energy in Q Units[1]
Fossil	Coal Oil and Natural Gas	12,000 1,800
Fissile	U^{235} (without breeders)	1,800
Fusile	Deuterium in the oceans	10^{10}

1. 1 Q = 10^{15} BTU = 1.05×10^{18} J

Americans consumed 75 Q in 1976. At present rates of consumption, we will exhaust our domestic supplies of all fossil fuels in 80 years.

methods of utilizing existant energy resources. Scientists and engineers have considered several alternative energy sources such as solar, wind, geothermal, and tidal power. There is at least one other - controlled thermonuclear fusion. The major incentive for developing a controlled thermonuclear reactor (CTR) is the enormous amount of energy it would make available to mankind. Fusile fuels (deuterium and tritium, both isotopes of hydrogen) make for an almost unlimited resource that would last man essentially indefinitely. Deuterium exists stably in all natural waters to the extent of 1 part in 6,666. Tritium is bred from lithium; the potential world reserves of lithium are estimated at 2×10^7 metric tons, enough to last about 30,000 years [1]. Fusion reactions produce almost no air-pollution, nor any byproduct that can be converted into dangerous weapons. They produce a minimum of manageable radioactive wastes, and, being highly efficient (due to the high temperatures of the working fluid), they produce much less thermal pollution per Mw(e) than either fossil or fissile energy.

1.2 BACKROUND

1.2.1 FUELING A CONTROLLED THERMONUCLEAR REACTOR

The general physics and engineering of fusion power will not be discussed here. Of all the many technologically formidable aspects of CTR design, this study will only deal with one - steady-state reactor fueling.

Long (magnet) pulse reactors are steady-state devices as far as fueling is concerned. The fractional fuel burn-up and diffusive losses (mainly the latter) are so large

that some method of refueling the magnetically confined plasma during the pulse is required. The advantages of steady-state fusion devices (fewer energy storage and switching problems, lower power densities, and more moderate demands on materials and structural supports, to name a few) make them extremely attractive candidates for first generation reactors. This means that an efficient solution to the fueling problem, as well as to those of providing adequate pumping or exhaust and adequate impurity control, is imperative to the evolution of a successful long pulse CTR design.

Although the importance of the fueling problem has been recognized for more than two decades, only a few analyses are available, and they appear to require unattractive technology (from the viewpoint of complexity and expense). The first study of CTR fueling (for stellarators) was made by Spitzer et al. [2] as early as 1954. More recently Rose [3], Gralnick [4], Kerbel [5], and others have considered the problem. Several fueling methods have been proposed, e.g. neutral beam injection, cluster injection [6], magnetic pumping [7], and a gas blanket solution [8]. Among the injection schemes proposed, the pellet method is advantageous because a relatively low injection energy per particle should be required in order to obtain penetration into the plasma. In comparison, neutral beams and atomic clusters require a much larger expendature of energy to reach the same plasma depth.

When a DT ice pellet enters a hot reactor plasma, a layer of gas and cold plasma develops by ablation, and thereby the remaining part of the pellet is protected from the fu-

TABLE 1.2

FUEL CHARACTERISTICS OF REFERENCE DESIGN FUSION REACTORS

Machine	Description	Size	Fuel Charge	τ_{burn}	Fueling
UWMAK I (1974)	Ignited long pulse tokamak with poloidal diverter	5,000 Mw(t) R = 13 m a = 5 m V = 6,400 m^3	$0.8 \times 10^{14} cm^{-3}$	5,400 sec	Pellets and Neutral Beams
ORNL (1973)	Ignited short pulse tokamak (unfueled)	1,000 Mw(t) R = 10.5 m a = 3.5 m V = 2,540 m^3	1.2 grams (2 g/day) 2×10^{14} cm^{-3}	172 sec	Neutral Beams (20 Mw, 20 keV, 500 A)
TFTR (1974)	Driven long pulse tokamak with poloidal diverter	5,300 Mw(t) R = 10.5 m a = 3.25 m V = 2,190 m^3	700 g/day 5×10^{13} cm^{-3}	100 min	Pellets (1 mm, 300 per sec, at 5×10^4 m/sec)
ERR I (Doublet) (1975)	Ignited short pulse deformed cross section tokamak (unfueled)	R = 4 m a_1/a_2 = 2/7 V = 400 m^3	2×10^{14} cm^{-3}	60 sec	Neutral Beams
EBTR-48 (1976)	Ignited steady state toroidally linked mirrors	4,000 Mw(t) R = 60 m a = 1 m V = 1,187 m^3	1.2×10^{14} cm^{-3}	Indefinite	Pellets

sion plasma energy flux [9]. This brings to mind another advantage of pellet fueling - the pellet evaporation process inhibits the formation of energetic charge-exchange neutrals, which are likely to be a problem in fueling schemes relying on neutral atom injection. Simple theoretical models [5] predict that a velocity of about 10^4 m/sec is sufficient for a fraction of the pellet to penetrate to the core of a reactor plasma before disassembling, ionizing, and becoming captured in the local magnetic field. This means a low injection energy per particle, but on the other hand, it is technologically difficult to accelerate a pellet with a radius in the millimeter range to such high velocities.

1.2.2 REACTOR FUELING BY PELLET INJECTION

As mentioned earlier, steady-state operation requires that the amount of fuel introduced into the reactor per unit of time be equal to the rate at which fuel is consumed and lost by diffusion out of the system. The rate of fuel input required per watt of heat produced is [10]

$$F = 5.5 \times 10^{11} \frac{(R_p)}{(R_w)} \cdot f_b^{-1} \quad \text{atoms/watt-sec} \qquad (1.1)$$

where R_p and R_w are the plasma and vacuum wall radii, and f is the fractional burn-up. Taking $\frac{(R_p)}{(R_w)} \simeq 0.7$ and $f_b \simeq 10\%$ (reasonable estimates for a low β toroidal machine such as a tokamak) Eq. 1.1 would indicate that a 5000 Mw(t) reactor requires fuel to be injected at the rate of

$$F = 1.92 \times 10^{22} \quad \text{atoms/sec} \qquad (1.2)$$

The energy expended in supplying fuel at this rate is the sum of the kinetic energy of the pellet at injection, E_u, and the refrigeration necessary to produce the solidified fuel. E_u is just

$$E_u = \tfrac{1}{2}\, m_p v_p^2 \tag{1.3}$$

where v_p is the initial injection speed, and m_p is the initial pellet mass. The power consumed in injection is then [4]

$$P_u = \frac{E_u F}{N} = \tfrac{1}{2}\, m_p v_p^2 \frac{(1.92 \times 10^{15})}{N} \quad \text{watts} \tag{1.4}$$

where N is the average number of fuel atoms per pellet, and E_u is in ergs. v_p must be selected so that a pellet of radius r_p will carry the fuel the desired distance into the reactor plasma. Figure 1.1 [4] shows the initial velocity, v_p, required to give a depth of penetration of 50% of the pellet mass, f_{50}, for different sizes of fuel pellets.

The next question is: What determines the initial size of the fuel pellet? The following criteria must be met:

1. The fuel pellet must be sufficiently large so that fuel is supplied rapidly enough to satisfy the fuel requirements of the reactor, without requiring the number of pellets injected per second to be excessively large.

2. The pellet must not be so large that it contains more than a small fraction of the total reactor fuel charge (< 10%). Large pellets will very rapidly cool the reactor plasma, cause instabilities, and interrupt the burn cycle.

The particle injection rate necessary to supply our hypothetical 5000 Mw(t) reactor (1.92×10^{22} atoms/sec) would be [4]

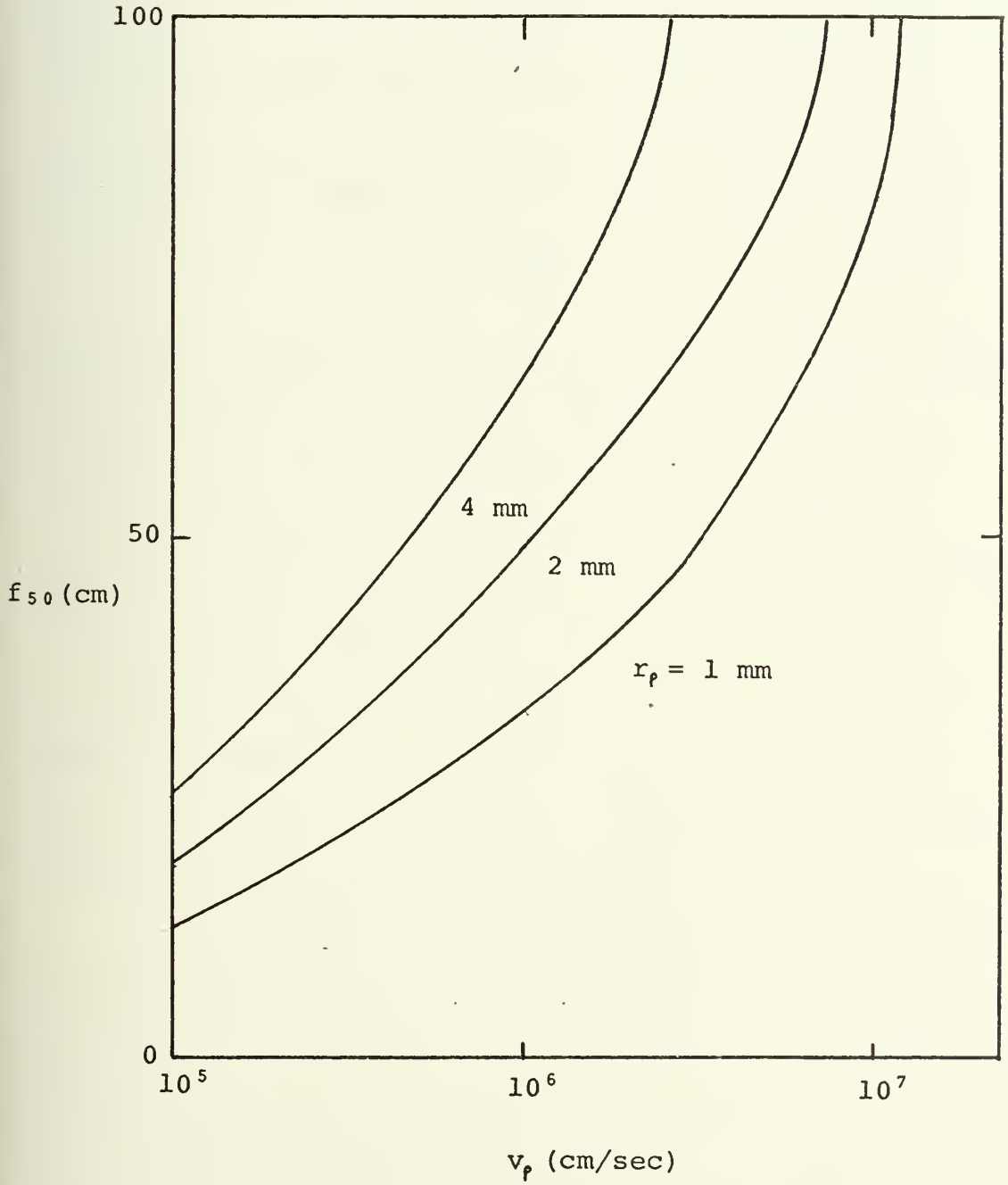

FIGURE 1.1: DEPTH OF FUEL PELLET PENETRATION AS A FUNCTION OF INJECTION SPEED [4]

$$R = \frac{0.085}{r_p^3} \tag{1.5}$$

where r_p is the pellet radius in mm. For a 5000 Mw(t) reactor with a major radius R_M of 5.20 m and a plasma radius R_p of 1.25 m, the total fuel charge of the reactor is [4]

$$C = 3.51 \times 10^{22} \text{ atoms} \tag{1.6}$$

Dividing by the number of atoms per pellet of radius r_p gives

$$\frac{C}{N} = \frac{0.16}{r_p^3} \tag{1.7}$$

Equations 1.6 and 1.7 show that a pellet of approximately 1 mm radius would be suitable for fueling this reactor. For this pellet size, the reactor charge is 210 times the fuel introduced in each pellet, so a feed rate of 85 pellets per second would do nicely. Larger pellets contain too large a percentage of the reactor charge, while reducing the size of r_p increases R rapidly. Figure 1.2 [4] shows the fueling rate and the percentage of the total charge contained in each pellet vs. pellet radius. For a 1 mm pellet, a value of f_{50} = 50 cm can be achieved with a v_p of 1.5×10^4 m/sec.

An experiment [11] was recently performed by Foster, in which 70 and 200 μm diameter pellets of solidified hydrogen were injected into ORMAK at a speed of 100 m/sec. The pellets penetrated 3.5 and 8 cm, respectively, into the plasma on a trajectory angled at 45 degrees to a radial line. Both the temporal and spatial distribution of the light emanating from the pellet-plasma interaction were recorded. The experiments are in agreement with the neutral shielded model proposed by Gralnick [4].

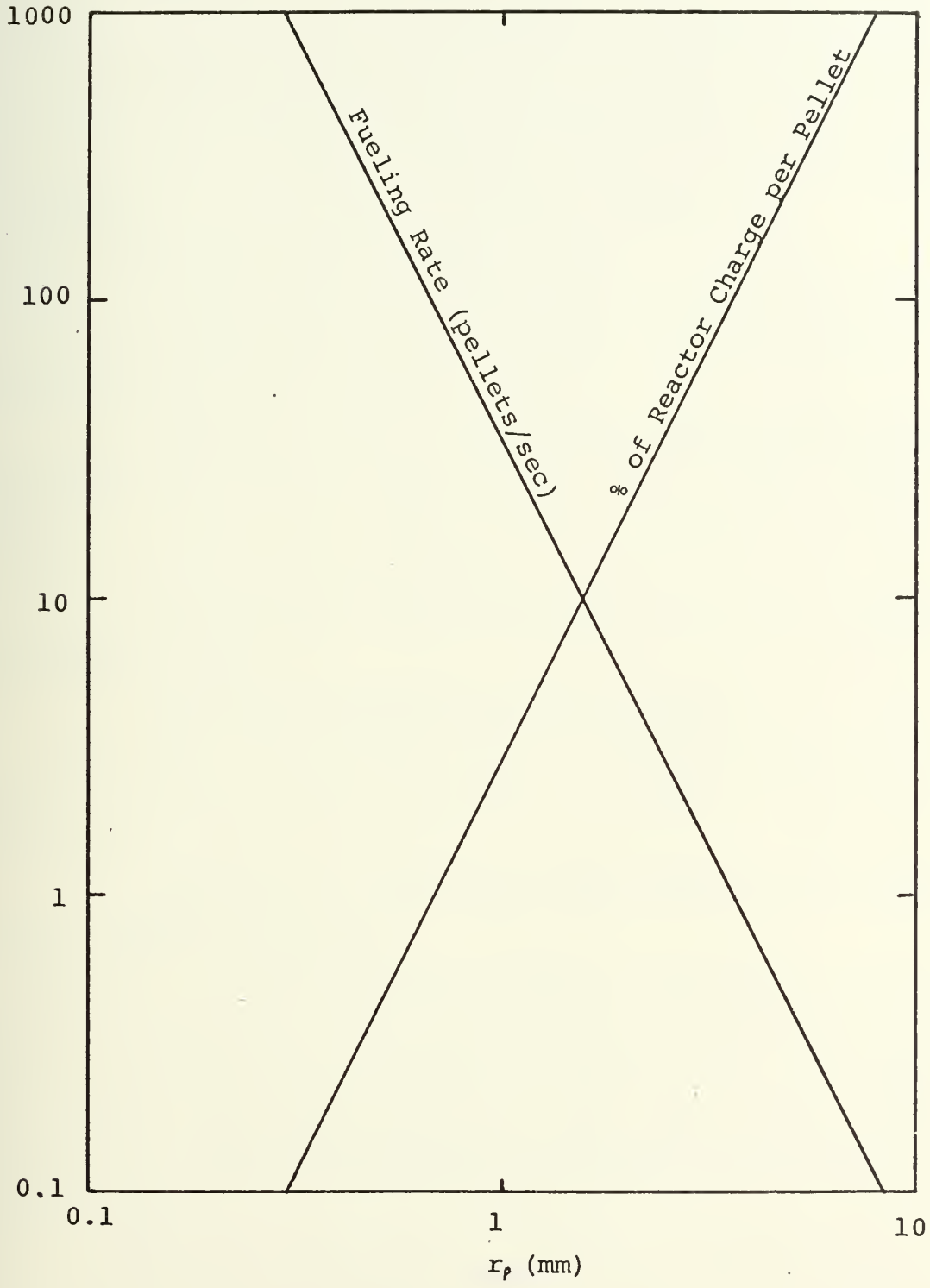

FIGURE 1.2: FUELING RATE AND PERCENTAGE OF REACTOR CHARGE PER PELLET FOR A 5000 Mw(t) CTR [4]

The neutral-shielded model has been applied to several proposed tokamaks to determine what size and speed a pellet must have to penetrate to the center of the discharge [12]. The pellet size was arbitrarily set so each pellet would contain 10% of the plasma ion content. The pellet speed necessary to penetrate to the center is shown in Table 1.3.

1.2.3 MACROSCOPIC PELLET ACCELERATORS

The parameters of a desirable pellet generator-accelerator apparatus would be [5]:

1. Pellet material: adjustible composition of hydrogen (deuterium and tritium), and tracers such as neon, oxygen, or argon.

2. Pellet size: atomic clusters to several millimeters in diameter-solid.

3. Injection velocity: 10^2-10^5 m/sec.

4. Rate of injection: one on demand to as many as 10^3 per second.

5. Direction of injection with respect to the direction of the magnetic field $\underline{B}$.

In addition, a valuable pellet injector should also be able to deliver the pellet at a prescribed moment with the influx of accompanying gas at less than 10^{-5} torr with a small angular spread so as to allow predictable trajectories through the plasma target.

One of the following injection methods (listed in Table 1.4, [13]) could be applied: electrostatic acceleration, laser acceleration, mechanical centrifuge, electron beam acceleration, gas dynamic acceleration, light gas gun, coaxial

TABLE 1.3

ESTIMATES OF MAJOR EXPERIMENTAL PELLET FUELING REQUIREMENTS FOR PELLETS CONTAINING 10% OF DEVICE TOTAL ION CONTENT AND FOR PERPENDICULAR INJECTION

[11]

Device	a (m)	T_e(keV)	N_e(m^{-3})	r (μm)	v (m/sec)
ORMAK	0.23	1.0	7×10^{19}	220	2,000
ISX	0.25	1.0	7×10^{19}	240	2,000
ORMAK	0.30	0.9	1×10^{20}	300	1,500
Upgrade	0.30	3.0[1]	1×10^{20}	300	5,000
PDX	0.47/0.57	1.0	3×10^{19}	300	1,500
		3.0[1]	1×10^{20}	475	3,000
PLT	0.45	1.7	5×10^{19}	360	3,000
		4.0[1]	1×10^{20}	450	6,000
TNS	1.25/2.0	24.0	4×10^{20}	3,000	6,000

1. With neutral beams.

TABLE 1.4

CATALOGUE OF ACCELERATING DEVICES FOR 2 mm DIAMETER DT PELLETS [13]

Device	Speed (m/sec)	Comments
Gas dynamic[1]	8×10^2	Uses low-pressure gas flow.
Light gas gun	1×10^4	Requires extremely high pressure.
Coaxial plasma gun	5×10^3	Introduces impurities into plasma.
Electrostatic[1]	6×10^2	Charging field 2.5×10^8 V/m, acceleration voltage 13×10^6 V.
Laser[2]	---	Present concepts (Q-switched) result in pellet destruction.
Electron beam[2]	---	May couple energy better than laser.
Mechanical centrifuge[1]	2×10^3 6×10^3	Aluminum rotor. High-performance composite rotor.

1. Estimates only.

2. Unproven concept.

plasma gun. Electrostatic acceleration has received a substantial amount of attention. Satisfactory velocities have been obtained with sub-millimeter size pellets, but the accelerating potential becomes unreasonably high with increasing pellet radius (Figure 1.3, [14]). Electron beams, mechanical centrifuges, and laser injectors all show some promise of success, and work is currently under way in the latter two areas. This paper is only concerned, however, with the last method: laser-driven pellet injection.

1.2.4 LASER-DRIVEN PELLET ACCELERATORS

Acceleration of pellets to hyper-velocities is possible by the interaction of a laser pulse with one side of the solid pellet surface. Part of the pellet mass is surface ablated producing a high velocity expanding plasma cloud that transfers its momentum to the solid surface. Acceleration experiments using giant (Q-switched) ruby laser pulses have been performed [15]. These resulted in the pellets being destroyed by the enormous impulse and power density of a 10 J laser with a pulse duration of only 50 nsec (power = 2×10^8 watts).

Another related method, would employ a pulsed laser operating in the conventional mode. Since the pulse duration is much longer ($\simeq$ 1 msec), the incident radiation intensities are many orders of magnitude lower than giant laser pulses, and hydrogen should be evaporated from the pellet surface as a high temperature neutral gas rather than a highly ionized plasma. The velocity of the blown off gas would be of the

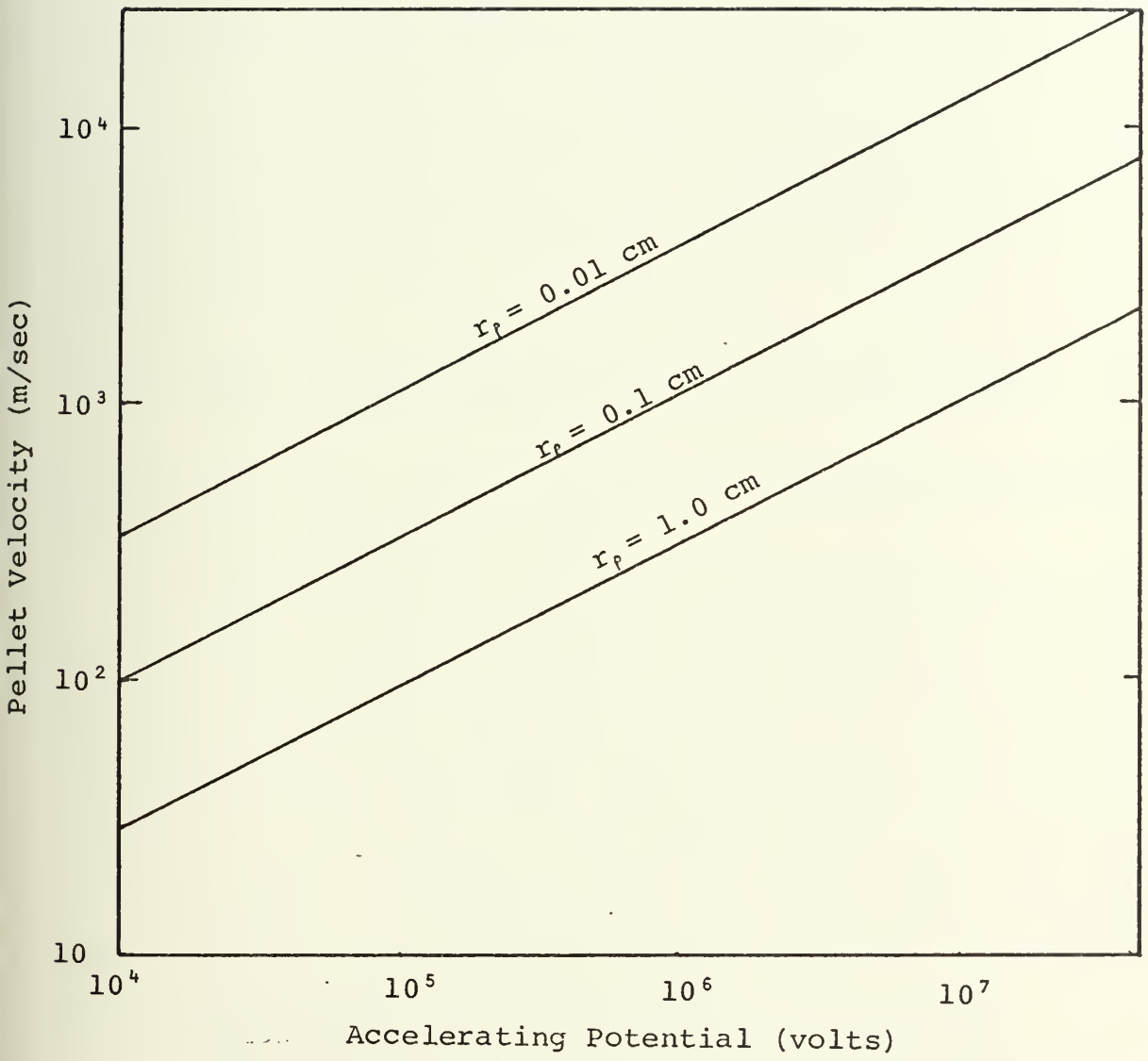

FIGURE 1.3: REQUIRED ACCELERATING VOLTAGE FOR FUEL PELLETS OF DIFFERENT RADII [14]

order of 10^3-10^4 m/sec, or roughly equivalent to the sonic velocity of gaseous hydrogen [16]. A pellet would, then, experience a more gradual acceleration over a much longer period of time. A 20 J laser having a pulse duration of 800 μsec would develop a reaction pressure of about

$$p \simeq \frac{20 \text{ J}}{(8 \times 10^{-4} \text{ sec})(10^4 \text{ m/sec})(10^{-6} \text{ m}^2)} = 2.5 \text{ MPa} \qquad (1.8)$$

A 1 mm pellet could probably withstand such a stress wave and be accelerated to a final velocity (assuming ideal energy coupling between the laser radiation and the pellet surface) given by [17]

$$v \simeq \frac{p\,\tau}{\rho\,\ell} = \frac{(2.5 \times 10^6)(8 \times 10^{-4})}{86 \times 10^{-3}} = 2.3 \times 10^4 \text{ m/sec} \qquad (1.9)$$

where ρ and ℓ are the pellet density and size respectively, and τ is the laser pulse length.

Thus, it appears that this method seems worthwhile, at least conceptually, to pursue. There are many practical problems with it that have yet to be resolved: energy coupling efficiency between the laser radiation and the pellet surface, maintaining pellet integrity throughout the acceleration process, and laser requirements such as energy, pulse duration, wavelength, and pulse repetition rate.

1.2.5 PELLET COMPOSITION, PROPERTIES, AND BEHAVIOR

When a pellet experiences an acceleration, opposing inertial forces result which give rise to a longitudinal compression of the pellet. The compression is accompanied by a proportionate amount of lateral tensile strain in both principle transverse directions. The constant of proportionality,

Poisson's ratio, typically has values in the range .25-.30. As long as the amount of lateral strain, ε, does not exceed the elastic limit of the material, the solid crystalline structure will remain stable. Common materials can withstand at most a few tenths of a percent of tensile strain before plastic deformation and destruction result.

The tensile strength of the pellet material, then, can impose an upper limit on its acceleration. The yield strength, given by

$$\sigma_y = E\ \varepsilon_{max} \tag{1.10}$$

where E is Young's modulus of elasticity, can lead to an even more conservative estimate. In the case of solid hydrogen and its isotopes, deuterium and tritium, the yield strength is a function of both temperature and deformation rate. Experimental measurements of uniaxial loading have been conducted by Bol'shutkin, Stetsenko, and their co-workers on polycrystalline parahydrogen and polycrystalline normal hydrogen [18], and polycrystalline deuterium [19]. Table 1.5 gives their values for several mechanical properties of deuterium. The maximum tensile strength of solid normal deuterium (n-D_2) is 57 g/mm^2 (5.6×10^5 N/m^2), which occurs at 6^0 K. The figures listed for deuterium should only be considered approximate. No mechanical data is available for solid tritium (T_2) or deuterium tritide (DT); the only density listed for solid tritium is 0.324 g/cm^3 at 4.2^0 K [20]. One would not expect much difference between the properties of D_2 and T_2 or DT, so it will be assumed that DT pellets exhibit the same

TABLE 1.5

PROPERTIES OF n-DEUTERIUM

[20]

T (^{0}K)	σ_T (g/mm^2)	ε (%)	σ_y (g/mm^2)	E (Kg/mm^2)	G	ρ (g/cm^3)	isothermal Poisson's Ratio	v (m/sec)
1.4	43.0	0.6	51.0	52.0	20.0	0.204[1]	---	---
3.0	50.0	0.8	34.0	49.6	19.4	---	---	---
4.2	54.0	1.0	29.0	48.2	18.1	0.204	0.31	1,920
5.4	52.0	2.0	27.5	46.5	17.8	---	0.31	1,920
8.0	45.0	3.0	26.0	44.0	16.8	---	0.31	1,920
11.6	43.3	6.2	22.0	42.0	16.2	0.200	0.30	1,910
15.6	29.1	13.0	14.4	41.1	15.8	0.196	0.30	1,890
16.4	21.4	22.3	---	---	---	---	0.30	1,860

1. Para-deuterium.

v = lateral speed of sound in solid n-D_2.

These mechanical properties are valid for a deformation rate of 4.4×10^{-3} sec^{-1}.

mechanical characteristic as D_2 pellets.

If the pressure given by the maximum tensile strength of deuterium were distributed uniformly over one side of a cube of dimension ℓ, the acceleration would be given by [17]

$$a_{max} = \frac{\Delta p}{\ell \rho} \tag{1.11}$$

Substituting 57 g/mm^2 for Δp, 0.20 g/cm^3 for ρ, and 1.5 mm for ℓ, one would then expect a maximum tolerable acceleration on the order of 2×10^6 m/sec^2. To attain a terminal velocity of 10^4 m/sec, an accelerating path of 1 m would be required.

A similar argument can be made when the pellet experiences larger impulsive loads which are applied over time periods that are shorter than the time required for the elastic stress wave to propagate through the pellet ($\simeq$ 1 μsec for a 1 mm pellet) [17]. In this case, however, that amount of applied pressure in excess of the elastic limit (σ_y) is propagated as a slowly moving plastic wave that deforms the pellet as it propagates, dissipating energy as heat. The pellet can probably remain intact if such large waves do not propagate more than a fractional distance into the pellet bulk.

Notice that the laser induced reaction pressure calculated in Equation 1.8 is a factor of two larger than the maximum tensile strength just used to find the maximum allowable pellet acceleration. Although these are rather crude estimates, it is apparent that the pellet materials will be stretched to their structural limits, and perhaps beyond.

In terms of laser wavelength, λ (in microns), and the density of the solid unshocked material, ρ_0, the fraction

of laser energy that is converted into kinetic energy of the shocked material is [15]

$$\eta = \frac{1}{2 + 5.4\ \lambda(\rho_0)^{1/2}} \tag{1.12}$$

This is an expression for the coupling efficiency mentioned in the previous section. A plot of this function is shown in Figure 1.4 for hydrogen and deuterium [15]. For wavelengths in the 0.5-1.0 μm range, the efficiency is poor (only a few percent), and for 10 μm radiation it is only a few tenths of a percent. In this respect, a ruby laser (λ = 0.6943 μm) should be slightly superior to carbon dioxide (λ = 1.02 μm), or neodymium glass (λ = 1.06 μm).

According to Milora et al. [15], the pellet velocity is

$$v_p = 0.58\ (E/\lambda)^{2/3}(\rho_0)^{-1}(r_p)^{-7/3}(\tau)^{1/3} \tag{1.13}$$

where E is the laser energy, τ the pulse length, and r_p is the pellet radius (which is taken as the laser focal radius). The internal energy of the pellet is, then

$$e = \frac{v_p^2}{2} \tag{1.14}$$

All parameters are in SI units.

Thus, if one is to believe this theoretical model, the velocity is most sensitive to pellet radius, and is dependent to a lesser extent on laser energy and wavelength, and solid density, ρ_0. The burn time, τ, is not an important parameter. The result that the internal energy is proportional to the square of the pellet velocity is an important consequence. This would place quantitative limit on v_p, since the internal

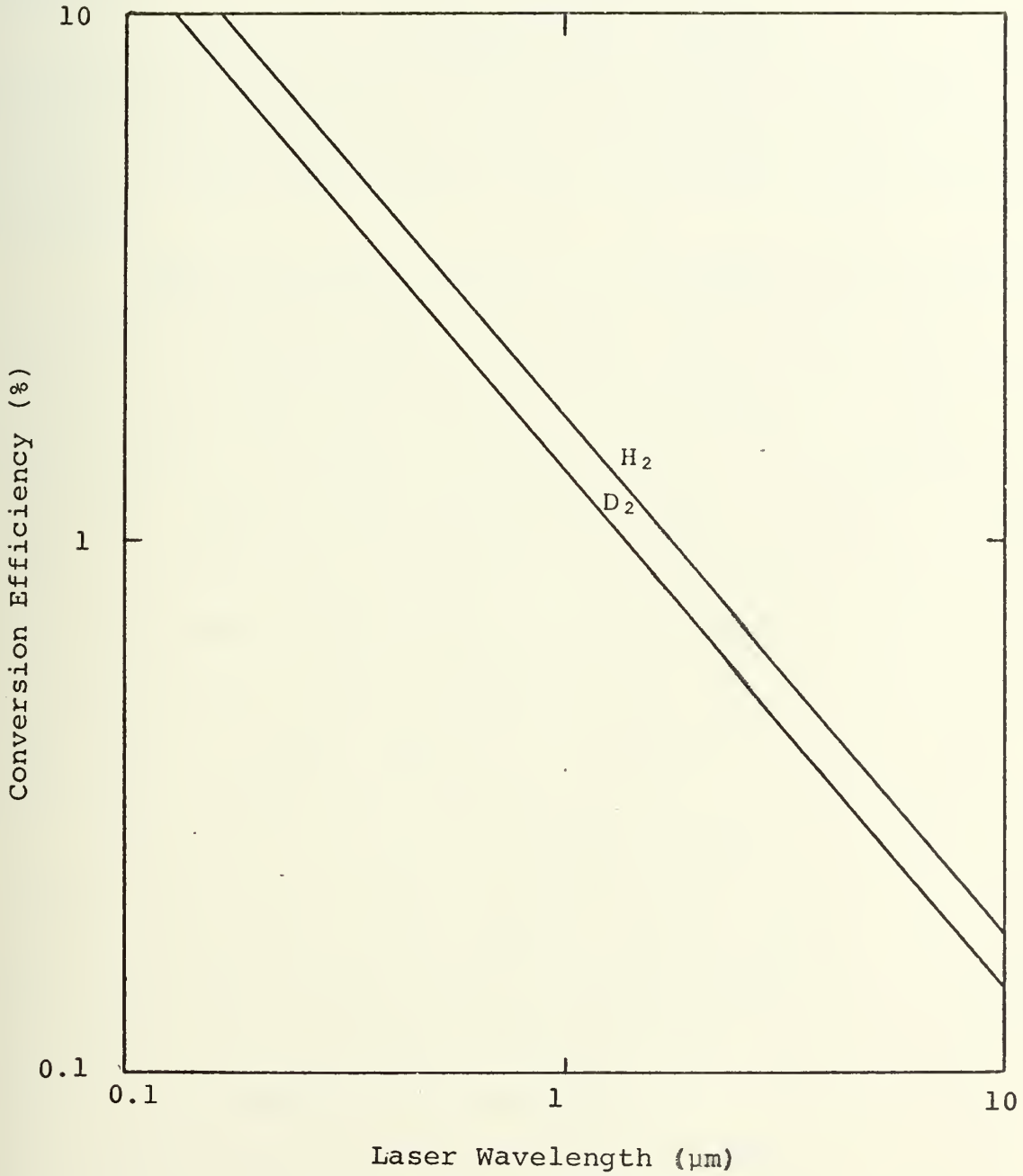

FIGURE 1.4: CONVERSION EFFICIENCY OF INCIDENT LASER ENERGY TO PELLET KINETIC ENERGY SHOWING λ DEPENDENCE FOR HYDROGEN AND DEUTERIUM [15]

energy must be kept below the value which would lead to vaporization of the pellet bulk. For hydrogen isotopes, the heat of vaporization varies approximately as $10^6/M$, where M is the molecular weight [20]. This result limits velocities given by

$$v < \left(\frac{2 \times 10^6}{M}\right)^{1/2} \quad \text{m/sec} \qquad (1.15)$$

For molecular hydrogen, an upper limit of only 10^3 m/sec is obtained. Even lower values would result with deuterium and tritium.

There are ways, however, to circumvent this restriction. It has been suggested that one might also consider ionic crystals such as LiD and LiT for fuel pellets, if indeed the dissociation of frozen DT pellets proves to be problematic in achieving larger plasma penetration depths, or fully ionized ablation plasmas for achievable pellet injection velocities [5]. The larger binding energy of ionic crystals would seem to help preserve pellet integrity, more orderly ablation, and thus assure a higher degree of ionization of ablating fuel, although contributing somewhat to the Z_{eff} of the fueled plasma (Z_{eff} determines the amount of Bremsstrahlung radiation power lost in the reactor power balance). Unfortunately, very little data concerning LiD and LiT crystalline structures is easily accessible due to security classifications (LiD is an essential component of thermonuclear warheads).

1.3 ORGANIZATION AND OBJECTIVES OF THE THESIS

This first chapter serves to define the problem and presents relevant backround information regarding pellet fueling of CTR's. In Chapter II, the author's laser-driven

pellet acceleration device is described in detail, noting how certain components could be improved in later versions, and how they fit into the total picture of reactor system design. Chapter III contains the experimental procedures and results using the accelerator of the previous chapter to launch 1.5 mm diameter cellulose triacetate pellets. These were chosen to simulate solid DT fuel pellets, thereby avoiding the complications involved with adding cryogenic systems to the apparatus. Chapter IV summerizes the results and draws conclusions as to the future success of the laser pellet acceleration concept for CTR fueling, based on comparisons of the properties of cellulose triacetate and DT. It also recommends certain topics which warrant further examination and experimentation.

CHAPTER II

LASER PELLET ACCELERATOR DESIGN

2.1 INTRODUCTION

The design of this laser pellet accelerator was carried out in a "build as you go" manner, utilizing equipment and materials on hand in the laboratory, some of which had to be scavenged from old experiments (e.g. the vacuum system) or machined from scratch (e.g. the laser supports, and the barrel assembly). This made performance optimization quite difficult at times due to the short time frame allowed to complete the experiment. There was substantial difficulty involved in procuring pellets of a suitable size and shape. As a consequence, it was not possible to make a choice of the pellet composition; proper size and shape had priority. Some aspects of the design evolved through trial and error, such as the velocity diagnostic system, which had to be drastically altered to obtain good results.

The pellet acceleration device employed here may be broken down, for purposes of explanation, into several sections: the ruby laser system, the vacuum system, the barrel assembly, the velocity diagnostic system, the pellets, and the accessory equipment. All of the equipment is relatively inexpensive (compared to other CTR components) and readily available, which further adds to the attractiveness of this method of fuel injection.

2.2 LASER SYSTEM

The Korad K-1 Series Ruby Laser (λ = .6943 μm), being over ten years old, is fairly obsolescent by current laser technological standards, but it is quite well suited to this experiment. It can be operated in a conventional long pulse mode, as well as in one of several Q-spoiled short pulse modes by inserting a pockels cell at the rear end of the laser cavity. Since we were interested only in the conventional mode, the pockels cell and its associated shutter electronics were not required.

The laser system, as used here, consists of:

1. laser head assembly
2. 100% reflecting sapphire rear cavity mirror
3. 45% reflecting sapphire front (output) cavity mirror
4. cooling system
5. power supply
6. focusing lens
7. mounting beam and support platform

The laser head includes the aluminum chassis, which houses a single spiral xenon flash lamp that serves to optically pump the laser material. The lasing medium is a chromium-doped ruby rod, 4 in. by 9/16 in. in diameter, which rests inside the xenon lamp helix. The rod and flash lamp are immersed in a circulating water coolant bath enclosed inside the housing (Figure 2.1). The water cooling system consists of a fifteen gallon reservoir, an electric pump, a freon refrigeration system with adjustable temperature control, an ion exchange filtration

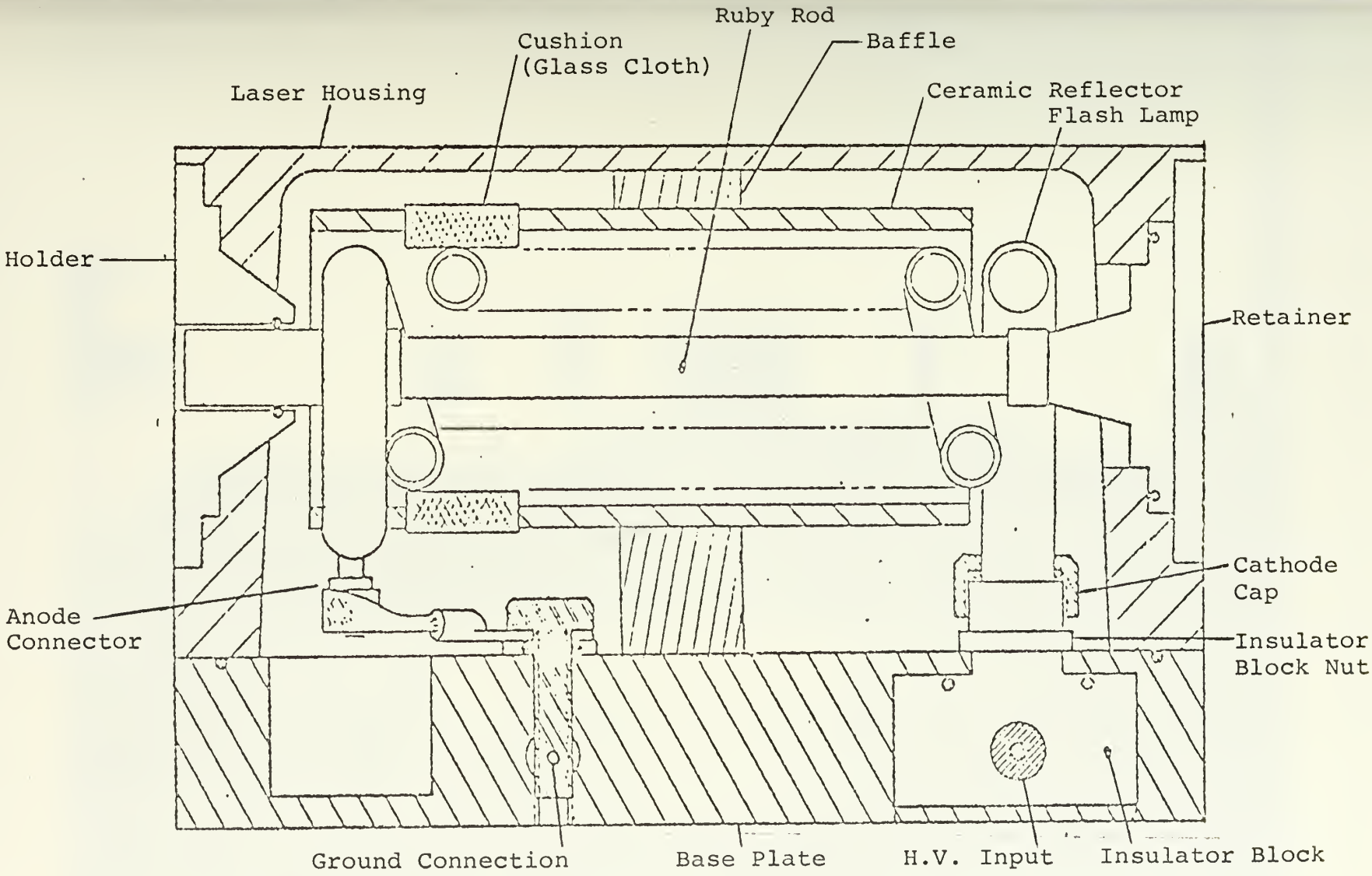

FIGURE 2.1: K-1 LASER HEAD - INTERNAL VIEW

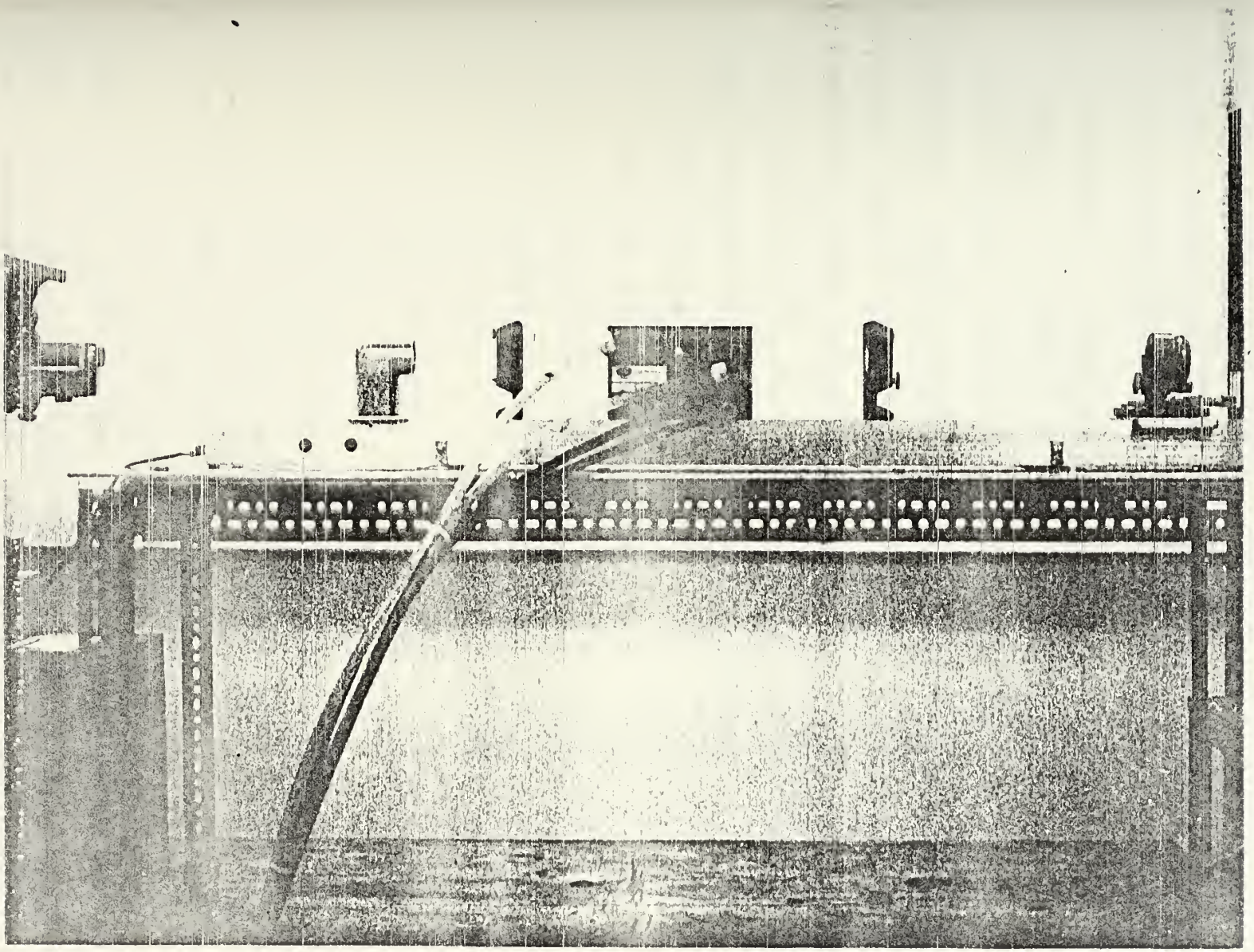

FIGURE 2.2: LASER CAVITY, FOCUSING LENS, AND SUPPORT PLATFORM

cartridge, and coolant tubing to the laser head. The power supply contains a high voltage capacitor bank (5.0 KV capacity), and the charging and firing electronics. In order to focus the laser beam into the muzzle of the barrel, a low quality, 40 mm diameter, double-convex, flint glass lens (f = 435 mm) is mounted on a sliding aluminum base in front of the laser output reflector (Figure 2.2). The laser head and the two reflectors (which comprise the laser cavity) are mounted on an aluminum channel beam. This beam is, in turn, bolted to an aluminum platform of adjustable height. A laser cover of aluminum sheet, painted flat black, serves to shield both instruments and personnel from stray laser radiation.

2.3 VACUUM SYSTEM

The vacuum system components are:

1. mechanical pump
2. diffusion pump
3. gate valve
4. baffle chamber
5. baffle
6. ionization gauge and controller
7. thermocouple gauge and controller
8. vacuum chamber
9. front vacuum window

There are two pumps in this system: a low vacuum mechanical pump, and a high vacuum diffusion pump. The former is a Kinney Model KD-30 electric pump, and the latter a Consolidated Vacuum Corporation 6 in. diffusion pump filled with Convoil-20 pump oil. Directly on top of the diffusion pump rests a gate valve,

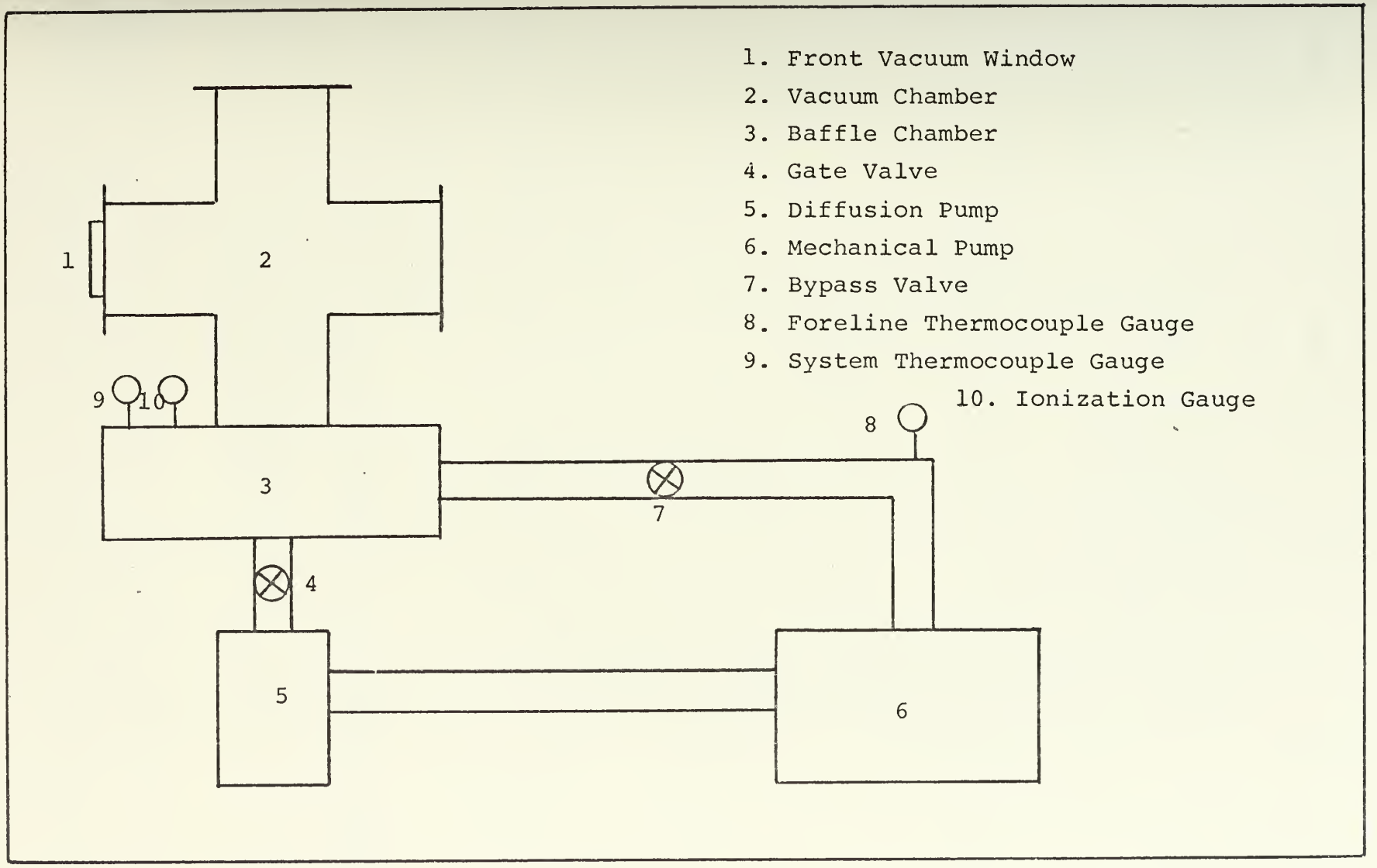

FIGURE 2.3: VACUUM SYSTEM LAYOUT

and then a baffle chamber (see Figure 2.3 for the layout) which houses a homemade, disk shaped, water cooled, copper baffle. The baffle prevents pump oil from rising into the vacuum chamber, and also serves to catch anything from above that could foul the diffusion pump (e.g. pellets). One Varian thermocouple gauge monitors the foreline pressure between the two pumps, while another measures the system pressure inside the baffle chamber. The ionization gauge and its controller (both made by the MIT Research Laboratory of Electronics) measure the system pressure inside the baffle chamber once it has gone below the range of the thermocouple gauge (< 20 mtorr). A thermal switch attached to the diffusion pump acts as an over-pressure protector in the event of coolant loss. The vacuum chamber, which surrounds the barrel assembly, is a crossed section of 6 in. O.D. Pyrex glass pipe sealed by ¼ in. thick brass plates with O-rings. One of these plates has a 4.5 in. hole, over which fits a 1 in. thick, optically flat, glass window that allows the laser beam to be transmitted into the barrel.

2.4 BARREL ASSEMBLY

The barrel assembly is made of only three components:

1. barrel support
2. stainless steel barrel
3. copper barrel

The barrel support consists of a ½ in. O.D. brass tube, perforated along its length to allow better evacuation. It fits vertically (see Figure 2.4) through a Cajon Ultra-torr vacuum

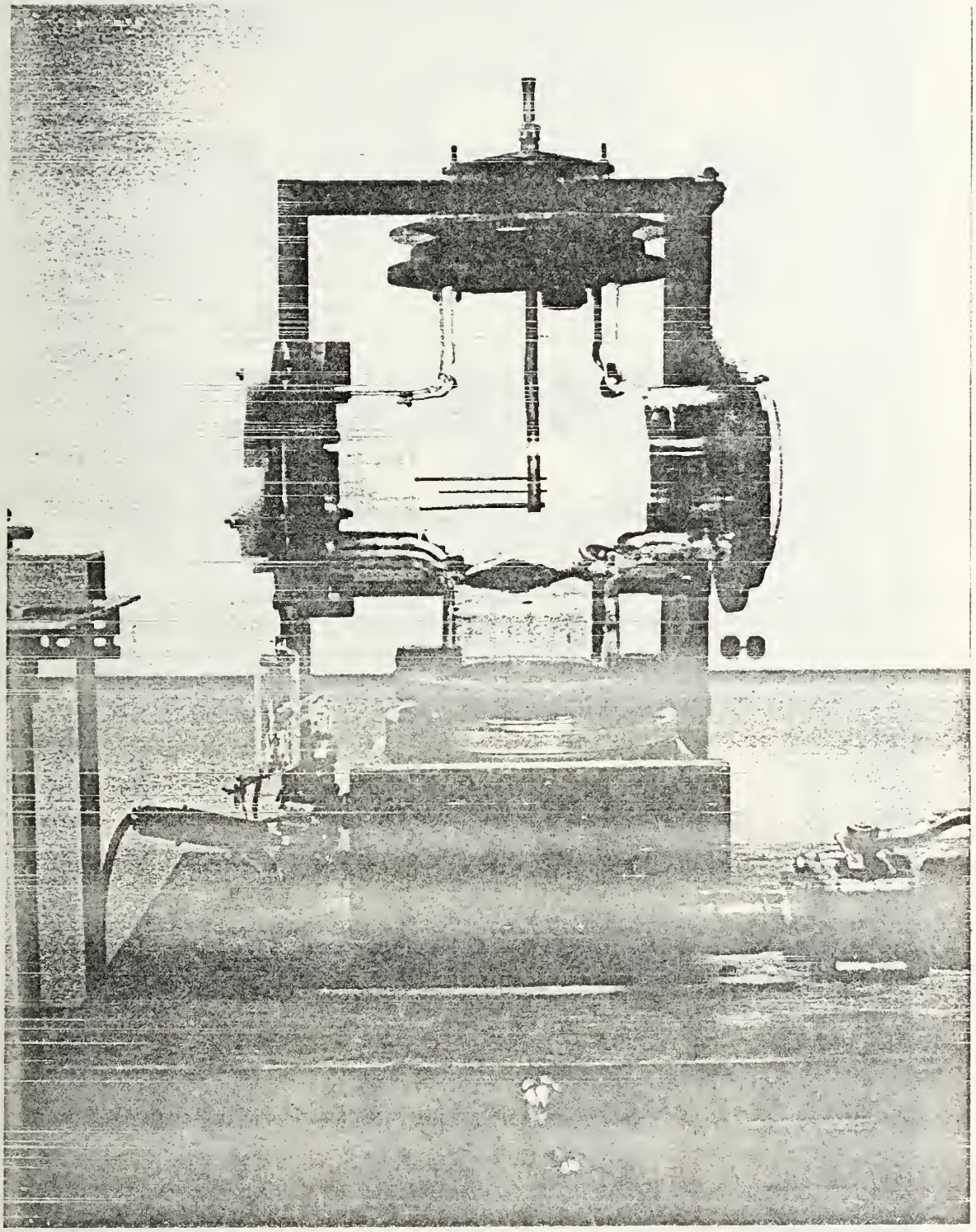

FIGURE 2.4: VACUUM CHAMBER WITH BARREL ASSEMBLY INSTALLED

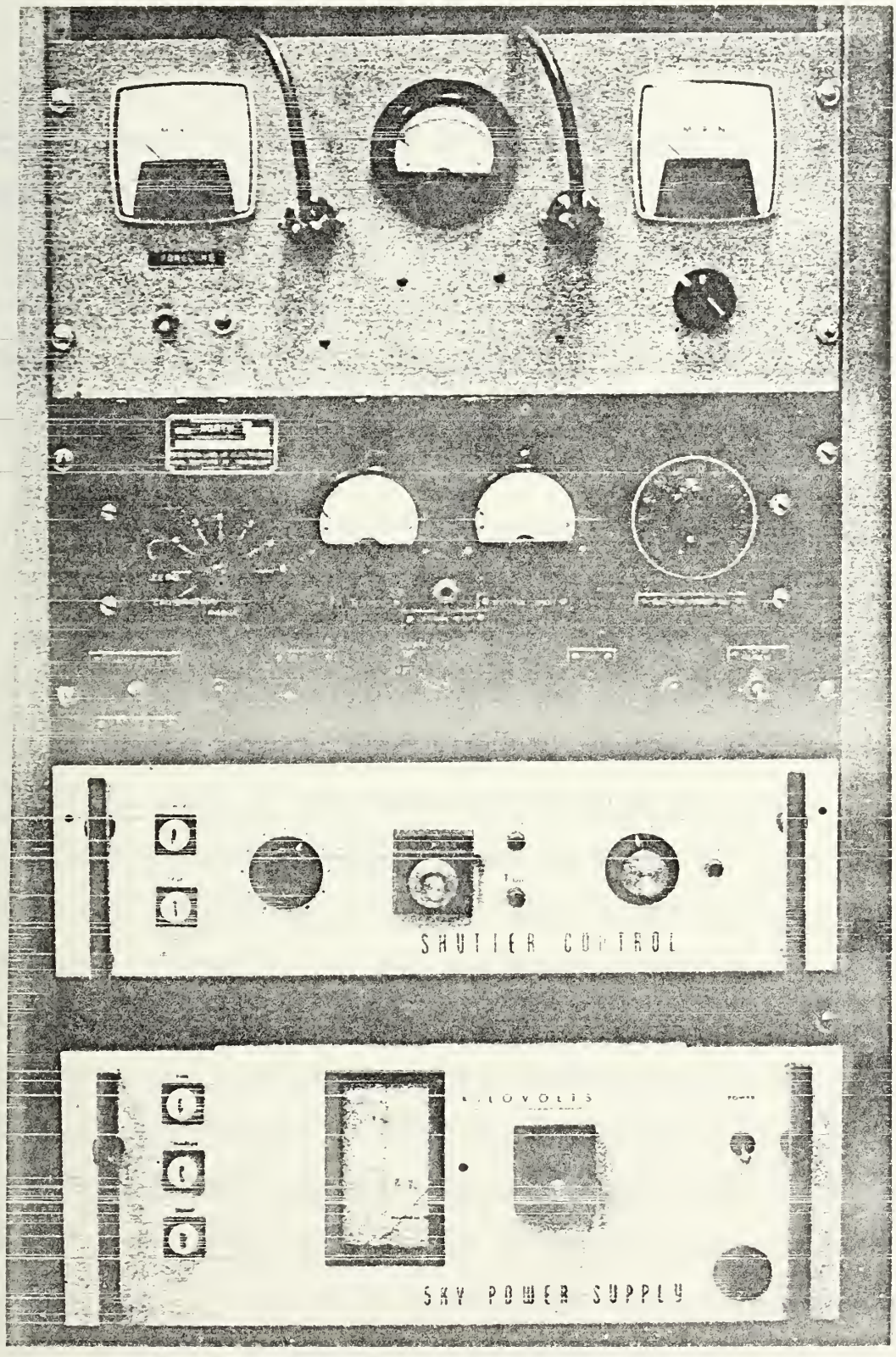

FIGURE 2.5: LASER POWER SUPPLY AND VACUUM GAUGE CONTROL PANEL

fitting soldered into the top plate on a brass bellows, which is, in turn, bolted (with an O-ring) onto the top plate of the vacuum chamber. This bellows arrangement makes barrel adjustments possible in all directions. The top of the tube is sealed with a rubber stopper, while the bottom holds the two barrels, one soldered above the other (a third stainless steel barrel was soldered in but not used). The barrels, used one at a time, serve three purposes: 1) they hold a pellet in position until the laser can be fired at it, 2) they confine (hopefully) most of the ablative gases behind the pellet, and 3) they guide the pellet during its acceleration and give it a straight trajectory. The stainless steel barrel is a 4 5/8 in. (117 mm) long tube, with an O.D. of 3/16 in. (4.8 mm), and an I.D. of 63 mils (.063 in., which equals 1.60 mm). The "muzzle" end has an opening 121 mils (3.1 mm) in diameter, which tapers in 3/4 in. to the I.D. of the bore. The copper barrel is 4 7/8 in. (124 mm) long, with an O.D. of 1/8 in. (3.2 mm), and a bore diameter of 66 mils (1.68 mm). Its muzzle is also enlarged to the same dimensions as the stainless steel barrel, to enable more of the laser beam to be channeled into the bore. The barrels may be selectively used by simply raising or lowering the support tube through the Cajon fitting. They can then be aligned with the laser by means of three adjustment screws on the bellows. The reasons for using two barrels is to examine the effect of bore diameter and bore material (copper has a reflectivity of 0.63, while stainless steel is only 0.55 [21]) on pellet velocity.

2.5 VELOCITY DIAGNOSTIC SYSTEM

In order to obtain a simple and reasonably accurate measurement of pellet velocities after they have been accelerated through the barrel, the technique of stroboscopic photography was used. For this purpose, the following equipment was acquired:

1. Model 100 Polaroid Land Camera, Close-up Kit, and laser filter
2. photodiode, and associated circuitry
3. adjustable time delay
4. double-flash stroboscopic light source

The light source is a Type 2307 Double Flashlight Source manufactured by Edgerton, Germeshausen and Grier, Inc. Its designer, Professor Emeritus Harold E. Edgerton of MIT (the inventor of xenon strobe lamps, and a pioneer in that field), was kind enough to loan it out. It is a device designed to measure the velocity of fast moving phenomena by taking two pictures, separated by a known time interval, on a single photograph. A variable time interval, τ_i, between exposures of 5-100 μsec is set by means of a dial on the rear panel (Figure 2.6). The light source is positioned so that it looks across the vacuum chamber at the barrel from one side, and is focused on the aperture of the camera, which is situated on the other side of the vacuum chamber. The camera is, then, focused on the subject (the barrel muzzle and the emerging pellets), using the Close-up Kit and a ruby filter to shield out the glare from the laser. In this fashion, one can get double-exposure silhoutte photographs of the pellets after they have

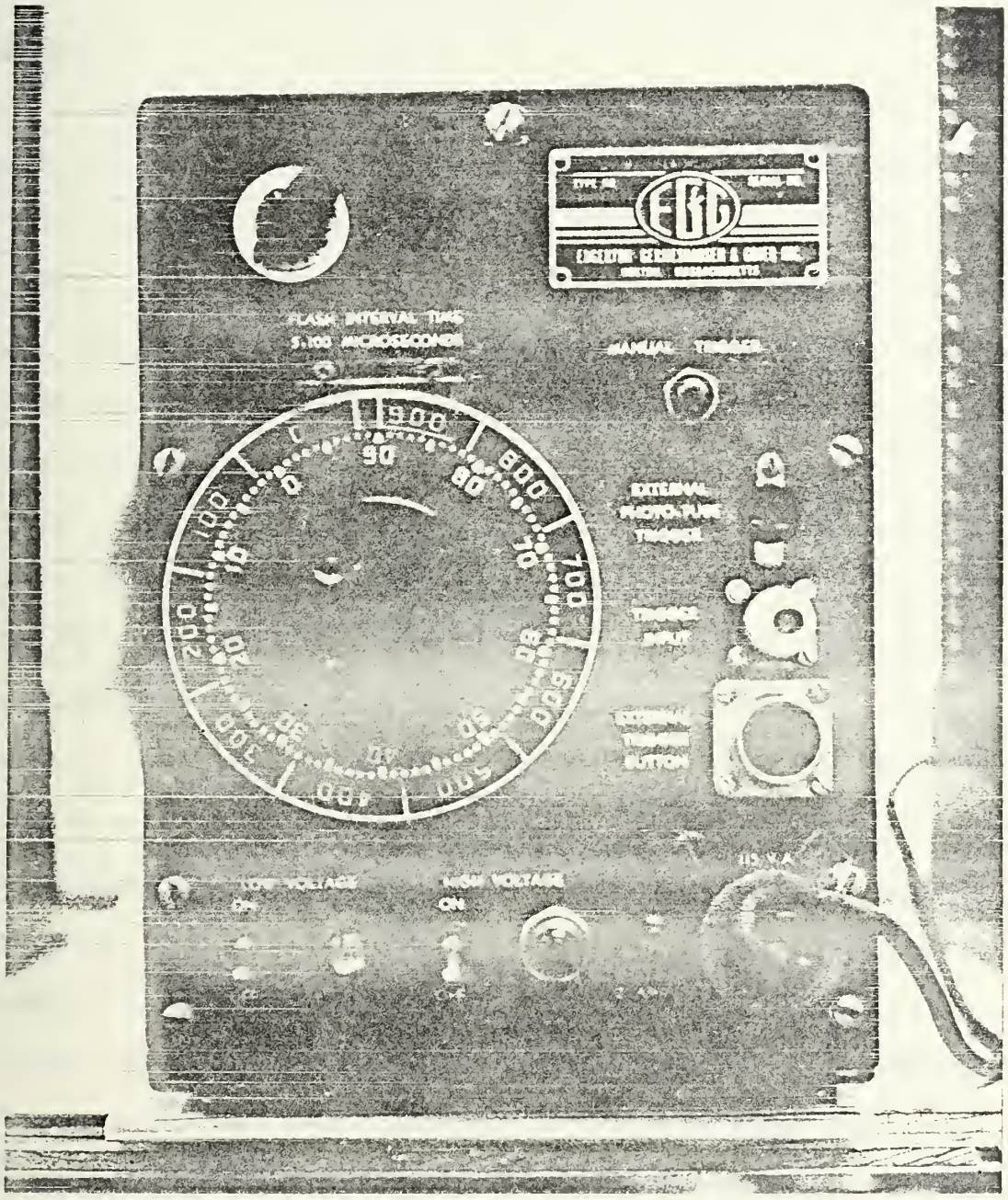

FIGURE 2.6: E.G.G. DOUBLE FLASHLIGHT SOURCE, REAR PANEL

left the muzzle by darkening the room, and manually holding the camera shutter open during the entire pellet firing sequence.

In order to catch the pellets in flight after they leave the muzzle, but before they have escaped the camera's field of view, an adjustable time delay is needed. The laser does not actually commence lasing until several hundred μsec after the xenon flash lamp has begun to fire (this time delay varies from shot to shot). The time delay, then, should not begin running until lasing commences (and pellet acceleration begins). To accomplish this, a United Detector Technology PIN-10 diode was fastened to the front of the light source lens, looking into the light source chassis (due to its high sensativity, the diode must not look directly at the laser). In this position, the diode can detect the laser the instant that it begins to lase, and also monitor the time interval between strobe flashes. A current amplification circuit (Figure 2.7) was built to boost the diode's output for display on an oscilloscope. A Tektronix Model 7633 Storage Oscilloscope provides a visual display of the laser pulse shape from the amplified diode output, and also features adjustable time delay circuitry. The scope output is connected to the external trigger on the rear panel of the light source.

To summerize the sequence of events: 1) the capacitor bank discharges, and the xenon flash lamp fires, 2) the laser commences to lase, and is detected by the diode, 3) the diode begins sending a signal, which is amplified, to the oscillo-

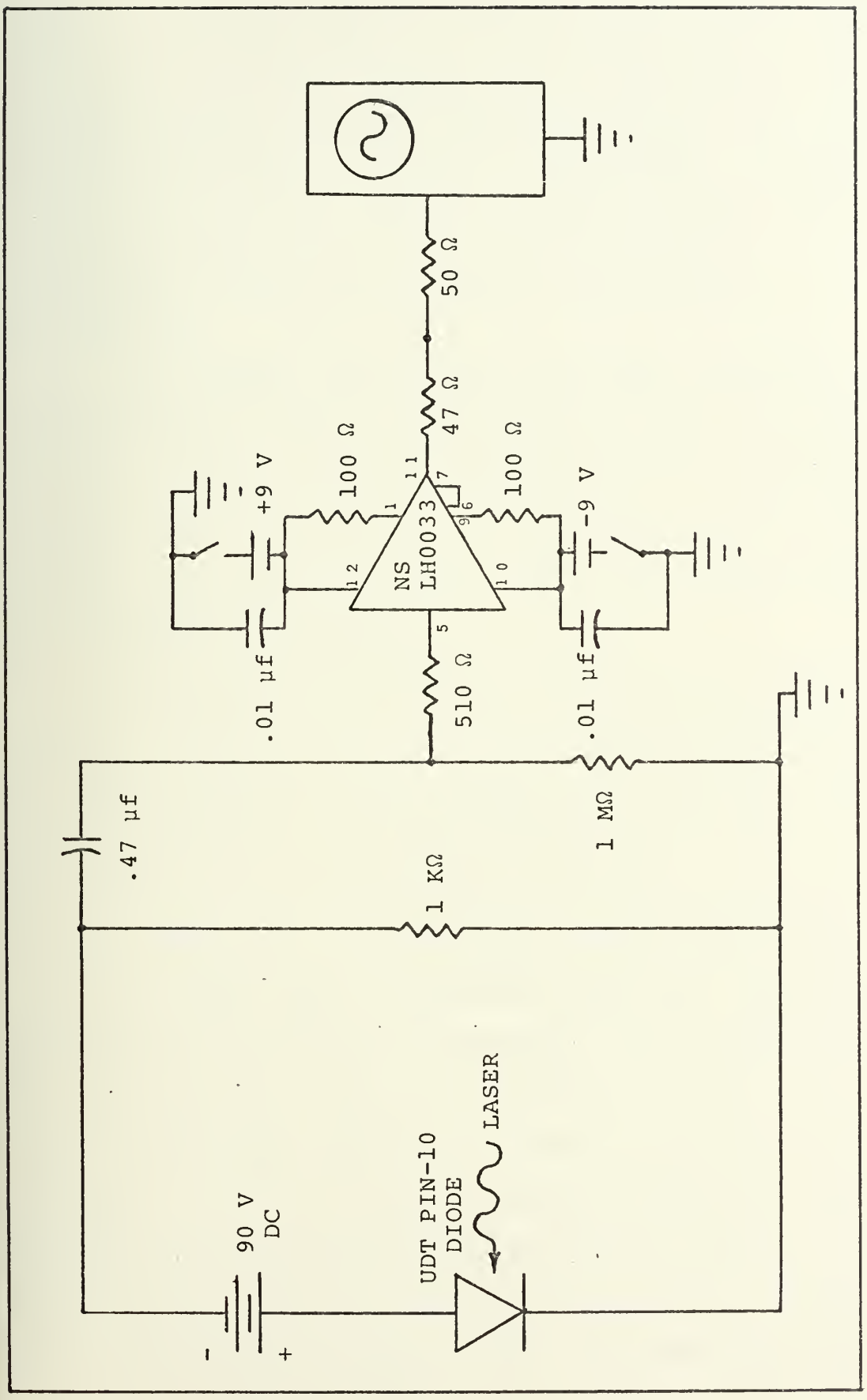

FIGURE 2.7: PHOTODIODE CURRENT AMPLIFIER

scope, 4) the diode signal triggers the oscilloscope, and starts the time delay running, and 5) after τ_b μsec, the oscilloscope triggers the Double Flashlight Source, which illuminates the pellets in flight on a photograph. The camera shutter is opened just before the laser is fired, and not closed until after the light source has flashed.

2.6 PELLETS

The pellets used in this experiment are black cellulose triacetate spheres, approximately 60 mils (1.5 mm) in diameter. Several thousand were purchased from the Allen Field Company, Inc. of New York City. Their shape and mass vary somewhat; see Figures 2.8 and 2.9 for their diameter and mass distributions respectively.

Cellulose triacetate is a member of the cellulosic group of plastics made by treating cellulose with acetic acid and acetic anhydride in the presence of a catalyst [22]. Since plastic properties can be controlled by the amount and type of plasticizer (e.g., abietic acid, $C_{19}H_{29}COOH$, and its derivatives) added, the cellulose ester plastics can be produced with a very wide range of physical properties. The physical properties are catagorized according to flow temperature (or flow designation), which is an indication of the amount and type of plasticizer added. In our case, a plastic with a flow designation of H3 was used to fabricate spherical pellets in a centerless stone grinding process [23,24]. Table 2.1 shows some selected physical properties of cellulose triacetate with a flow designation of H3 [25]. Cellulose ester plastics

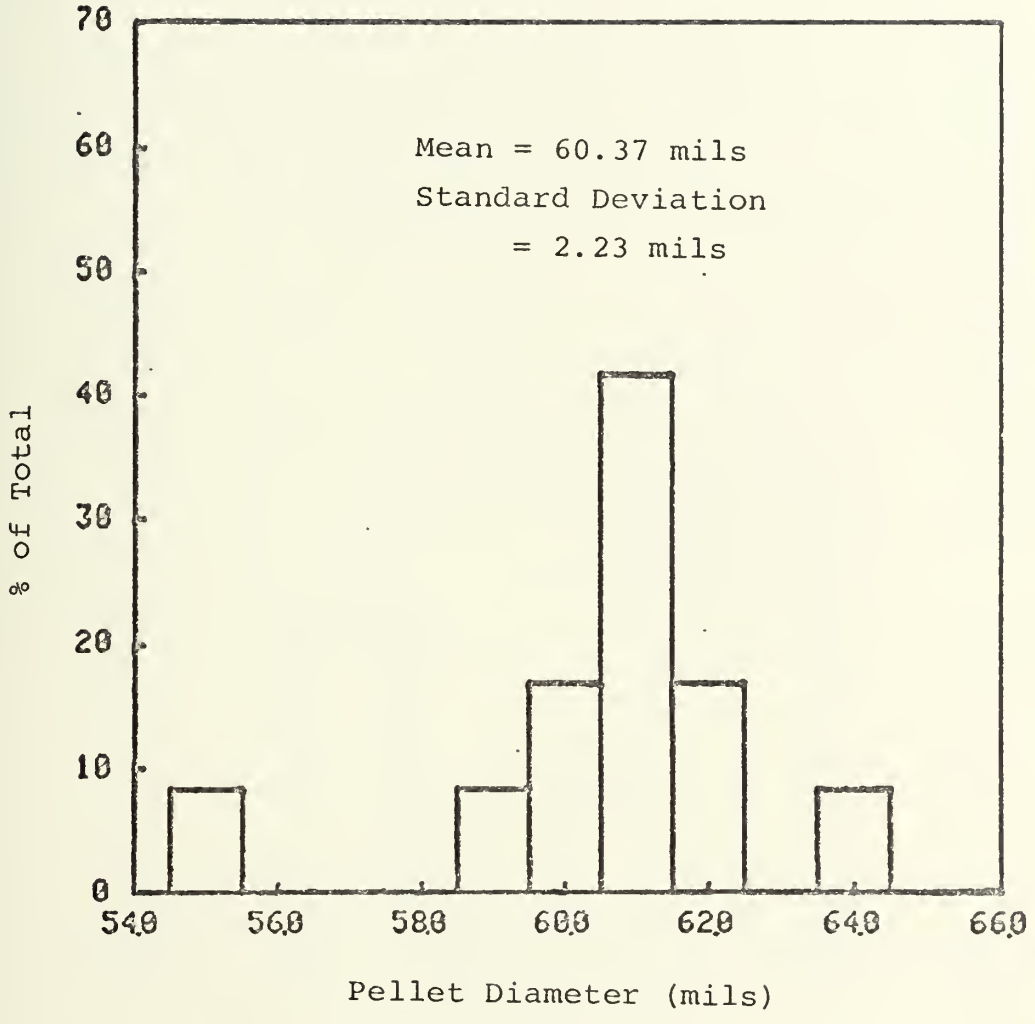

FIGURE 2.8: CELLULOSE TRIACETATE PELLET DIAMETER DISTRIBUTION

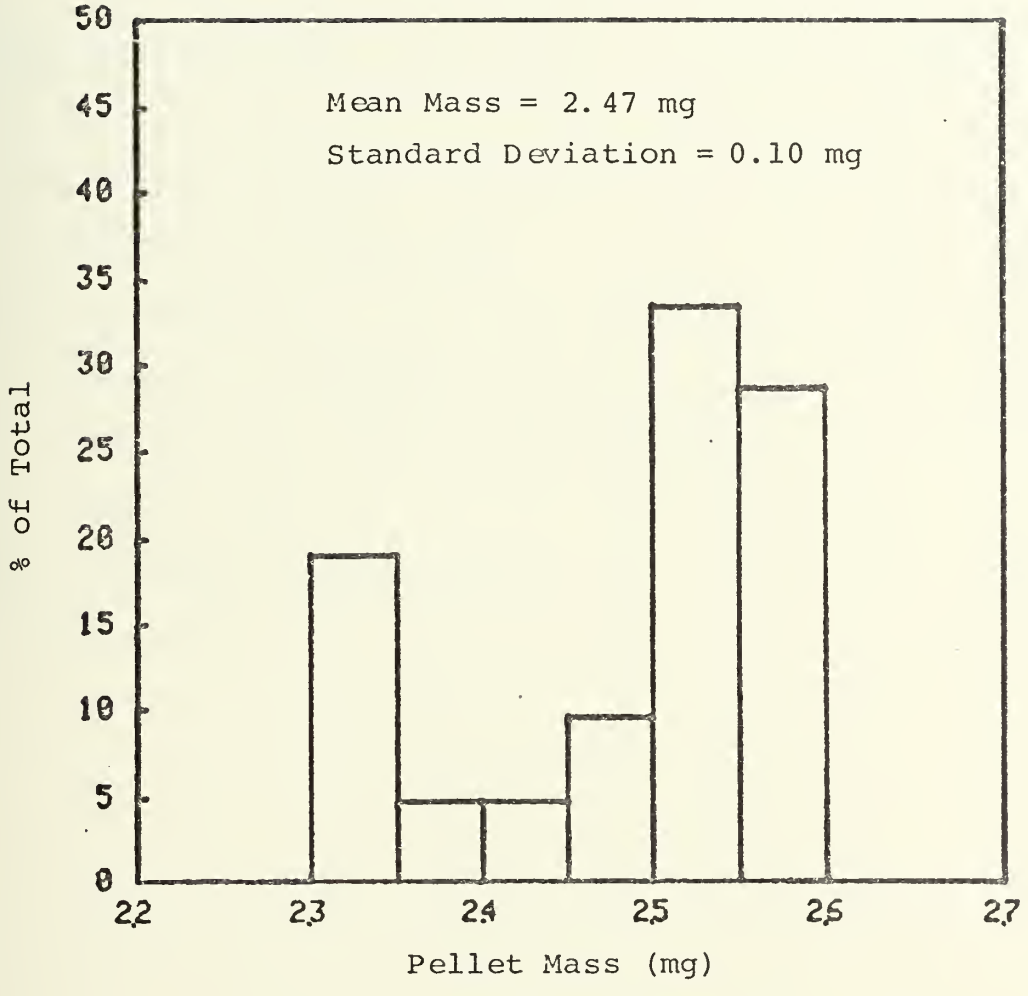

FIGURE 2.9: CELLULOSE TRIACETATE PELLET MASS DISTRIBUTION

TABLE 2.1

SELECTED PHYSICAL PROPERTIES OF CELLULOSE TRIACETATE

(Flow Designation H3)

[25]

Flow Temperature, ^{0}F (^{0}C)	329 (165)
Specific Gravity	1.29
Rockwell Hardness, R scale	94
Tensile Strength at Fracture, psi	5,200
Elongation at Fracture, %	28
Flexural Strength at Yield, psi	8,300
Deflection Temperature, 264 psi load, ^{0}F (^{0}C)	149 (65)
Deformation Under Load, %	15
Compressive Strength at Yield, psi	8,000
Specific Heat, cal/g	0.4

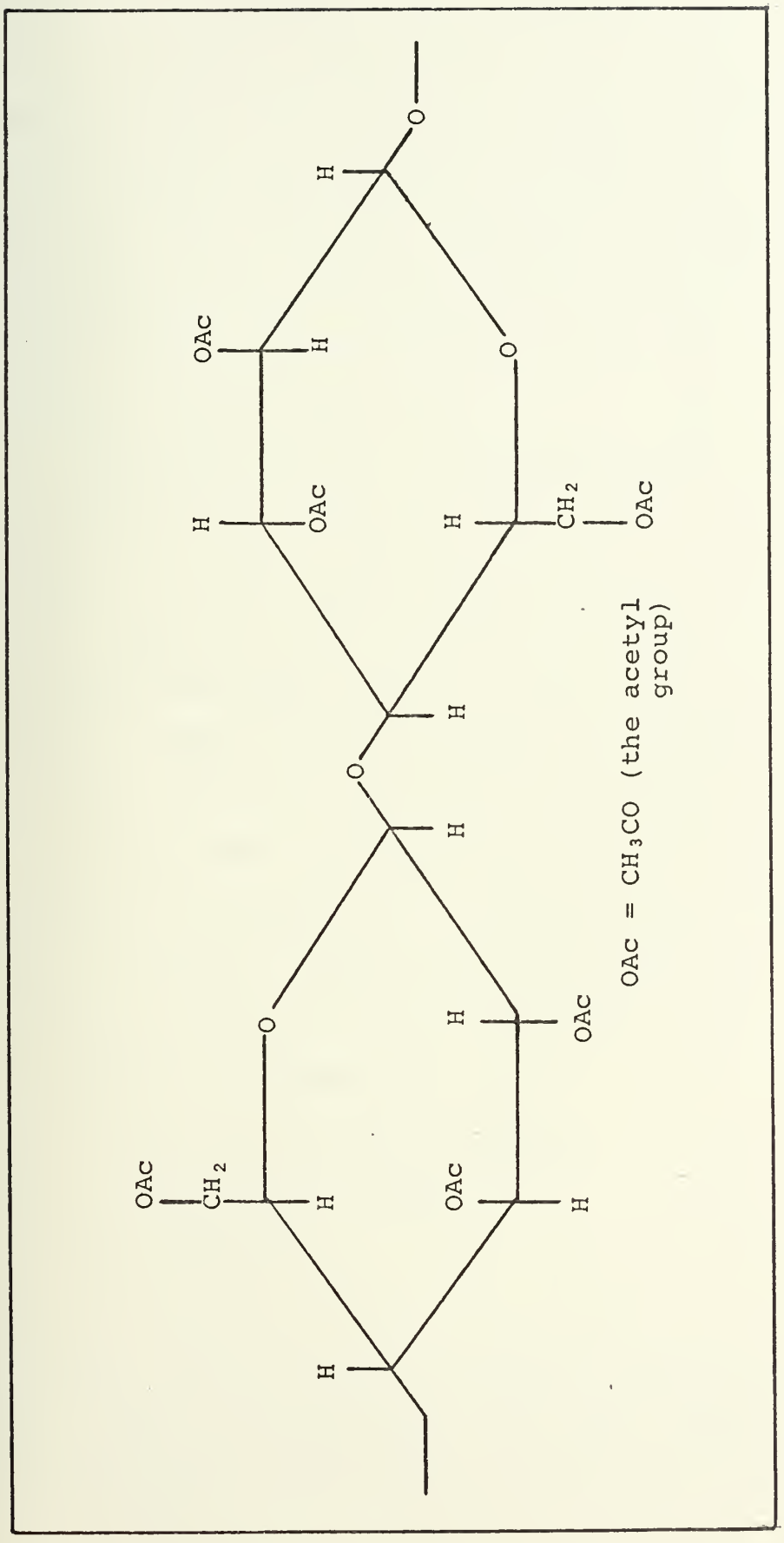

FIGURE 2.10: MER STRUCTURE OF CELLULOSE TRIACETATE

are among the toughest of the thermoplastics and have high impact resistance, meaning that they will absorb a large amount of mechanical energy with minimal structural damage. In this sense, these pellets do not serve as good models of solid DT, since the latter substance is comparatively brittle. Notice also, that cellulose triacetate possesses a tensile strength on the order of 100 times higher than that of solid deuterium (1 psi = 6900 N/m^2).

Beeswax pellets (at room temperature) have been used in an acceleration experiment very similar to this one, by Dimock et al. [26]. By spark induced evaporation of these pellets, they were able to achieve velocities of slightly over 100 m/sec. They claim beeswax to have "plastic" properties similar to those of solid hydrogen, although it is ten times more dense; cellulose triacetate is more dense by only a factor of six. When irradiated by a laser, they would resemble DT pellets in absorptivity of the beam better than black cellulose triacetate, although cellulose triacetate is also available in white and other transparent colors.

2.7 ACCESSORY EQUIPMENT

Accessory equipment includes:

1. helium-neon laser
2. thermopile
3. ramrod

A low power Model 133 Spectra Physics helium-neon (λ = .6428 μm) laser is used to:1) align the ruby laser cavity, 2) align the ruby laser beam with the bore of the barrel, and 3) find the

focal point of the 435 mm lens. To perform the latter two functions, a beam expander must be fitted into the helium-neon beam.

In order to measure ruby laser output energies, a Model 101 Control Data Ballistic Thermopile is placed in the beam's path. It furnishes an output voltage, which is proportional to the input radiant energy, to the input of an externally connected microvoltmeter. The calibration factor of this particular unit was 199 μV/J.

A 7 in. section of 35 mil stainless steel wire serves as a ramrod to push the pellets to a certain depth down the barrel, measured in millimeters from the muzzle opening inward. A microclip acts as an adjustable limiter on the ramrod to restrain it from pushing pellets beyond the desired depth.

2.8 SUMMARY

Thus, it is seen that the equipment and method of acceleration in this experiment are relatively simple. There should not be much difficulty with integrating several laser pellet injectors into a reactor design. Recall that for the 5000 Mw(t) tokamak mentioned in Section 1.2.2, the fueling requirement calculated was 85 one millimeter pellets injected per second. This would mean installing at least ten injection ports in the blanket surrounding the vacuum wall, with an injection rate of about two pellets per second per port. The ports and necessary laser equipment could be fitted in between the poloidal magnet structures around the outer toroidal perimeter of the reactor. An even better idea [27] is to situate

the laser-barrel assemblies away from the blanket, just outside of the magnet structures, and guide the accelerated pellets through the blanket and into the reactor vacuum chamber by means of evacuated drift tubes. This would alleviate the need for high energy resistant materials in the laser-barrel assemblies.

The best injection angle for the fuel pellets would be perpendicular to $\underline{B}$ (the shortest path into the plasma center). There should be no problems associated with particle drifts, such as there are with neutral beams injected at this angle [28], since the energy per particle in the pellets is so low.

The determining factors in choosing barrel materials are: 1) high energy flux resistance (especially if it has to be near the plasma), 2) high reflectivity of the particular laser radiation wavelength, 3) good resistance to cyclic laser loading, fatigue, erosion, and creep, and 4) good vacuum properties. Stainless steel looks good from all but the second viewpoint, although it may be acceptable. The refractory metals (molybdenum, niobium, vanadium, etc.) should also be considered. Some materials with high reflectivities, like copper, aluminum, and silver, would definitely not meet the other requirements stated above.

In terms of laser requirements, one would need: 1) a rapid sustained rate of fire (two shots per second or better), adequate reliability (at least as good as most of the other reactor components, and 3) reasonable efficiency. Both carbon

dioxide and neodymium glass lasers are likely candidates due to their relatively long operating lifetimes and fire rate capabilities. A satisfactory laser system should not require maintenance or replacement more often than the scheduled maintenance shutdown periods for the entire plant (four or five times a year).

Due to the complexity and rate at which the reactor plasma conditions fluctuate, the entire fueling operation will probably have to be computer monitored and controlled. The fueling rate through each injection port at any given moment, must conform exactly to the local plasma conditions in order to avoid quenching and creating instabilities.

CHAPTER III

EXPERIMENTAL PROCEDURE AND RESULTS

3.1 LASER CAVITY ALIGNMENT

The optical unit contains two elements which must be aligned with respect to the laser axis. These are the rear and output reflectors discussed in Section 2.2. The ruby rod, when lasing, emits plane polarized radiation. The plane of polarization is referred to as the "C" plane. The output reflector has a preferred plane of transmission, which can be determined by rotating the reflector under a polarizing sheet of plastic whose direction of polarization is known. In order to achieve maximum laser output, the output reflector must be rotated in its mount until its direction of polarization is parallel with the "C" plane of the rod marked on the laser housing.

The next task is to align both reflectors so that their faces are centered on the rod axis, and are perpendicular to it. To accomplish this, the rear reflector is removed, and the helium-neon laser is mounted and aligned behind the ruby cavity so that the beam is colinear with the ruby rod axis. Colinearity can be achieved by adjusting the helium-neon beam until it is centered on the rod cross section, and the beam reflection from the rod face returns to the beam origin. The adjustment screws on the output reflector mount are then used to return the beam reflection from the reflector face back on itself. Finally, the rear reflector can be replaced

in its mount and aligned in the same manner. The ruby laser is now ready to fire; the helium-neon laser should be left in place, since it will be needed to align the ruby laser beam with the bore of each barrel.

3.2 LASER-BARREL ALIGNMENT

The laser and the vacuum system were, unfortunately, built on two separate tables. This fact makes the process of aligning the laser beam with the longitudinal barrel axis a headache, to say the least. The helium-neon laser, with a beam expander attachment, is first adjusted so that its focal spot (through the lens) falls exactly on top of that of the ruby. Scrap pieces of Polaroid film work nicely for finding the ruby spot. Crude laser-barrel alignment can be accomplished by moving and shimming the tables relative to one another, and by adjusting the laser support platform legs. The bellows adjustment screws on the barrel assembly are then used to achieve final colinear alignment of the beam with the axis of the selected barrel's bore. The focusing lens mount should now be positioned along the rail so that the beam spot falls just inside the barrel breech opening.

This alignment is quite delicate and was difficult to maintain while running the experiment. The author would strongly suggest that all components in future devices of this sort be constructed on one solid structural foundation.

3.3 LASER OUTPUT ENERGY MEASUREMENT AND CALIBRATION

In order to determine the total ruby laser energy output per pulse as a function of power supply capacitor bank

voltage (CBV), thermopile measurements are taken at various bank voltages. The values graphed in the top curve of Figure 3.1 were obtained by placing the thermopile directly in the beam's path, without any windows or lenses to attenuate it. There is a good linear releationship between the CBV settings and the laser output for CBV's above 3.8 KV. Notice also, that there is a shot-to-shot variation in laser energy of less than 5% at each CBV setting.

The laser beam encounters several obstacles in its path before reaching its intended target (a pellet). These are, in order, the beam focusing lens, the vacuum chamber front window, and the mouth (or breech) of the barrel. Measurements are taken from behind each of these obstacles to find the degree of laser attenuation along the beam's path. These values are displayed in the remaining curves in Figure 3.1. Due to the linear relationship established by the first set of measurements, it was not deemed necessary to take more than one or two data points to determine the other curves. Upon transversing the focusing lens, the beam is attenuated ≃ 16%, and loses another ≃ 12% across the front window. The difference in reflectivities of machined stainless steel and copper is apparent; the energy drops another ≃ 54% in passing through the steel barrel, and only ≃ 45% more through the copper. Keep in mind that a pellet would receive more radiation (depending on its depth in the barrel) than would the thermopile sitting at the end of the muzzle. These figures could be improved somewhat by using a higher quality focusing lens, and barrel materials with better

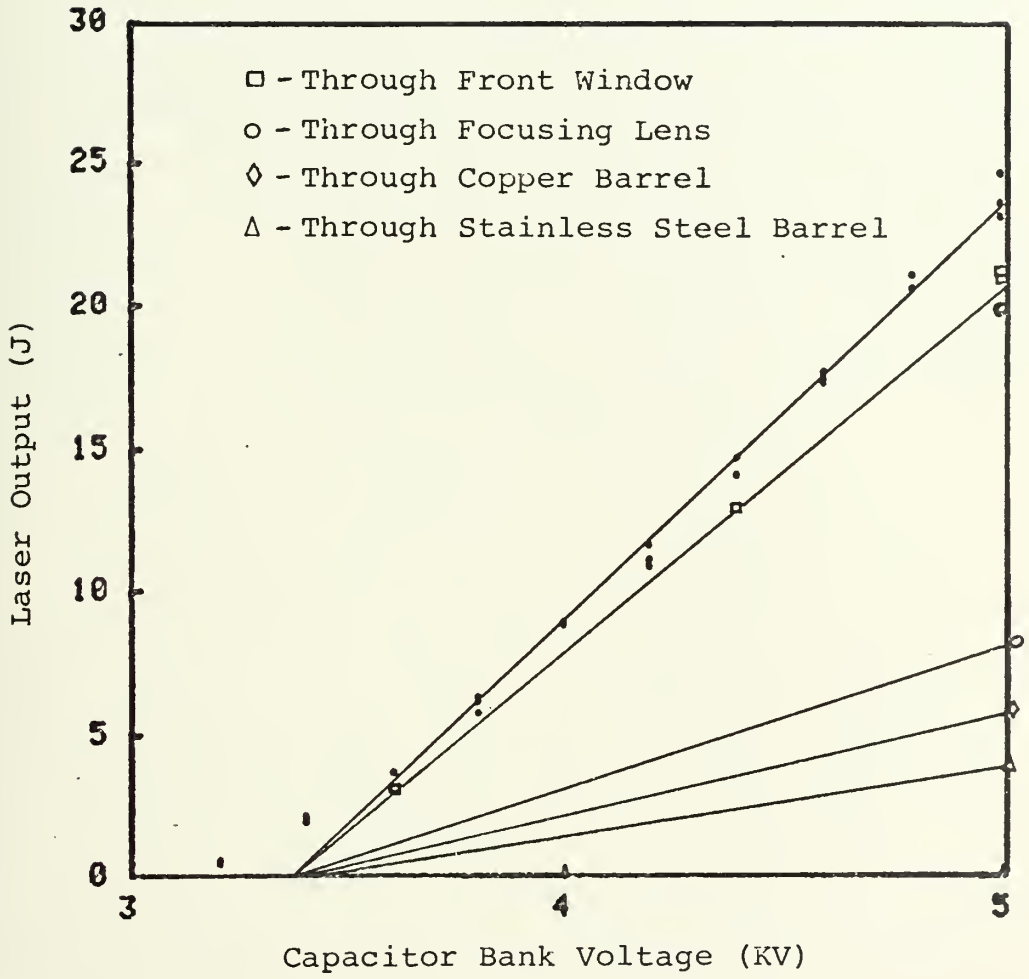

FIGURE 3.1: LASER OUTPUT AS A FUNCTION OF CAPACITOR BANK VOLTAGE

reflectivities.

3.4 LASER PULSE SHAPE MEASUREMENT

To determine the time history of the ruby laser pulse, the photodiode and its amplifier circuit (described in Section 2.5) are situated at a place in the room where the diode can still detect the laser, but not be overloaded. Figure 3.2 is a photograph of the laser's oscilloscope trace with a CBV setting of 3.5 KV, which corresponds to a laser output of ≈ 2.5 J. The trace was triggered at the instant that voltage was applied to the xenon flash lamp. Notice that lasing does not commence until 600-800 μsec after the flash lamp begins to fire. As stated earlier, this delay seems to vary randomly within that range of time. The actual laser pulse length is 800-900 μsec long; it also varies slightly from shot to shot.

3.5 STROBE INTERVAL MEASUREMENT

A large part of the velocity measurement accuracy depends upon how well the time interval between flashes (and photograph exposures) can be known. To determine the shot-to-shot reproducability of this interval, τ_i, for a particular dial setting, the photodiode may again be used. By mounting it on the front lens face of the Double Flashlight Source, it is possible to monitor τ_i on the oscilloscope over several trials. It was discovered that the dial readings for τ_i are not completely accurate; the actual intervals are generally 10% longer than the dial would indicate. Figure 3.3 a) shows the actual interval between flashes for seven shots with a dial setting of 100 μsec. There is a maximum shot-to-shot

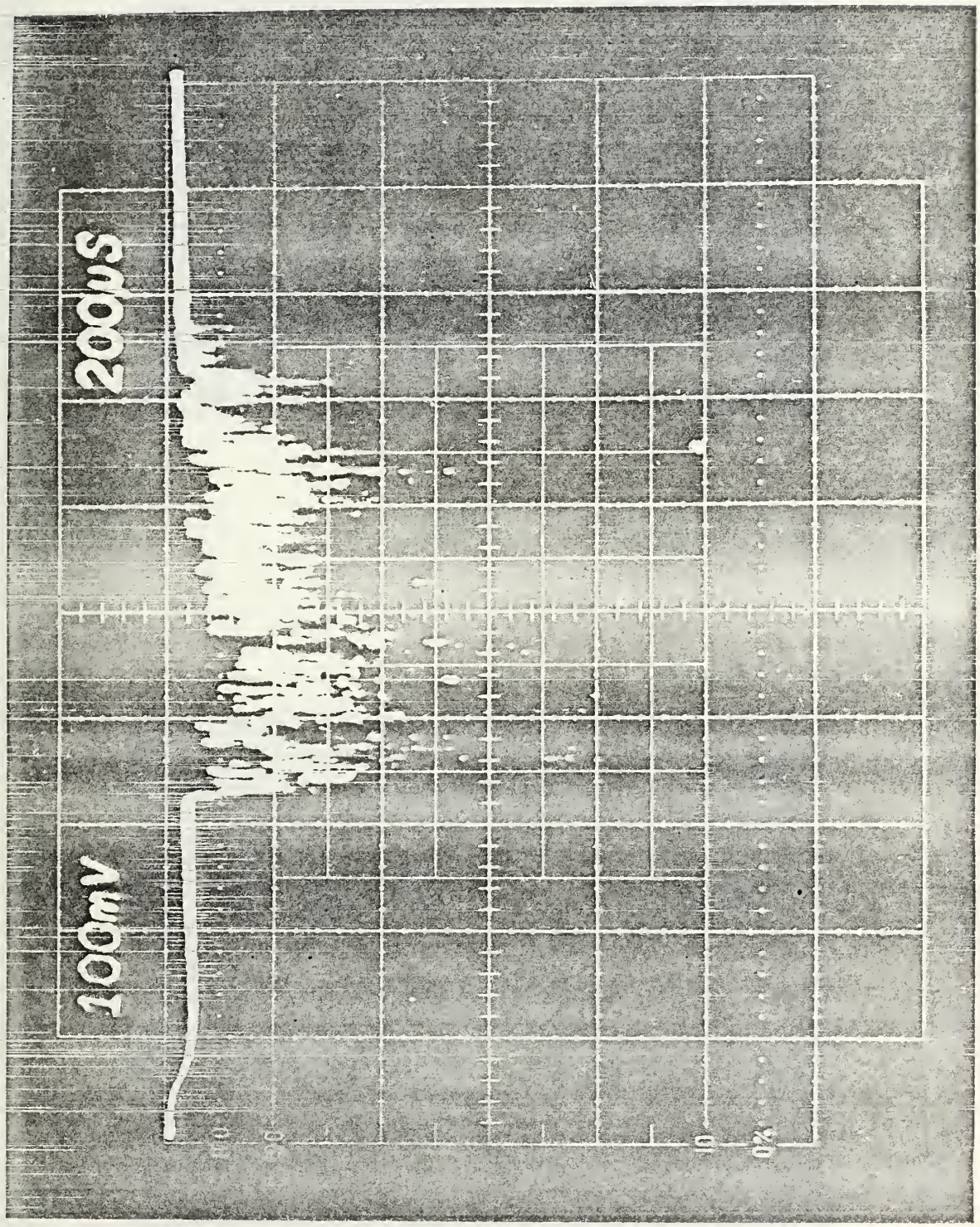

FIGURE 3.2: LASER PULSE SHAPE

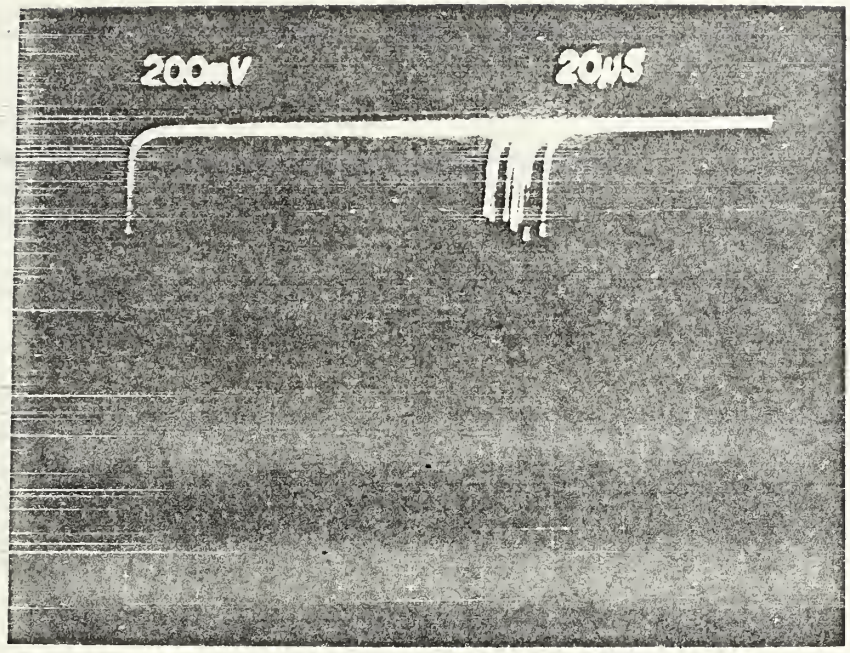

(a)

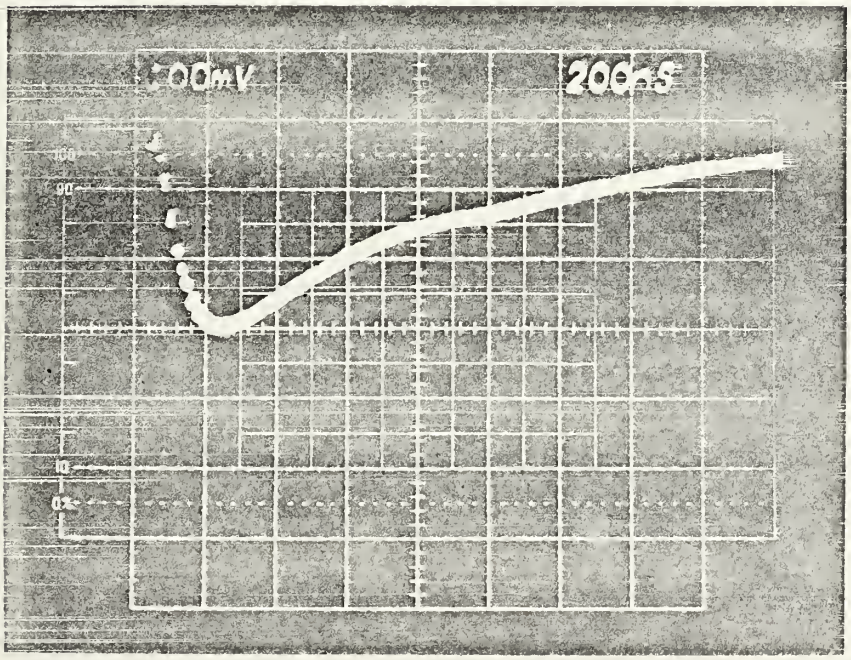

(b)

FIGURE 3.3: STROBE FLASH INTERVAL VARIATION (a) AND PULSE SHAPE (b)

interval variation of ≃ +20%. Each flash lasts for only ≃ 1 μsec (Figure 3.3 b)).

3.6 PELLET FIRING AND VELOCITY MEASUREMENT

3.6.1 PROCEDURE

The parameters that were varied during the experiment are:

1. barrel depth (s = 5 to 95 mm, in steps of 10 mm)
2. vacuum chamber pressure (either atmospheric, or ≃ 10^{-4} torr)
3. barrels (either stainless steel, or copper)
4. laser power supply voltage (CBV = 3.8 to 5.0 KV, in steps of 0.3 KV)

In order to measure pellet velocities, a scale reference between the actual distance and the distances traveled by pellets in the photographs is needed. For this purpose, a steel rule was held up to the barrel with one end flush against the muzzle and photographed (Figure 3.4). This scale factor was found to be 1.80 to 1.

The first step is to select a barrel, align it with the laser beam, and arrange the velocity diagnostic equipment as described in Section 2.5. The camera was fitted with Close-up lens No. 3; the focus was set at 3.5 ft. and the f stop at 13. The pellets can then be loaded by hand, one at a time, into the muzzle of the appropriate barrel, and pushed down the bore a predetermined distance (referred to as barrel depth, s) with the wire ramrod. If a shot in vacuum is desired, the rear end plate of the vacuum chamber must be placed over the rear opening

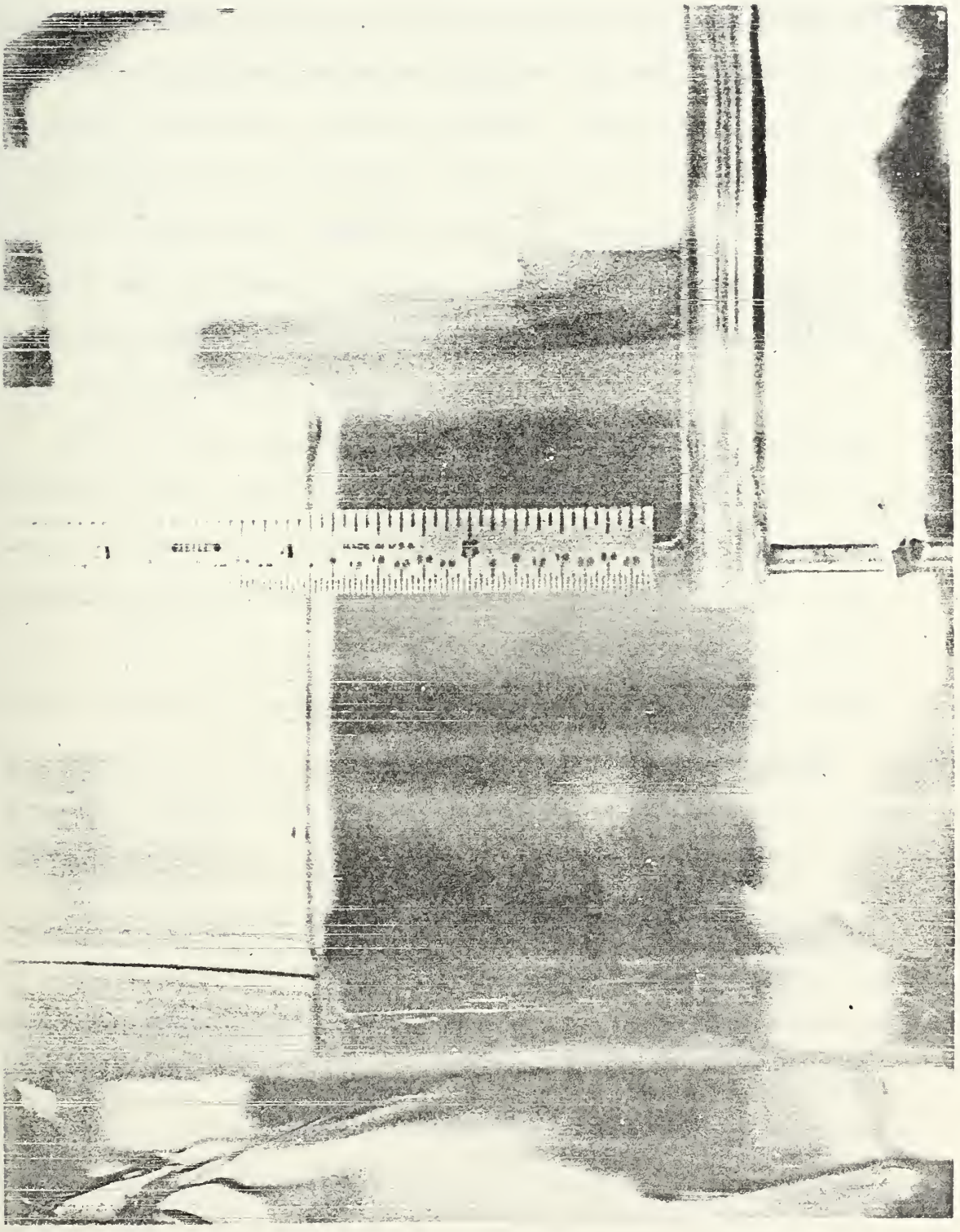

FIGURE 3.4: PELLET PHOTOGRAPH SCALE REFERENCE

(enlarged)

to seal it. With the gate valve closed and the bypass valve opened, the mechanical pump is started. When the chamber pressure drops below 100 mtorr on the system thermocouple gauge, the diffusion pump may also be started (do not forget to turn on the pump and baffle cooling system). After the diffusion pump has warmed up, the bypass valve can be closed and the gate valve opened. The chamber pressure should drop to 100 μtorr within fifteen to twenty minutes. At this pressure the aerodynamic drag force on a pellet can be considered negligible, and the accelerator is ready to fire.

The firing sequence begins with darkening the room and charging the laser power supply. When the selected voltage has been reached, the laser fire button will be illuminated. The camera operator will then manually open the shutter, and the laser operator fires the laser. The pellet will be accelerated, and after a preset delay time, τ_b, the Double Flashlight Source will fire, illuminating the pellets on film. Finally, the camera shutter may be closed and the room lights turned back on.

Estimating the proper delay time setting involves a bit of guess work and luck; not every shot could be recorded on film. The best guideline to follow is the pellet's initial barrel depth. The deeper the pellet is pushed into the bore, the longer it takes to emerge from the muzzle. At atmospheric pressure, the pellets were caught and recovered by a plastic bag draped over the rear opening of the vacuum chamber. In vacuum, they were retrieved by stretching a piece of double-stick masking tape across the pellet's trajectory in the

chamber. Pellets would usually pass through the tape, bounce off of the rear end plate, and stick to the back of the tape. When firing the accelerator, eye protection must be worn by all personnel due to the high intensity level of the ruby laser radiation.

3.6.2 DATA COLLECTION

The first series of shots (Numbers 1-49) were taken through the stainless steel barrel at atmospheric pressure, with the laser operating at full power (5.0 KV, 4.4 J through the bore). These shots were begun at a barrel depth of 5 mm and continued to 95 mm, taking at least two or three shots at each depth to establish the degree of velocity variation. All data can be found in Table A.2 of the Appendix. Figure 3.5 is a velocity vs. barrel depth plot of the first day's run (Numbers 1-36), and Figure 3.6 shows two separate runs from the second day's work (Numbers 37-44, and 45-49). Only one of these shots was taken under vacuum conditions (Number 35). A typical pellet photograph can be seen in Figure 3.7.

The next series of shots (Numbers 50-92) were fired through the copper barrel. In an effort to improve upon the pellet velocities measured in the previous series, the front vacuum window was removed to maximize the amount of laser energy through the barrel (now ≈ 8.0 J). Shot Numbers 51-54 were made at atmospheric pressure at this maximum laser energy. To study the effect of added mass, the front window was replaced, and two pellets at a time were loaded and fired from various barrel depths at atmospheric pressure (Numbers 55-59). The

laser energy through the barrel at that time was ≈ 6.6 J. A typical double-pellet photograph is shown in Figure 3.9..

The next two runs of this series were performed to determine the difference between pellet velocities in air, and in vacuum. Shot Numbers 60-70 were carried out at atmospheric pressure, while Numbers 71-80 took place under 100 μtorr of vacuum. Once again, the laser energy through the barrel was ≈ 6.6 J. Figures 3.11 and 3.12 contain plots of velocity vs. barrel depth under atmospheric and vacuum conditions respectively. To learn how pellet velocity behaves as the laser energy is systematically varied, Shot Numbers 81-85 were taken (in air) at different laser power supply CBV settings. The initial pellet barrel depth was held constant at s = 55 mm. The laser energy through the barrel was measured after each shot. A plot of velocity vs. laser beam energy can be seen in Figure 3.13.

The final run of the series (Numbers 86-92) involved glueing two pellets together with Elmer's Glue-all and accelerating them in air from different barrel depths. This was done to again study the effect of increased mass. The glue was deemed necessary to hold the pellets together, since earlier two-pellet attempts resulted in the two pellets emerging from the muzzle at different times and with different velocities. The last shot (Number 92) contained four pellets glued together in a linear fashion. It was fired in air from a depth of 55 mm; the photograph appears in Figure 3.14 a). A velocity vs. barrel depth plot of this run is shown in Figure 3.15.

After each shot, the partially ablated pellet, providing

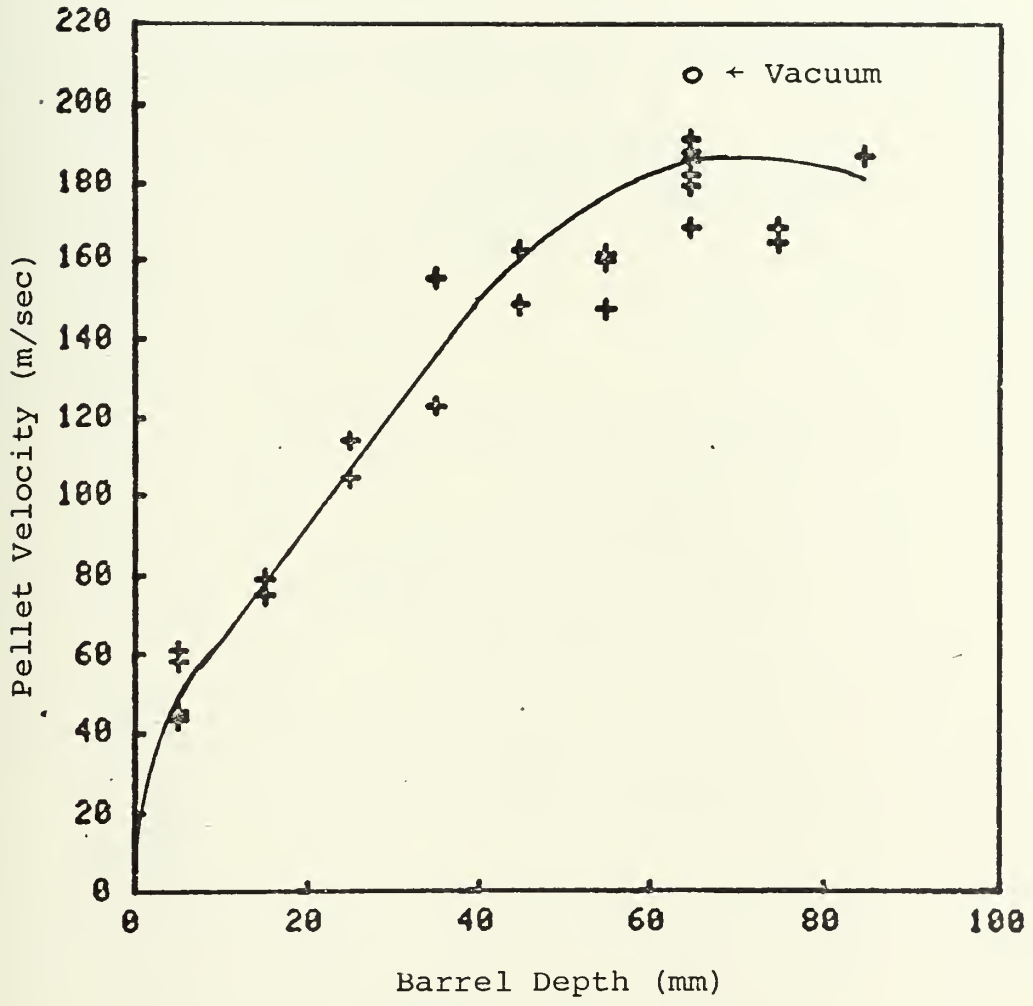

FIGURE 3.5: PELLET VELOCITY AS A FUNCTION OF BARREL DEPTH FOR SHOT NUMBERS 1-36 (Stainless Steel Barrel, Atmospheric Pressure, $E_l \simeq 4.4$ J)

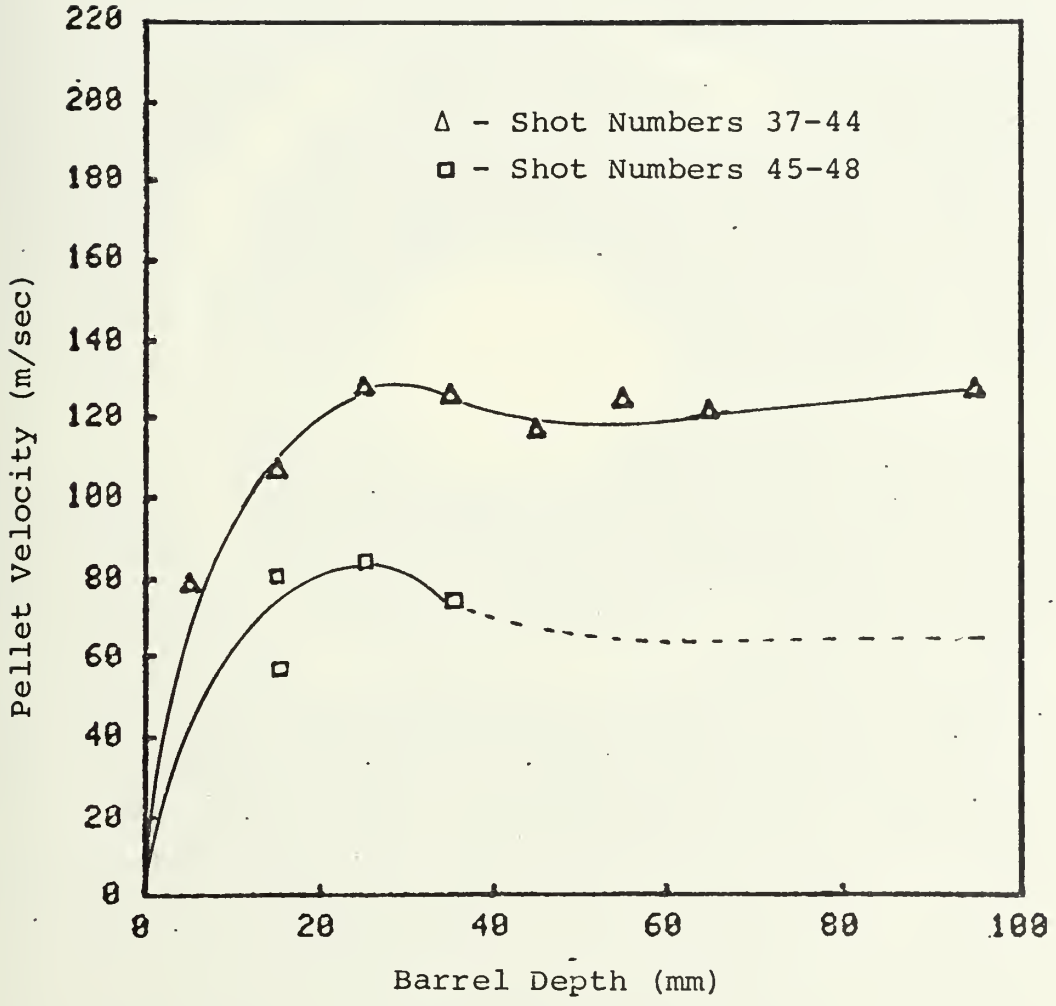

FIGURE 3.6: PELLET VELOCITY AS A FUNCTION OF BARREL DEPTH FOR SHOT NUMBERS 37-48 (Stainless Steel Barrel, Atmospheric Pressure, $E_l \simeq 4.4$ J)

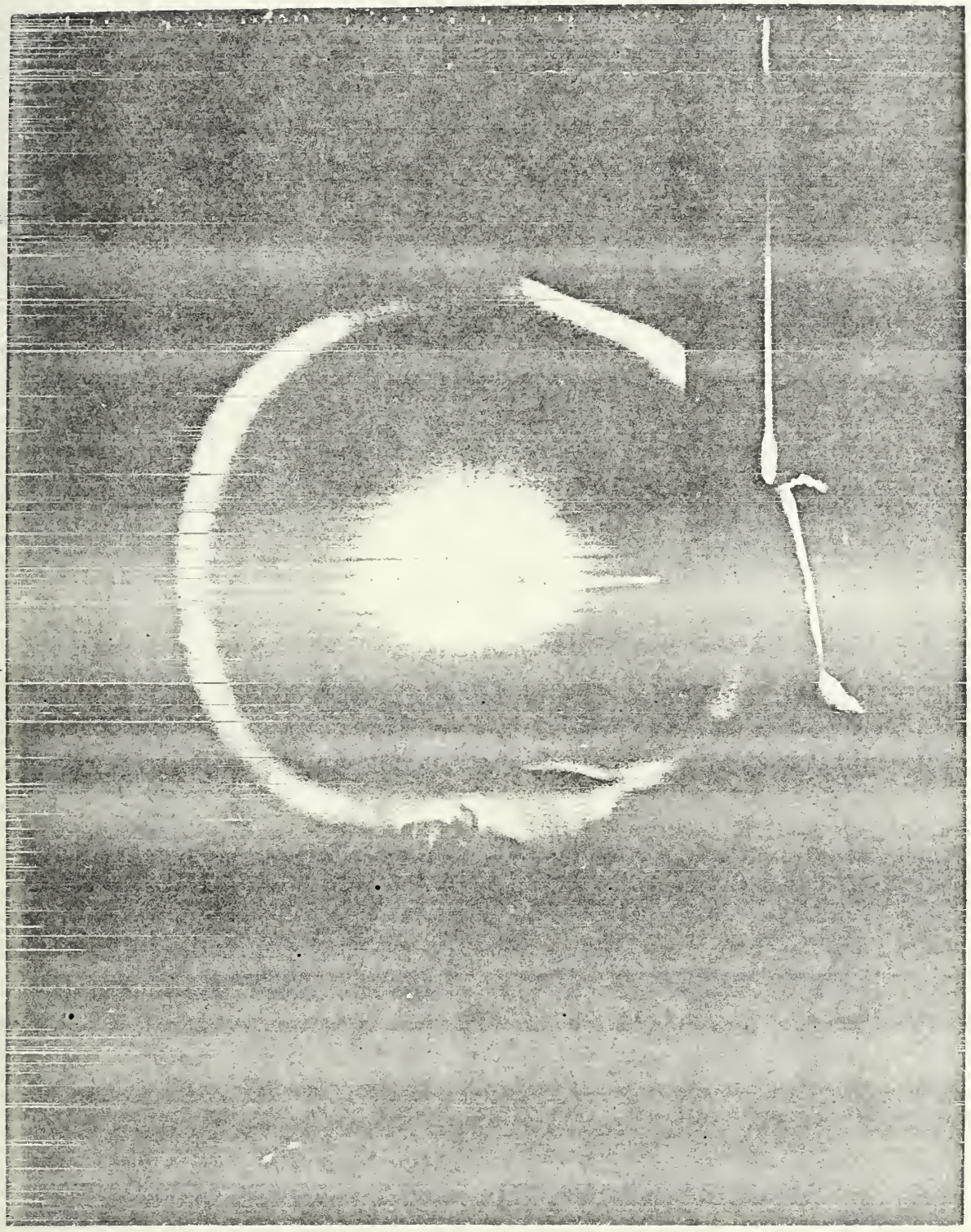

FIGURE 3.7: TYPICAL DOUBLE-EXPOSURE PELLET PHOTOGRAPH

(enlarged)

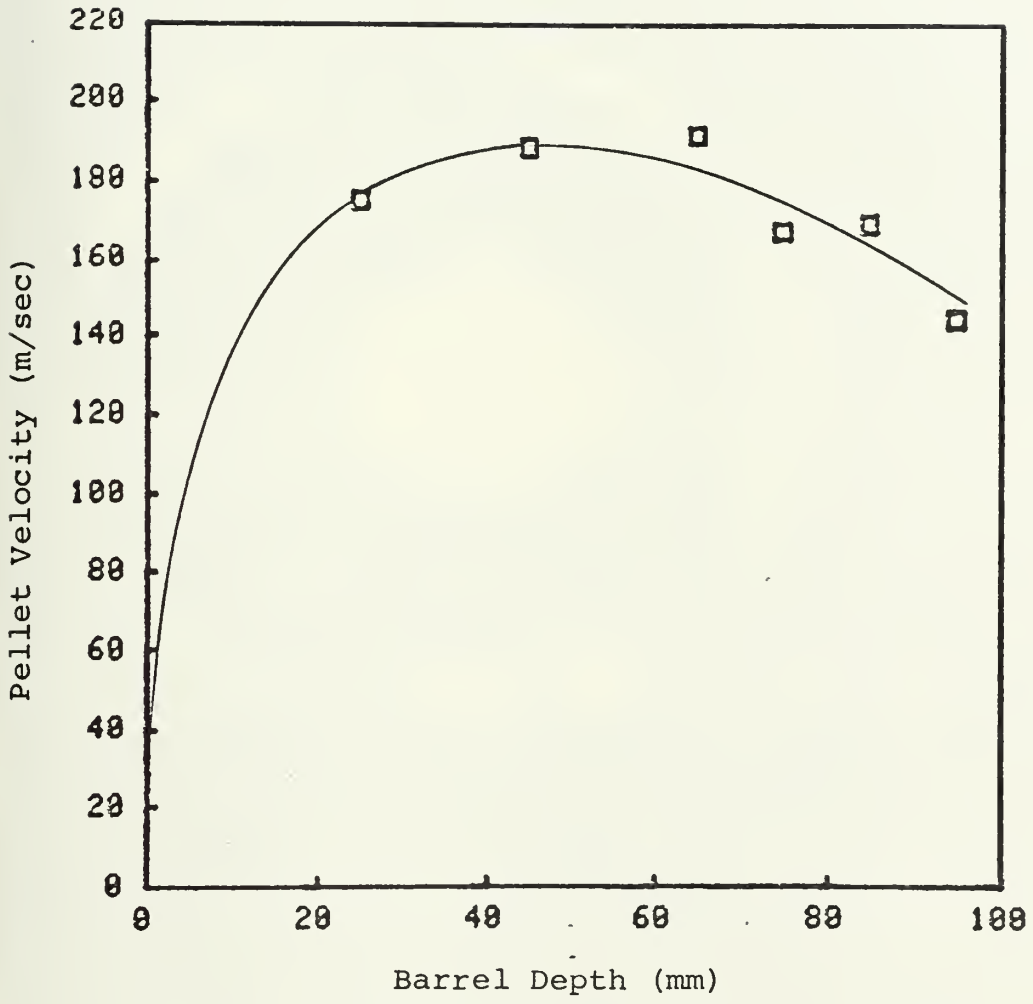

FIGURE 3.8: PELLET VELOCITY AS A FUNCTION OF BARREL DEPTH FOR SHOT NUMBERS 49-54 (Copper Barrel, Atmospheric Pressure, $E_l \simeq 8.0$ J)

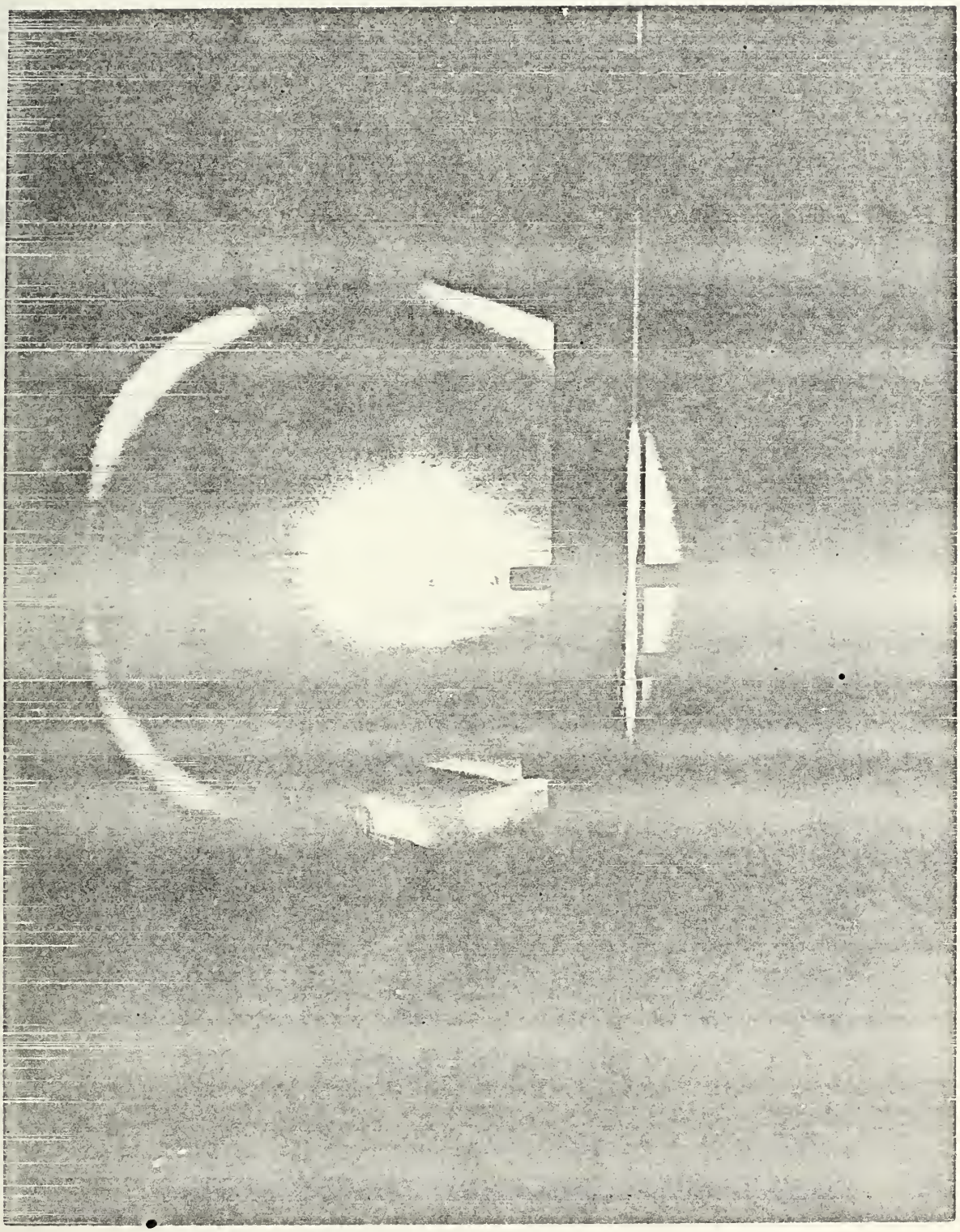

FIGURE 3.9: TYPICAL DOUBLE-EXPOSURE DOUBLE-PELLET PHOTOGRAPH (enlarged)

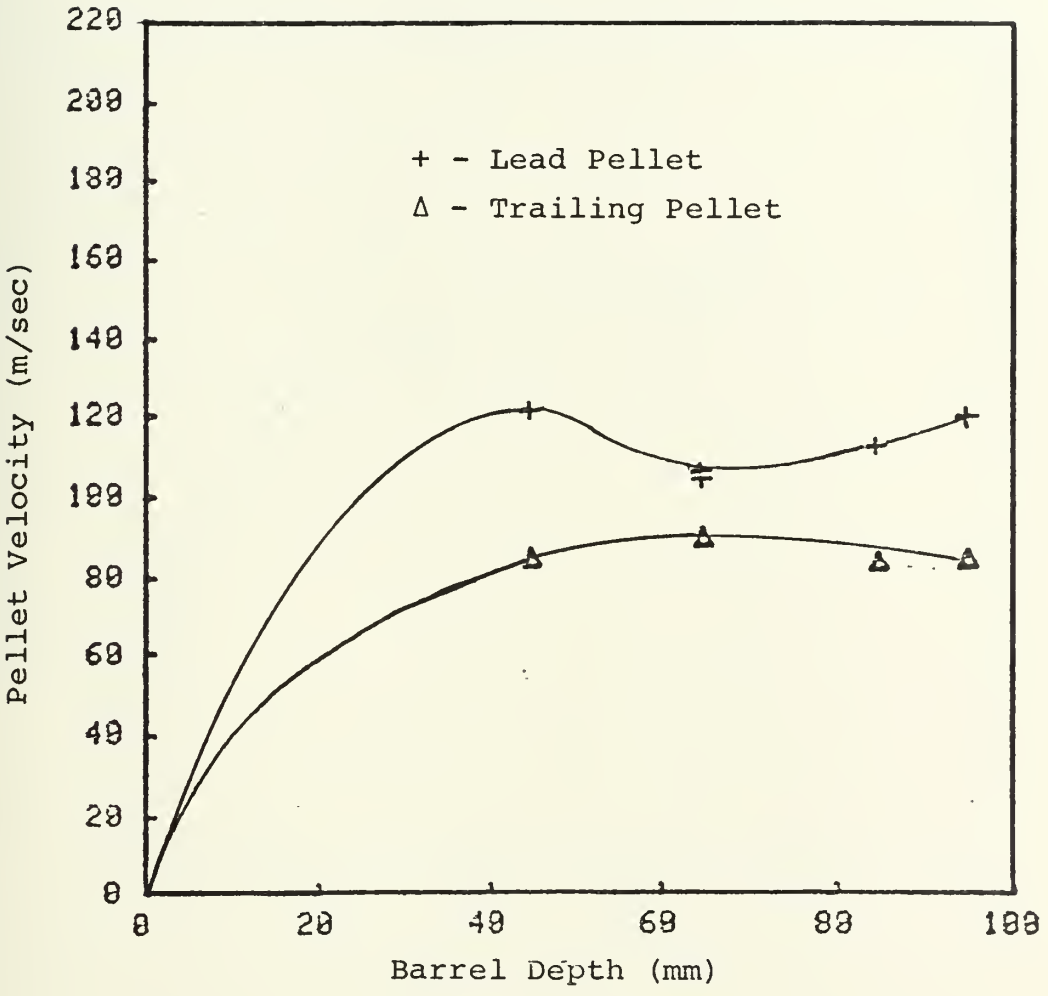

FIGURE 3.10: PELLET VELOCITY AS A FUNCTION OF BARREL DEPTH FOR SHOT NUMBERS 55-59 (Copper Barrel, Atmospheric Pressure, $E_l \simeq 6.6$ J)

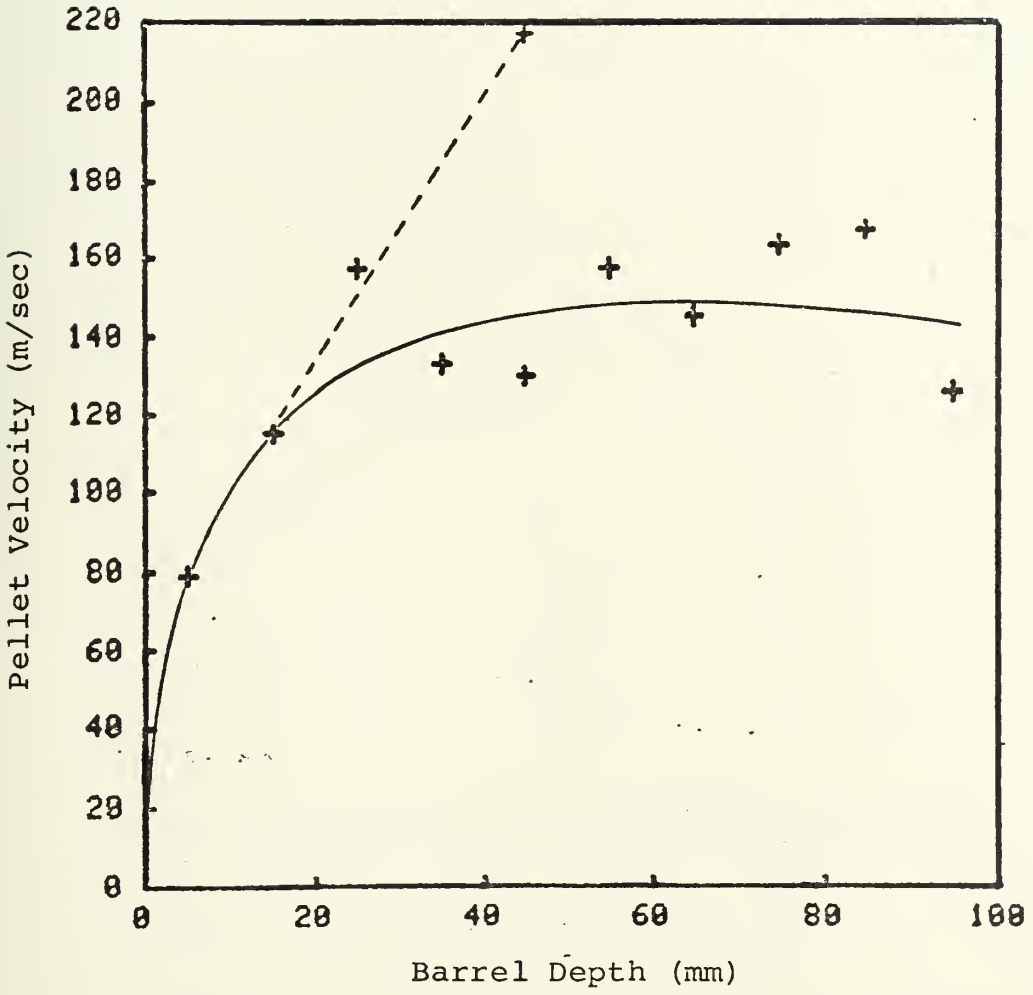

FIGURE 3.11: PELLET VELOCITY AS A FUNCTION OF BARREL DEPTH FOR SHOT NUMBERS 60-70 (Copper Barrel, Atmosheric Pressure, $E_l \simeq 6.6$ J)

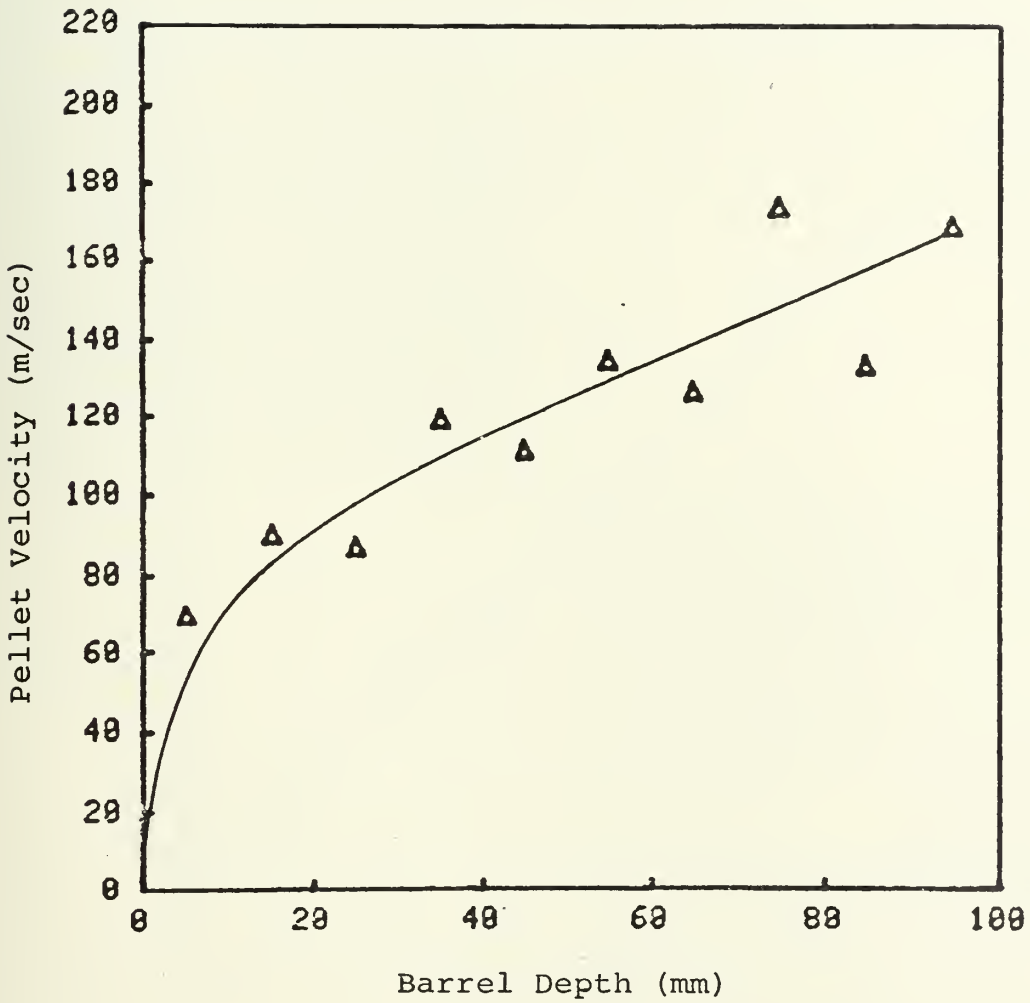

FIGURE 3.12: PELLET VELOCITY AS A FUNCTION OF BARREL DEPTH FOR SHOT NUMBERS 71-80 (Copper Barrel, Vacuum, $E_l' \simeq 6.6$ J)

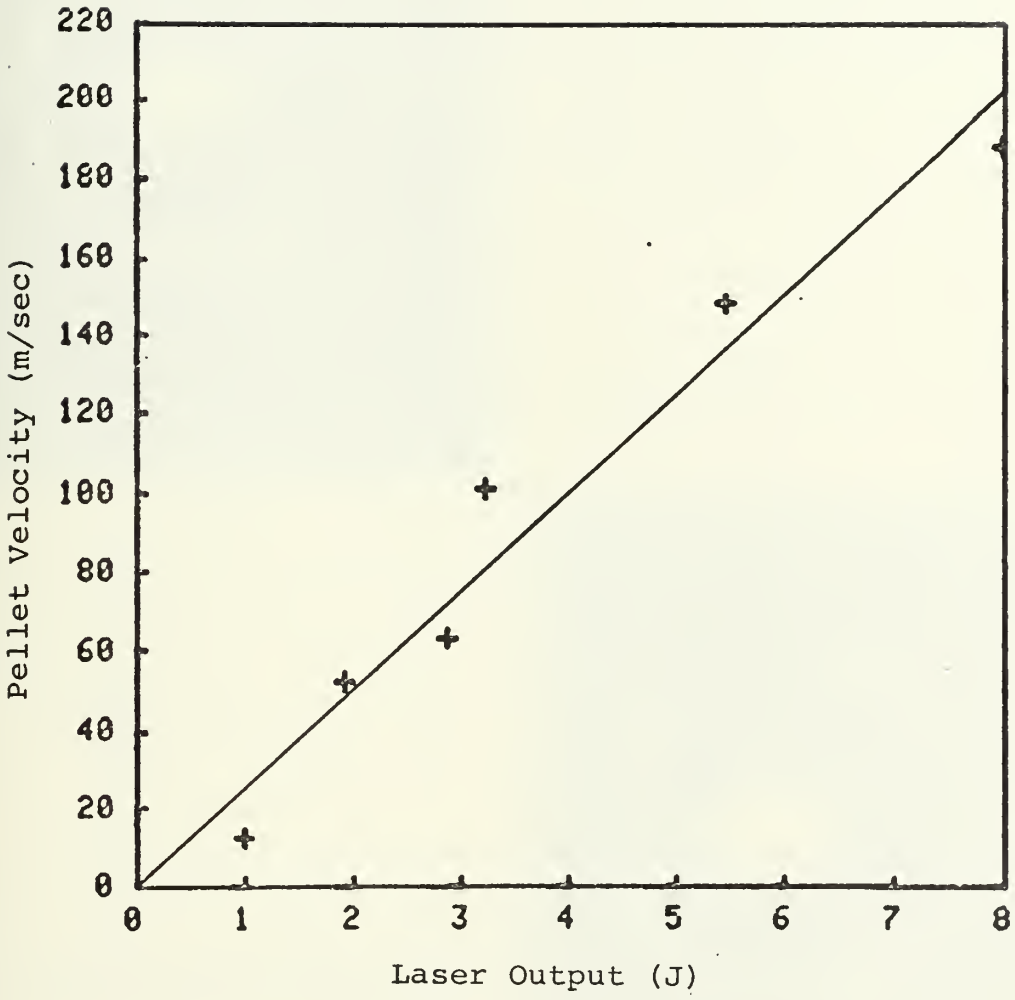

FIGURE 3.13: PELLET VELOCITY AS A FUNCTION OF LASER OUTPUT

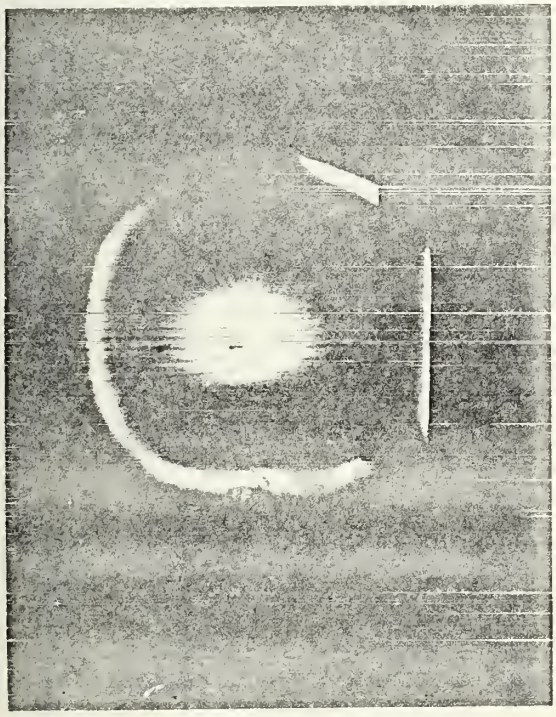

(a)

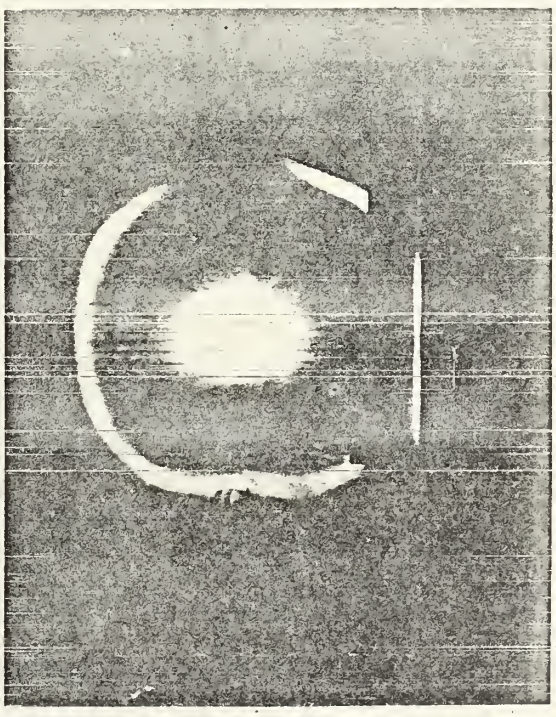

(b)

FIGURE 3.14: TYPICAL DOUBLE-PELLET (a) AND QUADRUPLE- PELLET (b) DOUBLE-EXPOSURE PHOTOGRAPHS (actual size)

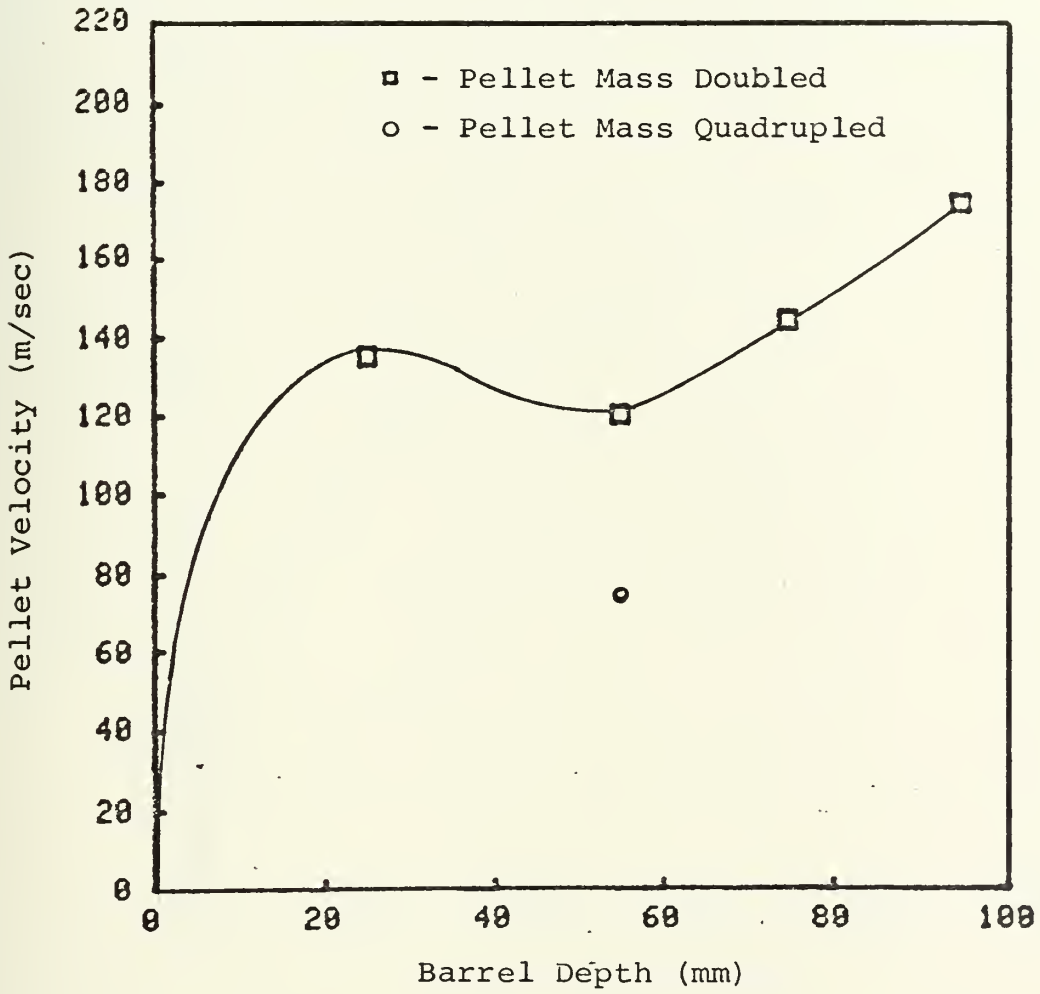

FIGURE 3.15: PELLET VELOCITY AS A FUNCTION OF BARREL DEPTH FOR SHOT NUMBERS 86-92 (Copper Barrel, Atmospheric Pressure, $E_l \simeq 6.6$ J)

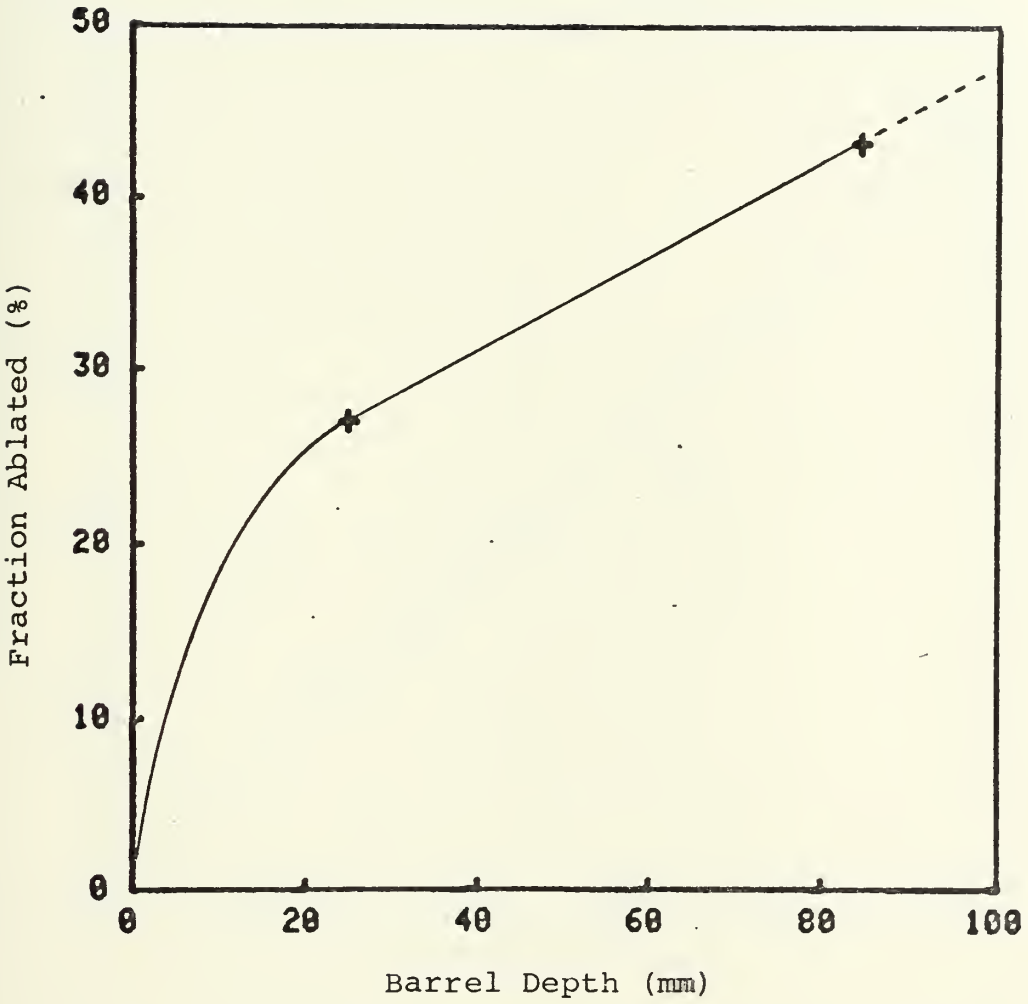

FIGURE 3.16: FRACTION OF PELLET ABLATED AS A FUNCTION OF BARREL DEPTH FOR SHOT NUMBERS 49-54 (Copper Barrel, Atmospheric Pressure, $E_l \simeq 8.0$ J)

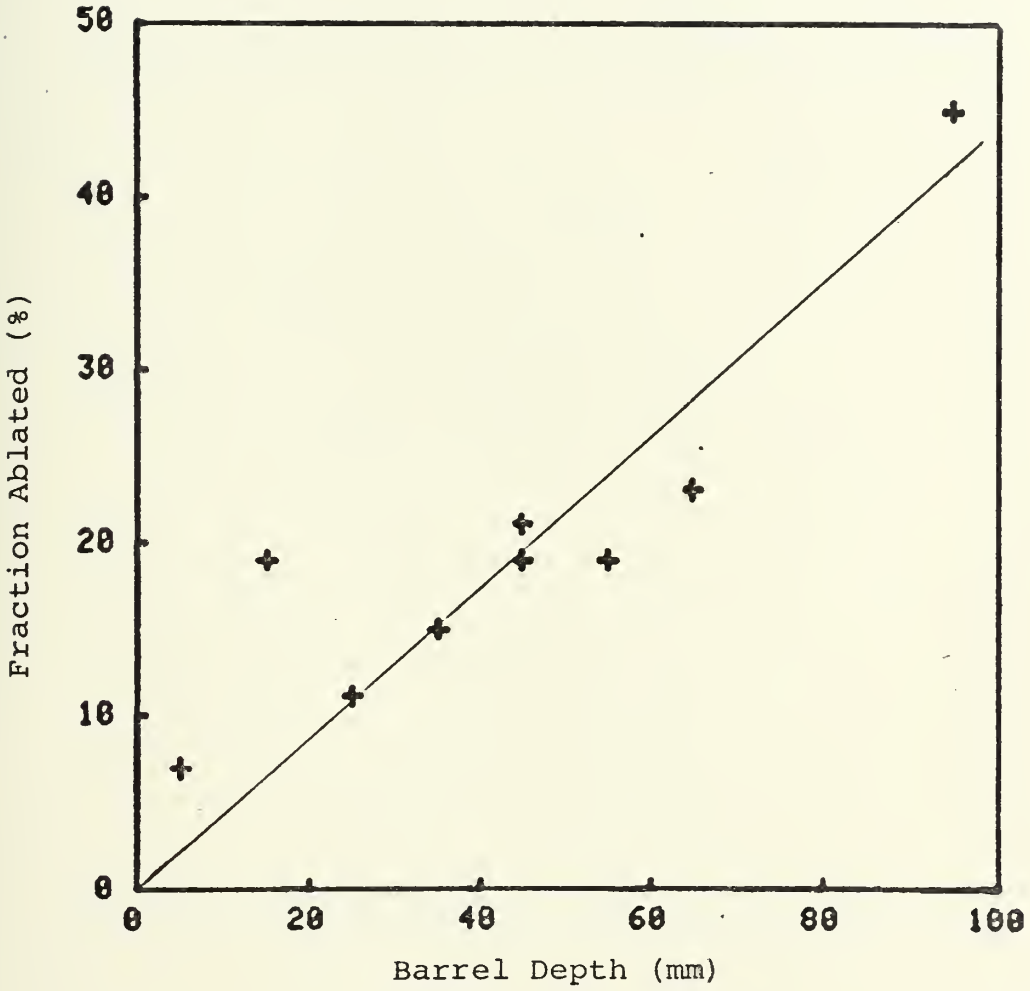

FIGURE 3.17: FRACTION OF PELLET ABLATED AS A FUNCTION OF BARREL DEPTH FOR SHOT NUMBERS 60-70 (Copper Barrel, Atmospheric Pressure, $E_l \simeq 6.6$ J)

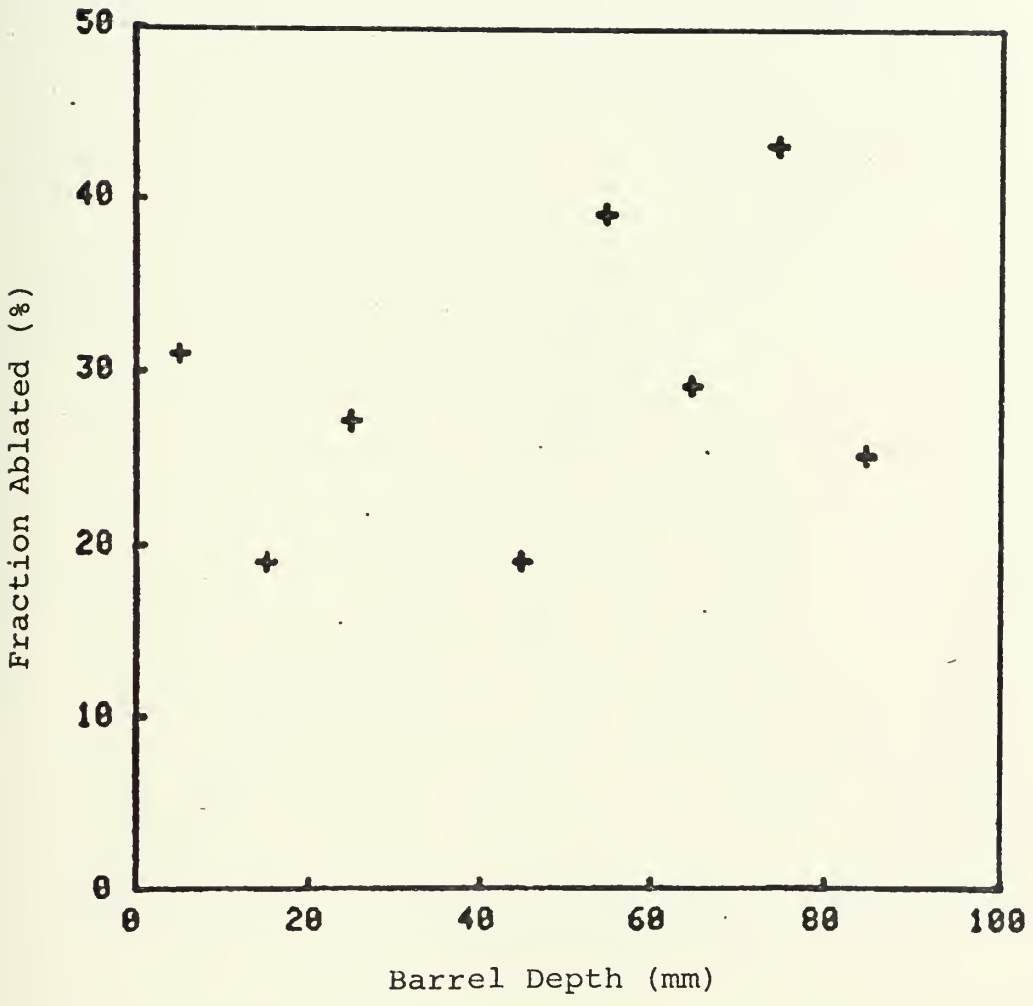

FIGURE 3.18: FRACTION OF PELLET ABLATED AS A FUNCTION OF BARREL DEPTH FOR SHOT NUMBERS 71-80 (Copper Barrel, Vacuum, $E_l \simeq 6.6$ J)

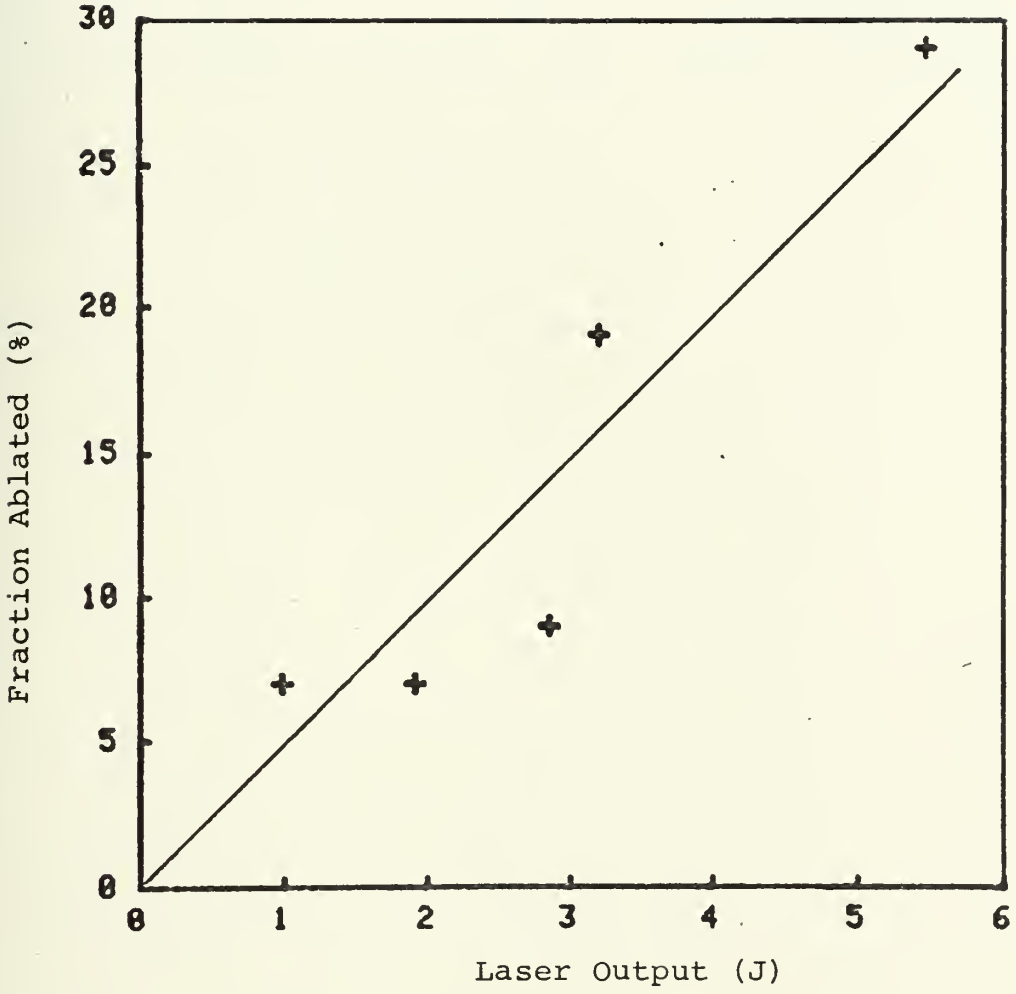

FIGURE 3.19: FRACTION OF PELLET AS A FUNCTION OF LASER OUTPUT

it could be found, was sealed in a small envelope until it could be weighed on an analytical balance (to within 0.05 mg; less than 5% error), and its mass recorded. An estimate of the degree of pellet vaporization was made by dividing the recovered pellet masses by the mean unablated pellet mass (2.47 mg), and subtracting that figure from 100%. Figures 3.16-19 contain plots of the fraction of pellet mass ablated vs. barrel depth and laser output for shots taken through the copper barrel.

3.6.3 DATA REDUCTION AND ANALYSIS

It would be appropriate at this time, to point out to what extent the data from this experiment can be considered accurate, and then suggest possible sources of experimental error. It was previously mentioned that the time interval between strobe flashes varied an average of 10% above the value indicated on the dial. Throughout the experiment, the dial was set for a time interval of 90 μsec. The distances between pellet exposures in the photographs were carefully measured (from pellet leading edge to leading edge) with a pair of calipers under a magnifying lens to within 0.03 mm. Pellet velocities could then be calculated by multiplying the photograph distances by the scale factor (1.80) and dividing by an average strobe time interval of 100 μsec. Thus, the largest source of pellet velocity measurement error appears to be τ_i , and the figures listed for v_p in Table A.2 should be accurate to within, at most, 10%.

In order to account for variations in v_p when all of

the parameters for certain shots are identical, attention should be turned to Figure 2.6. Since these pellets are not rigorously spherical and their diameters vary slightly, they cannot all fill up the bore cross section to the same degree. On the average there is a pellet-bore diameter clearance of 3 mils in the steel barrel, and 6 mils of clearance in the copper. Laser energy jitter (measured in Section 3.3 to be < 5%) and laser-barrel misalignment must also be considered here. Consequently, the pellets do not all receive the same amount of laser radiation, and more importantly, there will always be some amount of ablative gas "blow-by" around in front of the pellet as it is pushed down the bore. This blow-by will probably increase as more of the pellet is ablated. The sum of all these measurement errors and fluctuations turns out to be no greater than 15% of the pellet velocity.

Errors in alignment will inevitably arise over a normal period of system operation. This is probably the cause of the disparity between the two velocity curves in Figure 3.6. Since the laser output through the bore is directly dependent upon such delicate alignment, the pellets may not receive the same amount of radiation from one run to the next.

By knowing the time delay, τ_p, between the onset of lasing and the first flash from the light source for each shot and then extrapolating backward in the photographs, the amount of time required by each pellet to emerge from the muzzle, τ_B, may be estimated. This should be approximately equal to the amount of time each pellet spends being irradiated (and ablated)

as it travels down the bore, since the pellet usually emerges from the muzzle before the laser pulse has been terminated. Pellets at shallow barrel depths may continue to be irradiated for a short time after they leave the barrel. The amount of time each pellet spends in the barrel is plotted against barrel depth and laser output in Figures 3.20-25.

There are several observations from all these graphs that deserve mention. In all cases, the pellet seems to experience a rapid acceleration in the first 10 to 20 mm of its path, followed by a regime of more gradual, if not nil, acceleration. Pellets do not appear to be affected by the presence of air in their path; they do not travel appreciably faster in a vacuum, although the flat portion of the velocity curve does suggest a slightly upward slope. This comes as quite a surprize, since one might guess that there would be a problem with choked flow as a pellet pushes against the air in front of it in the barrel. Due to the fact that the pellet velocity was measured just after it cleared the muzzle, the full effect of aerodynamic viscous drag cannot be determined.

Pellet velocity rises linearly with increasing incident laser energy, but so too does the fraction of it that is ablated (except in vacuum). The ablation is seen to take place over only one side of the pellet. In the upper limit, as laser output increases, the pellet velocity might rise accordingly, but the end product would be of such small mass as to be useless for fueling purposes. Because the fraction ablated in air and the time spent in the barrel both increase with barrel depth,

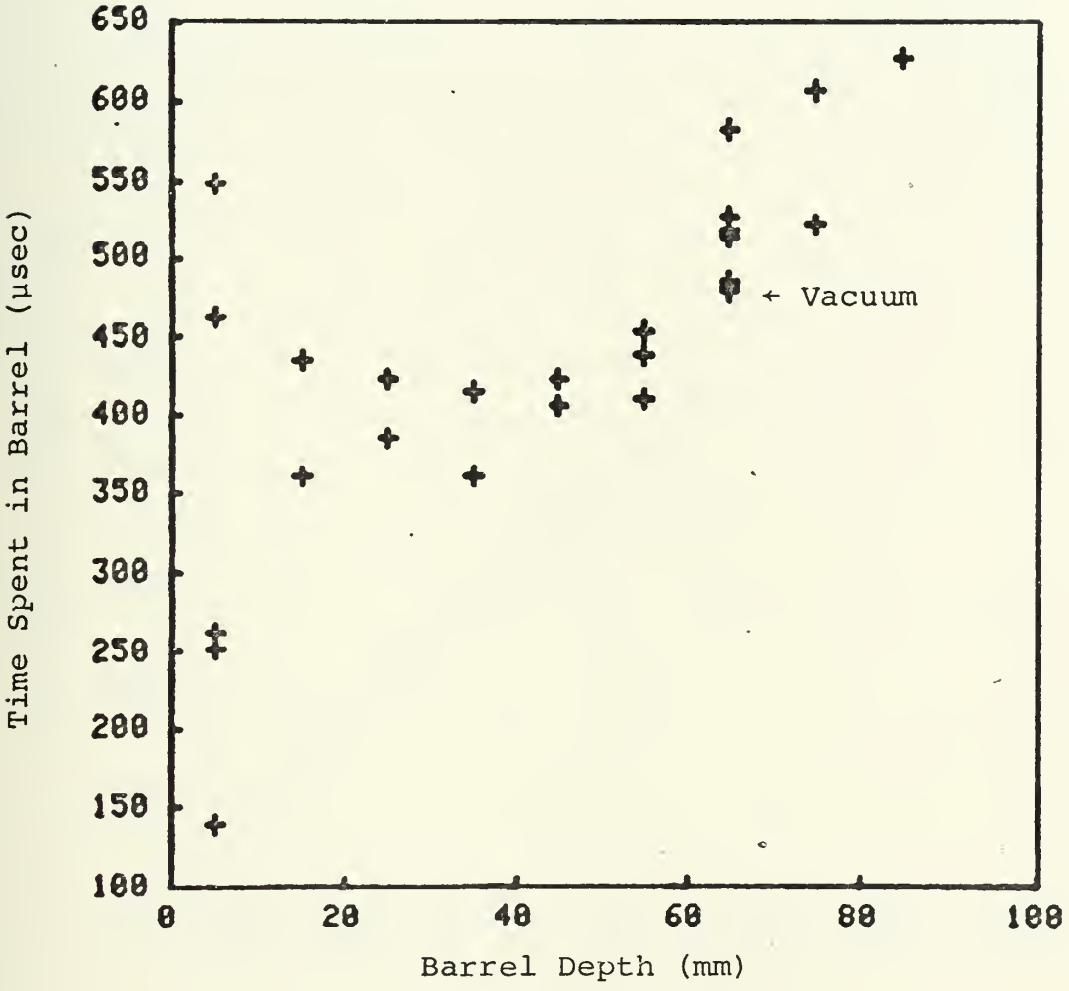

FIGURE 3.20: TIME SPENT IN BARREL AS A FUNCTION OF BARREL DEPTH FOR SHOT NUMBERS 1-36 (Stainless Steel Barrel, Atmospheric Pressure, $E_l \simeq 4.4$ J)

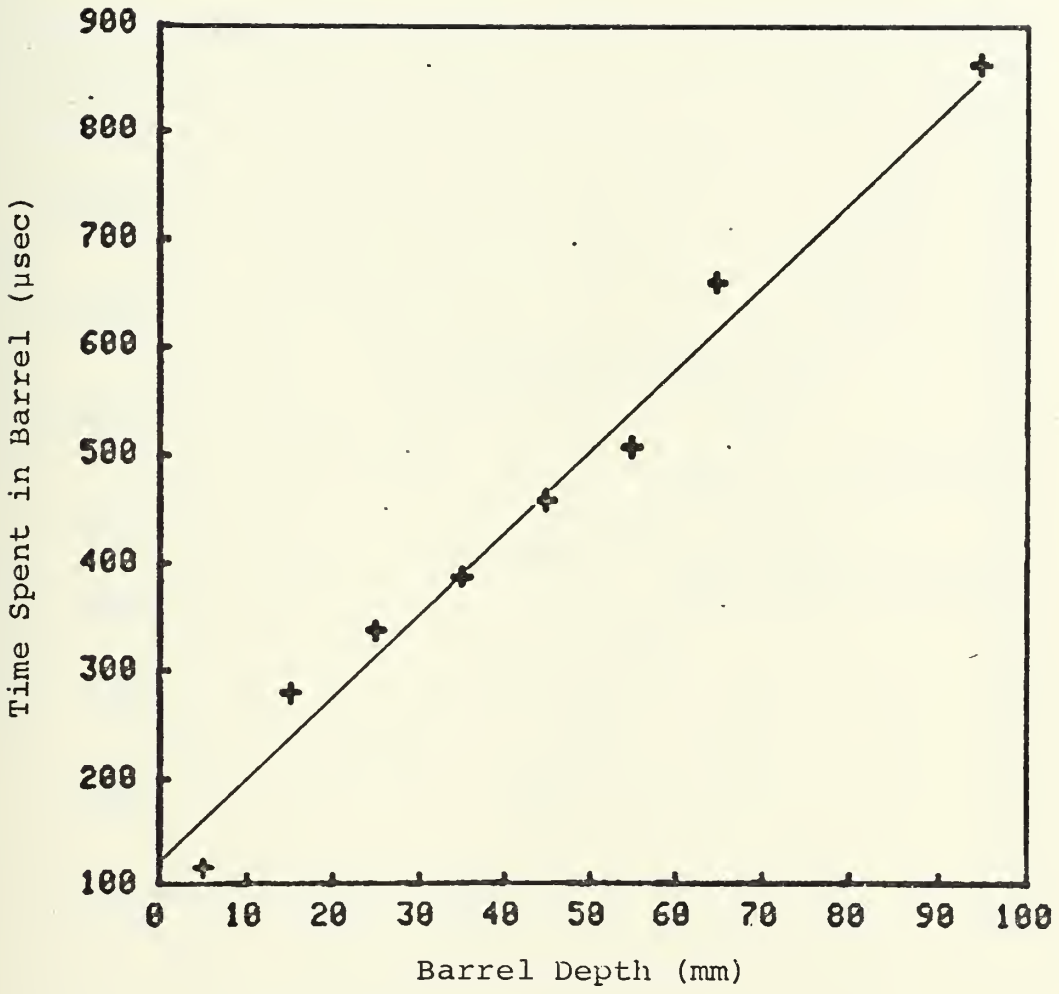

FIGURE 3.21: TIME SPENT IN BARREL AS A FUNCTION OF BARREL DEPTH FOR SHOT NUMBERS 37-44 (Stainless Steel Barrel, Atmospheric Pressure, $E_l \simeq 4.4$ J)

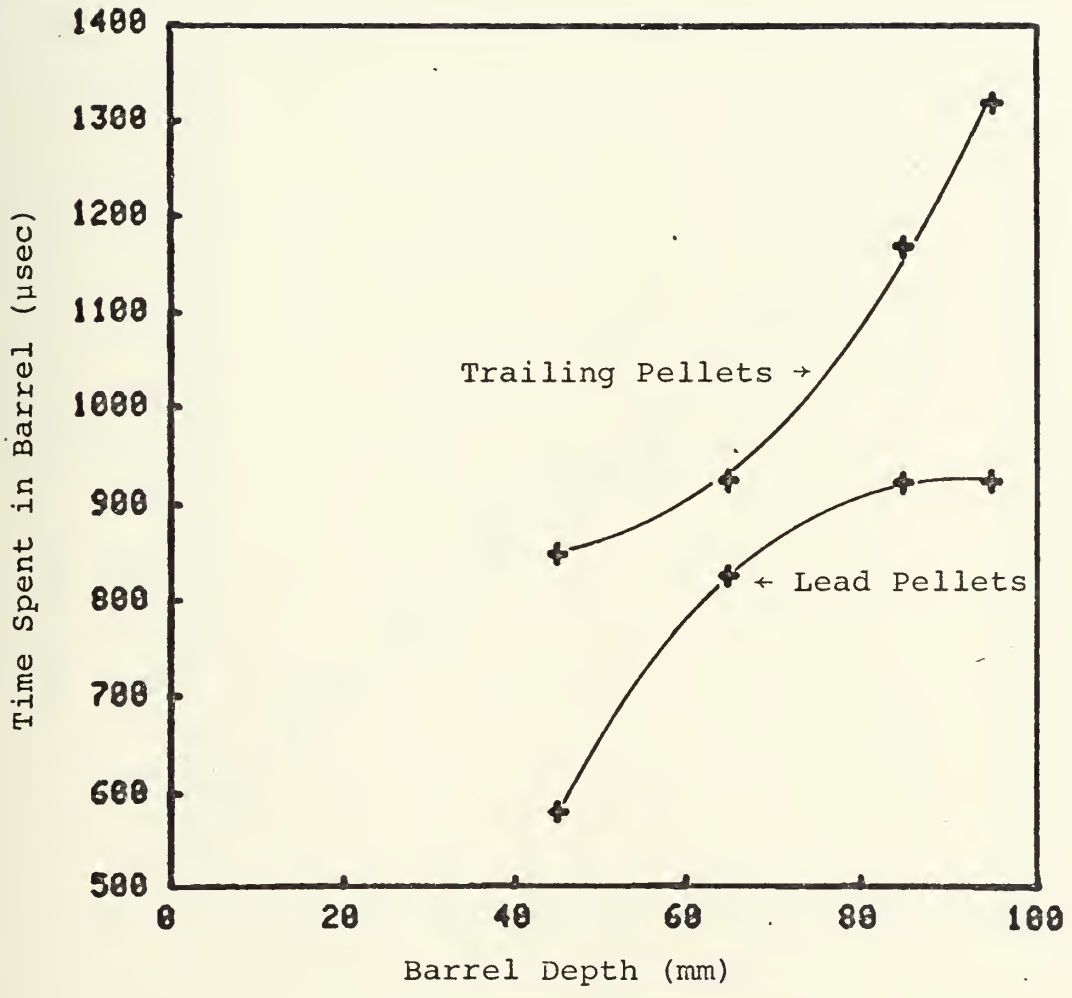

FIGURE 3.22: TIME SPENT IN BARREL AS A FUNCTION OF BARREL DEPTH FOR SHOT NUMBERS 55-59 (Copper Barrel, Atmospheric Pressure, $E_l \simeq 6.6$ J)

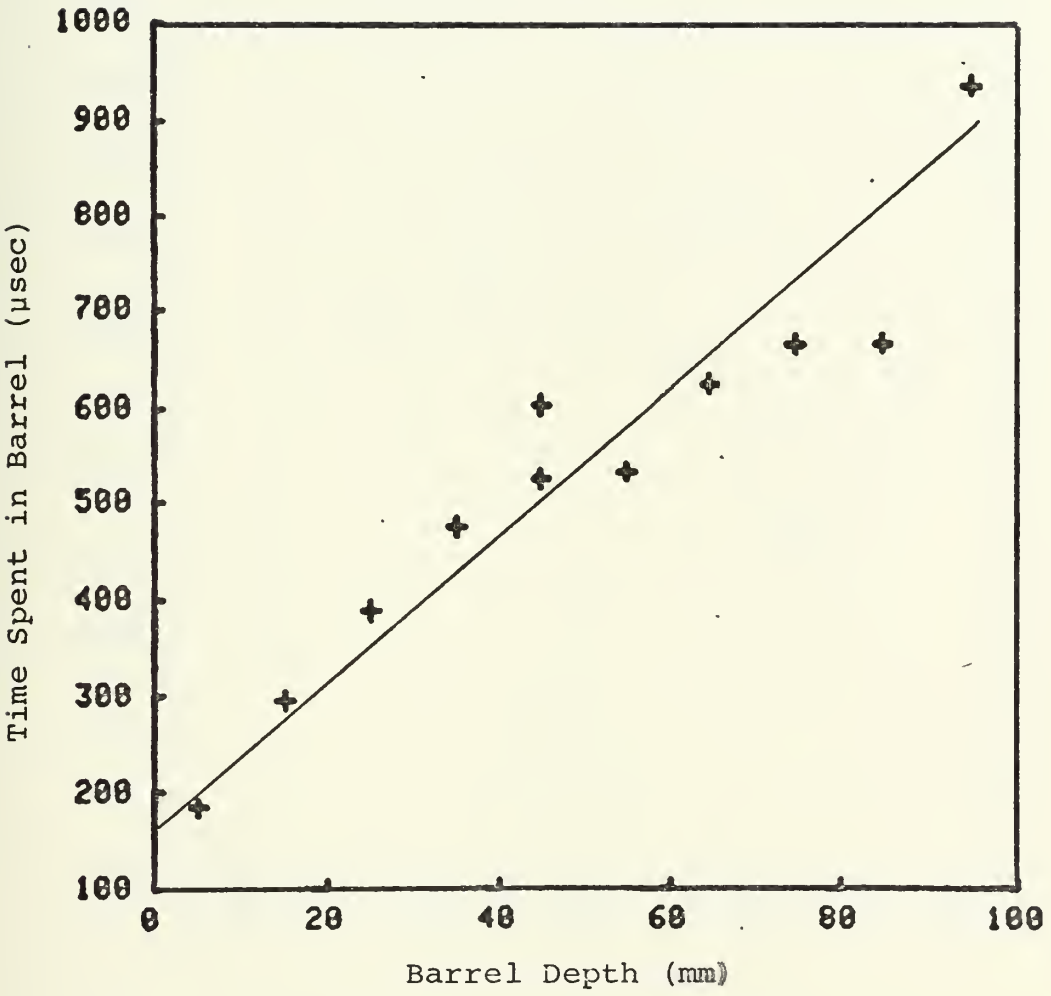

FIGURE 3.23: TIME SPENT IN BARREL AS A FUNCTION OF BARREL DEPTH FOR SHOT NUMBERS 60-70 (Copper Barrel, Atmospheric Pressure, $E_l \simeq 6.6$ J)

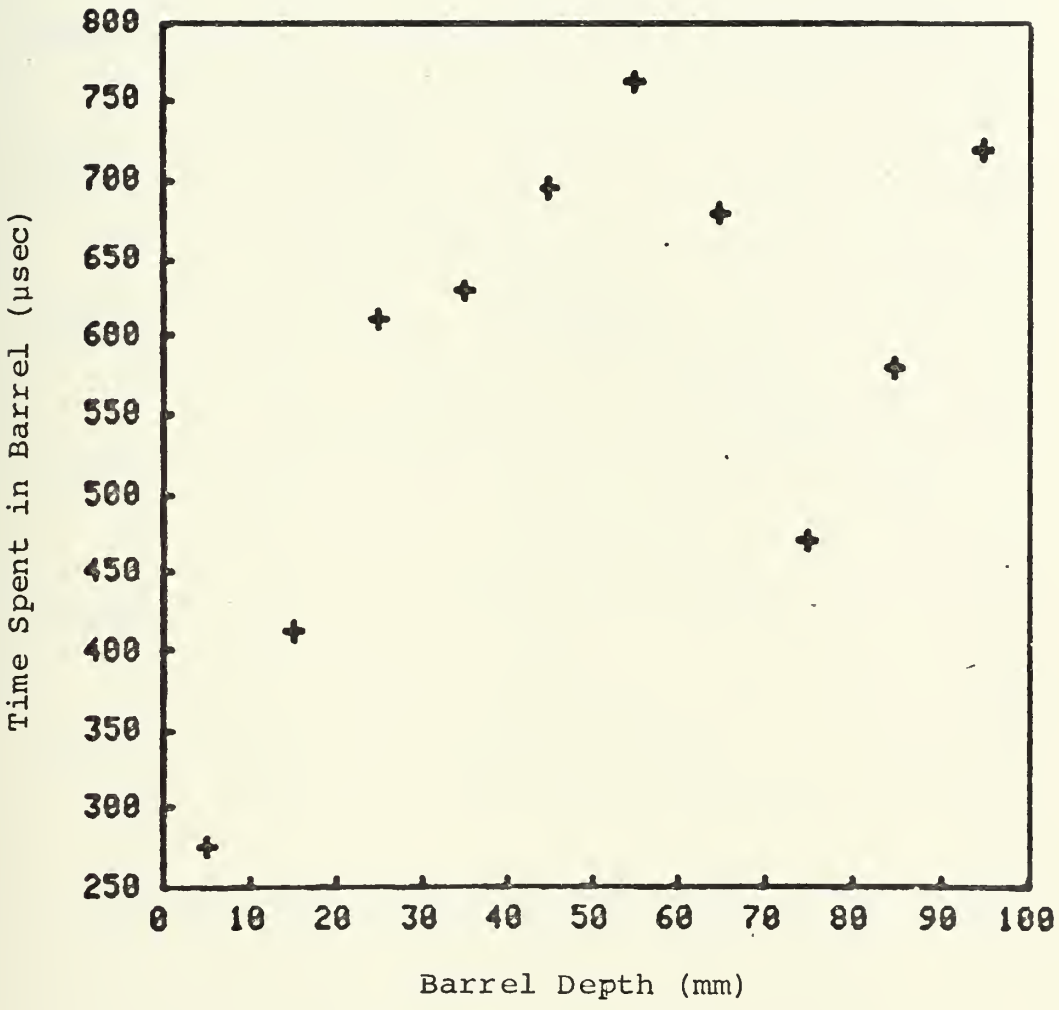

FIGURE 3.24: TIME SPENT IN BARREL AS A FUNCTION OF BARREL DEPTH FOR SHOT NUMBERS 71-80 (Copper Barrel, Vacuum, $E_l \approx 6.6$ J)

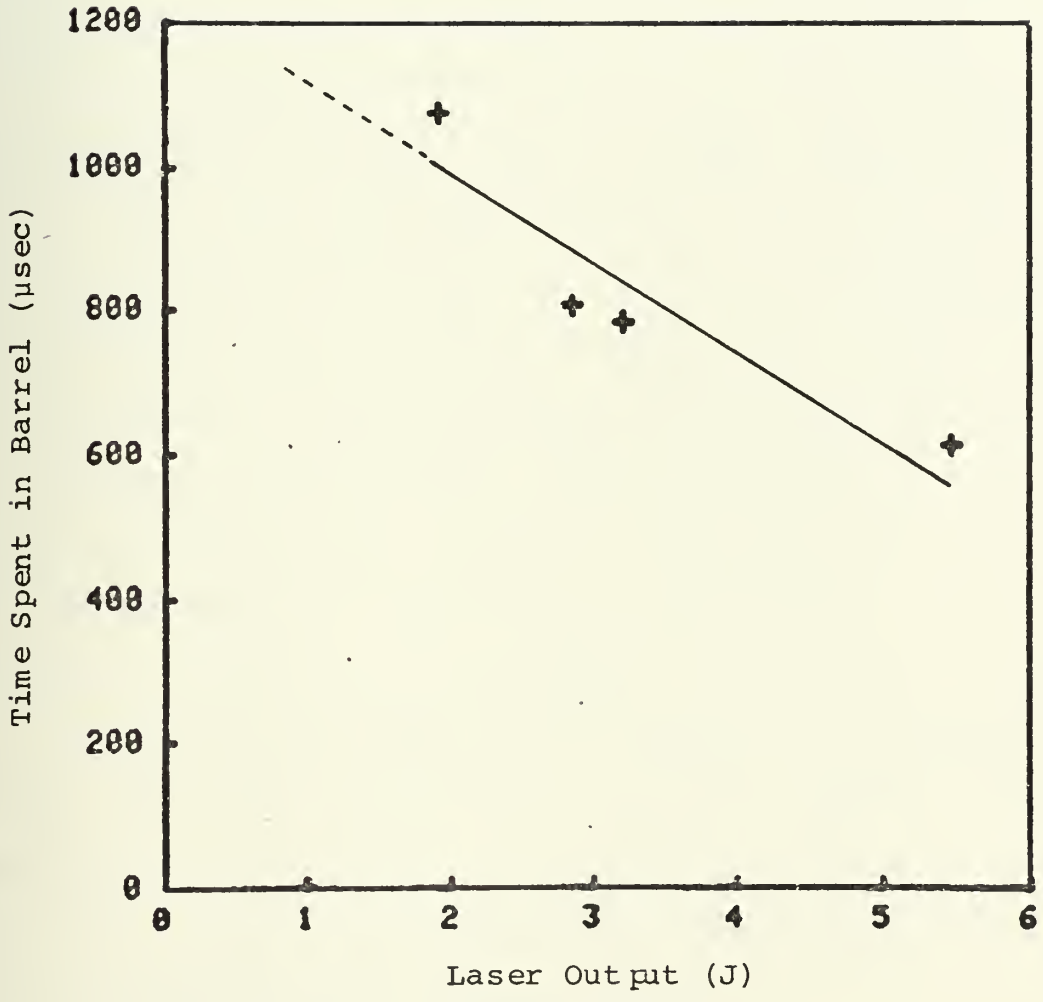

FIGURE 3.25: TIME SPENT IN BARREL AS A FUNCTION OF LASER OUTPUT

the pellet is shielded very little by the ablative gases. This would confirm our earlier assumption that the gas evaporates as neutral molecules instead of as an ionized plasma. In vacuum, however, there is clearly no such correlation between the fraction ablated (or the time spent in the barrel), and barrel depth (see Figures 3.18 and 3.24). In all cases, there is no definite relationship between the pellet velocity and the fraction of it ablated.

In the unglued double-pellet shots, the lead pellet always emerges long before, and at a higher speed than the trailing one. The lead pellet velocities are comparable to those of single-pellet shots, as are the velocities of the double-pellets which were glued together. By doubling the mass and maintaining the same velocity, one has effectively doubled the particle's kinetic energy. This insensativity to increased pellet mass would seem to indicate that some sort of velocity limiting phenomenon is at work here. When pellet mass is increased by a factor of four, however, the velocity is finally cut in half. The fact that the lead pellets are slightly burned suggests that there is some, but not much, ablative gas blow-by occurring. Friction between the pellet and the sides of the bore is an extremely nonlinear effect, but one would not expect it to be responsible for these results.

CHAPTER IV

DISCUSSION AND CONCLUSIONS

Since the pellets travel just as fast when their mass is doubled as they do singly, and seem to be continuously ablated as they travel down the bore, one might suspect that the velocity limitation phenomenon has to do with gas dynamics, in particular, the speed of sound in the ablative gas behind the pellet.

After it has been vaporized from the pellet bulk, the gas may absorb more of the laser energy and be heated to higher temperatures. The rate at which the expanding gas transfers momentum to the pellet bulk may be limited by the gas sonic velocity. This effect is already known to limit the speed of pellets accelerated by light gas guns [17]. The thermodynamic sound velocity, W, is defined by [16]

$$W^2 = - v\left(\frac{\partial p}{\partial v}\right)_s \tag{4.1}$$

where p is pressure, v is specific volume, and s is entropy. For calculational purposes, however, the sonic velocity can be approximated by [29]

$$c_s = \frac{\gamma p}{\rho_0} = \left(\frac{\gamma k T}{M}\right)^{1/2} \tag{4.2}$$

where γ is the ratio of constant pressure to constant volume specific heats, k is the Boltzmann constant, T is the absolute gas temperature, and M is its molecular weight.

Suppose the pellets are limited to the gas sonic velocity. We can attempt to calculate T, and then compare it with

what we would reasonably expect the gas temperature to be. It is nearly impossible to know how such a complex substance as cellulose triacetate would vaporize, but let's assume that the cellulose rings remain intact. Each gas molecule would then have a mass of about 212 amu. A molecule as complex as this has many degrees of freedom so $\gamma \simeq 1$ (since $\gamma = (n-2)/n$, where n is the number of degrees of freedom). The corresponding gas temperature is 747^0 C, which is within reason. Thus, this theory is within the realm of plausibility, however, this cannot be considered to be conclusive proof.

In the ideal case, suppose the pellets behave like a rocket accelerating in the absence of aerodynamic and frictional resistance. The terminal pellet speed is then given by

$$v_p = v_{rel} \ln\left(\frac{M_0}{M}\right) \tag{4.3}$$

where M_0 is the initial unablated pellet mass (2.47 mg), and M is the mass of the accelerated pellet bulk. Assuming a blow-off gas velocity of 1000 m/sec relative to the pellet (v_{rel}), and an M of 1.9 mg (an average experimental value), a terminal pellet speed of 1300 m/sec would result. Obviously our experimental data cannot support this hypothesis, but it appears that this type of acceleration may take place over the first 20 mm or so of the pellet's path, since the pellets pick up most of their speed at that time.

In terms of energy coupling efficiency, defined by

$$\eta \equiv \frac{\text{pellet kinetic energy}}{\text{incident laser energy}} \tag{4.4}$$

the experimental results show that it is extremely poor, less than a percent. The model presented in Chapter I (Equation 1.12)

predicts a substantially higher value of 16%. The laser radiation provides sufficient local heating to induce a high velocity gas dynamic flow of ablated material directed away from the pellet surface which drives shock waves into the pellet bulk. It appears then, that most of the laser energy is imparted to the material engulfed by the shock waves in the form of internal energy (heat), rather than as directed kinetic energy. Even though η is so low, the amount of energy expended accelerating fuel pellets in this manner would have only a slight impact on the reactor power balance.

In the case of cellulose triacetate, maintaining pellet integrity during acceleration poses no problem whatsoever. This may not hold as true for DT ice, since its maximum allowable tensile stress is substantially lower by a factor of at least 100. An estimate of the maximum stress encountered by the pellets in this experiment can be made, and compared with the structural limits of DT. Recall that the maximum stress is dirctly related to the maximum acceleration experienced by the pellet (Equation 1.11). In Section 2.5, the maximum acceleration that could be tolerated by a solid DT pellet was calculated to be 2×10^6 m/sec^2. The experimental acceleration can be estimated by using the relation

$$a_{max} \simeq \frac{(\Delta v)^2}{\Delta s} \tag{4.5}$$

where Δs is the path length over which the acceleration acts, and Δv is the pellet velocity at the end of that path. The dotted curve in Figure 3.11 corresponds to the highest observed acceleration; it gives a Δv = 217 m/sec and a Δs =0.045 m. The

value of a_{max} is then 1.05×10^6 m/sec^2, which is just below the maximum allowable limit. This, indeed, indicates that there could be some difficulty in holding DT pellets together during acceleration.

4.2 CONCLUSIONS

The technological obstacles involved in laser fuel pellet injection are quite formidable, but not altogether impossible to overcome. The velocities achieved using cellulose triacetate pellets must be improved upon by at least a factor of five to meet most projected reactor fueling requirements. This may prove to be possible with hydrogen if pellet speed is limited by the ablative gas sonic velocity, since the speed of sound in this case lies in the 3×10^3 m/sec range. In this event, however, one may as well use a light gas gun instead.

Whereas only less than a third of the pellet's mass was vaporized in this experiment, one would expect higher ablation fractions in hydrogen at comparable levels of laser energy; but this alone would not mean proportionately higher terminal pellet velocities. Structural deformation and disintegration of solid hydrogen could prove to be problematic, and might necessitate the development of ionic crystal fuel pellets.

The difference in barrel performance between copper and stainless steel was not as great as first expected. Less laser energy is transmitted through the latter, and as a result, stainless steel may suffer crystal structure damage from the kind of continual laser irradiation expected in a reactor

fuel injector. In terms of velocity, neither material seemed clearly superior, although the advantage of higher reflectivity in copper may have been offset by the greater clearance around the pellet for blow-by to occur.

The key problem remaining for future consideration is confirming the mechanism by which the pellets are accelerated. If the blow-off gases are merely expanded by laser heating, pellet velocities will assuredly be sonic velocity limited. If, on the other hand, a rocket effect takes place which continually accelerates the pellet, the laser injection concept can probably be made successful. Perhaps refined laser acceleration techniques can be engineered to cause the latter effect to become dominant.

Laser fuel pellet injection is certainly an idea which deserves further examination and experimentation. The next logical step would involve the use of solid deuterium ice pellets in an acceleration study similar to this one. Serious thought should be given to varying the laser pulse length below 1000 μsec, in hopes that the rocket acceleration effect acts for a longer period of time. An even better extension of this idea [30] would be to use several repetitive mode-locked Q-switched pulses of moderate power. Several short, intense pulses may provide a corresponding number of rocket-like accelerations. Another suggestion would be to launch the pellets through a set of guide rails (instead of a solid barrel) to allow the blow-off gases to escape out the sides, and thus assure continuous pellet ablation by the laser radiation. This

should prevent any appreciable gas layer shielding of the pellet, if indeed it is the cause of velocity limitation.

APPENDIX

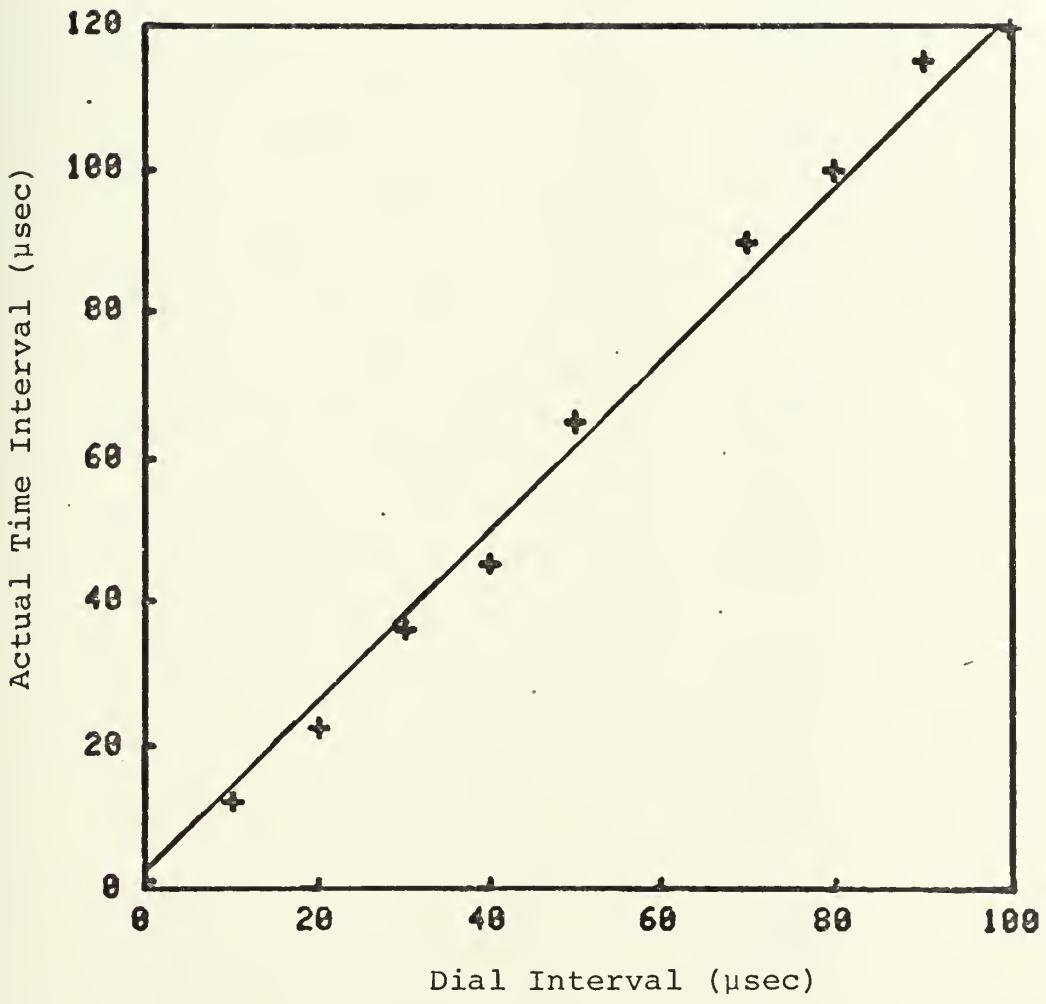

FIGURE A.1: STROBE DIAL TIME INTERVAL AS A FUNCTION OF ACTUAL STROBE TIME INTERVAL

APPENDIX

TABLE A.1

RUBY LASER CALIBRATION DATA

Capacitor Bank Voltage (KV)	Laser Output (J)
3.0 and below	Will not fire
3.2	0.367
3.2	0.402
3.2	0.528
3.4	1.88
3.4	2.04
3.4	1.81
3.6	3.62
3.6	3.59
3.6	3.59
3.8	6.13
3.8	5.78
3.8	6.28
4.0	8.84
4.0	8.79
4.0	8.89
4.2	10.80
4.2	11.56
4.2	11.06
4.4	14.67
4.4	14.67
4.4	14.07
4.6	17.19
4.6	17.59
4.6	17.34
4.8	20.60
4.8	21.11
4.8	20.60
5.0	23.12
5.0	24.62
5.0	23.62

APPENDIX

TABLE A.2

PELLET ACCELERATION DATA

Shot No.	s (mm)	v_p (m/sec)	f (%)	τ_s (μsec)	Remarks
1	5	61	7	463	Atmosphere, SS Barrel
2	5	44	Lost	549	$E_l \simeq 4.4$ J
3	5	58	15	251	
4	5	43	11	239	
5	5	45	15	262	
6	15	79	15	360	
7	15	75	15	435	
8	25	104	7	423	
9	25	114	7	385	
10	35	123	15	415	
11	35	155	Lost	360	
12	45	148	23	406	
13	45	162	21	423	
14	55	161	Lost	411	
15[1]	25	169	11	310	
16	55	147	11	454	
17	55	159	11	439	
18	65	168	15	481	
19	65	179	Lost	518	
20	75	168	15	522	
21	75	164	15	608	
31[2]	65	182	21	527	
32	65	191	17	514	

TABLE A.2 (Cont.)

Shot No.	s (mm)	v_p (m/sec)	f (%)	τ_a (μsec)	Remarks
33	65	186	19	486	Atmosphere, SS Barrel
34	65	188	Lost	582	$E_\ell \simeq 4.4$ J
35	65	207	Lost	479	
36	85	187	Lost	628	
37	5	79	11	114	
38	15	107	13	279	
39	25	128	7	335	
40	35	126	Lost	386	
41	45	117	9	457	
42	55	125	15	506	
43	65	122	15	661	
44	95	128	Lost	864	
45	15	57	3	218	
46	15	81	7	370	
47	25	85	Lost	457	
48	35	74	Lost	529	
49	65	191	Lost	590	Atmosphere, Cu Barrel
50	85	169	43	697	$E_\ell \simeq 8.0$ J
51	45	188	Lost	423	
52	75	167	Lost	641	
53	95	144	Lost	647	
54	25	175	27	291	
55	65	104 - 106	Both Lost 0	854 - 826	Atmosphere, Cu Barrel, 2 Pellets (unglued), $E_\ell \simeq 6.6$ J
56	65	90	27	924	

TABLE A.2 (Cont.)

Shot No.	s (mm)	v_p (m/sec)	f (%)	τ_b (μsec)	Remarks
57	85	113	Both	923	Atmosphere, Cu
		84	Lost	1169	Barrel, 2 Pellets
58	95	121	Both	925	(unglued)
		>81	Lost	>1320	$E_l \simeq 6.6$ J
59	45	122	Both	578	
		85	Lost	849	
60	95	126	41	936	Atmosphere, Cu Barrel
61	85	167	Lost	667	$E_l \simeq 6.6$ J
62	75	163	Lost	665	
63	65	145	23	625	
64	55	157	19	533	
65	45	217	19	603	
66	35	133	15	474	
67	25	157	11	388	
68	15	115	19	295	
69	5	79	7	183	
70	45	130	21	525	
71	95	168	Lost	719	$p \simeq 10^{-4}$ torr, Cu Barrel
72	85	133	25	579	$E_l \simeq 6.6$ J
73	75	173	43	470	
74	65	126	29	680	
75	55	134	39	762	
76	45	111	19	695	
77	35	119	Lost	629	
78	25	87	27	610	
79	15	90	19	412	
80	5	70	31	275	

TABLE A.2 (Cont.)

Shot No.	s (mm)	v_p (m/sec)	f (%)	τ_b (μsec)	Remarks
81	55	148	29	612	Atmosphere, Cu Barrel, $E_l \simeq 5.48$J
82	55	101	19	784	$E_l \simeq 3.22$ J
83	55	63	9	806	$E_l \simeq 2.86$ J
84	55	52	7	1078	$E_l \simeq 1.91$ J
85	55	12	7	--	$E_l \simeq 0.98$ J
86	55	120	--	722	Atmosphere, Cu Barrel, 2 Pellets (glued) $E_l \simeq 6.6$ J
87	75	165 111	--	897 1035	Broke apart
88	75	144	--	861	
89	95	66 56	--	443 549	Broke apart
90	95	174	--	982	
91	25	135	--	493	
92	55	74	--	1325	4 Pellets (glued)

1. Not plotted.

2. Data for Shot Numbers 22-30 invalidated by laser malfunction; data not plotted.

BIOGRAPHICAL NOTE

The author was born in Laramie, Wyoming on December 7, 1953. He was raised in Cheyenne, Wyoming, where he graduated at the top of his class at Central High School in 1972.

In July of 1972, he reported for duty as a Midshipman at the United States Naval Academy. After four years of study with a double major in Engineering Physics and Soviet Studies, he graduated with distinction and was awarded a Bachelor of Science degree and a commission as an Ensign in the United States Navy. While at the Academy, he participated as a member of the Plebe cross-country and rifle teams, and later, on an intramural level, in cross-country, track, and 150 lb. football. He was also active in Sigma Pi Sigma, Scuba Club, Sky-diving Club, the American Nuclear Society, and Russian Club. In his senior year, he served as president of the student chapter of ANS as well as president of Russian Club.

In 1976, he was authorized to accept a fellowship from the Nuclear Engineering Department at the Massachusetts Institute of Technology.

Upon completion of his one year of graduate work there, he will attend the U.S. Naval Nuclear Power School in Orlando, Florida and Arco, Idaho, followed by Submarine School in San Diego, California. By January 1979, he will finally be assigned to duty aboard a nuclear submarine of the U.S. Pacific Fleet.

REFERENCES

1. Class Notes, Course 22.610, "Controlled Fusion Power," Nuclear Engineering Department, Massachusetts Institute of Technology, Fall, 1976.

2. Spitzer, L., Grove, D.J., Johnson, W.E., Tonks, L., Westendorp, W.F., "Problems of the Stellerator as a Useful Power Source," U.S. Atomic Energy Commission Report NYO-6047, 1954.

3. Rose, D.J., "On the Fusion Injection Problem," Oak Ridge National Laboratory Technology Division Memo No.22, 1972.

4. Gralnick, S.L., "Solid Deuterium Evaporation in a Fusion Plasma," Nuclear Fusion, No.13, 1973.

5. Kerbel, G.D., "Fueling of Thermonuclear Reactors by Deuterium Pellets," Oak Ridge National Laboratory Plasma Engineering Memo No.35, 1975.

6. Bottiglioni, et al., "An Evaporation Model for H_2 Clusters Interacting with Electrons and Ions in a Plasma," Nuclear Fusion, No.14, 1974.

7. Samain, A., "Inward Diffusion of Tokamak-Trapped Particles by Slow Magnetic Pumping," Nuclear Fusion, No.12, 1972.

8. Verboom, G.K., and Rem, J., "The Temperature Profile in a Thermonuclear Reactor," Nuclear Fusion, No.13, 1973.

9. Jorgenson, L.W., Sillesen, A.H., and Oster, F., "Ablation of Hydrogen Pellets in Hydrogen and Helium Plasmas," Plasma Physics, Vol.17, 1975.

10. Carruthers, R., "Engineering Parameters of a Fusion Reactor," Nuclear Fusion Reactors Conference Proceedings, 1969.

11. Foster, C.A., Ph.D. Thesis, Nuclear Engineering Department, University of Illinois, 1977.

12. Milora, S.L., and Foster, C.A., Oak Ridge National Laboratory TM-5776, 1976.

13. Gralnick, S.L., Report No.58, Plasma Laboratory, School of Engineering and Applied Science, Columbia University, New York, 1972 (unpublished).

14. Mills, R.G., ed. A Fusion Power Plant, Princeton, New Jersey: Plasma Physics Laboratory, Princeton University, 1974.

REFERENCES (Cont.)

15. Milora, S.L., Foster, C.A., and Stewart, L.D., "Pellet Fueling Progress Report for the Quarter of January, February, and March," Oak Ridge National Laboratory, 1976 (unpublished).

16. McCarty, Robert D., Hydrogen Technological Survey - Thermophysical Properties, Washington, D.C.: National Aeronautics and Space Administration, 1975.

17. Milora, S.L., and Foster, C.A., "Pellet Fueling Progress Report for the Quarter of October, November, and December," Oak Ridge National Laboratory, 1975 (unpublished).

18. Bol'shutkin, D.N., and Stetsenko, Yu.E., "Trudy Fiziko-Tekhnicheski Institute Nizkikh Temperature, Akademiya Nauk UkrSSR, 1, 1968.

19. Stetsenko, Yu.E., et al., "Influence of Zero Energy on the Plastic Deformation of Hydrogen," Soviet Physics - Solid State, Vol.14, No.1, 1972.

20. Roder, H.M., et al.,"Survey of the Properties of Hydrogen Isotopes Below Their Critical Temperatures," National Bureau of Standards TN 641, 1973.

21. Weast, Robert C., ed. Handbook of Chemistry and Physics, Cleveland, Ohio: Chemical Rubber Company, 1970.

22. Wordingham, J.A., and Reboul, P., Dictionary of Plastics, New York: Philosophical Library, Inc., 1964.

23. Private Communication with Mr. Sidney Field of the Allen Field Company, Inc., July, 1977.

24. Private Communication with Kenneth L. Hoy, Ph.D., of the Chemicals and Plastics Research and Development Department, Union Carbide Corporation, July, 1977.

25. Encyclopedia of Polymer Science and Technology, Vol.3, New York: John Wiley and Sons, Inc., 1965.

26. Dimock, D., et al., "Pellet Acceleration Studies Relating to the Refueling of a Steady-state Fusion Reactor," Danish Atomic Energy Commission, Riso Report No.332, 1975.

27. Private Communication with Mr. Mark L. McKinstry of the Applied Plasma Physics Group, Nuclear Engineering Department, Massachusetts Institute of Technology, July, 1977.

REFERENCES (Cont.)

28. Class Notes, Course 22.612, "Plasmas and Controlled Fusion II," Nuclear Engineering Department, Massachusetts Institute of Technology, Spring, 1977.

29. Chen, Francis E., Introduction to Plasma Physics, New York: Plenum Press, 1974.

30. Private Communication with Professor Lawrence M. Lidsky of the Applied Plasma Physics Group, Nuclear Engineering Department, Massachusetts Institute of Technology, August, 1977.